

**Uncovering the Signaling Mechanisms of TransMEMbrane 16A**

by

**Maiwase Tembo**

Bachelor of Arts, Lake Forest College, 2015

Submitted to the Graduate Faculty of the  
Dietrich School of Arts and Sciences in partial fulfillment  
of the requirements for the degree of  
Doctor of Philosophy

University of Pittsburgh

2020

UNIVERSITY OF PITTSBURGH

DIETRICH SCHOOL OF ARTS AND SCIENCES

This dissertation was presented

by

**Maiwase Tembo**

It was defended on

April 14, 2020

and approved by

Jeffrey L. Brodsky, Ph.D., Professor, Department of Biological Sciences

Deborah L. Chapman Ph.D., Associate Professor, Department of Biological Sciences

Gerald R.V. Hammond Ph.D., Assistant Professor, Department of Cell Biology

Kirill Kiselyov, Ph.D., Associate Professor, Department of Biological Sciences

Dissertation Advisor: Anne E. Carlson, Ph.D., Assistant Professor, Department of Biological  
Sciences

Copyright © by Maiwase Tembo

2020

# Uncovering the Signaling Mechanisms of TransMEMbrane 16A

Maiwase Tembo, PhD

University of Pittsburgh, 2020

The  $\text{Ca}^{2+}$ -activated  $\text{Cl}^-$  channel, TransMEMbrane member 16A (TMEM16A), regulates diverse physiological functions including smooth muscle contraction, mucosal secretion and signal transduction. TMEM16A is an essential protein that we cannot live without. In fact, changes that enhance or reduce TMEM16A's activity result in diseases such as hypertension and inflammatory airway diseases, respectively. Despite its importance, we are just beginning to understand how TMEM16A channel activity is regulated. To study TMEM16A's regulation, I used electrophysiology techniques. Specifically, I recorded endogenous TMEM16A currents from *Xenopus laevis* oocytes using the inside-out configuration of the patch clamp technique. I observed that TMEM16A-conducted currents diminished within seconds of patch excision despite the continued presence of  $\text{Ca}^{2+}$ . Current rundown is common amongst channels regulated by the fatty acid phosphatidylinositol 4,5-bisphosphate (PI(4,5)P<sub>2</sub>). I demonstrated that TMEM16A current depletion in the membrane patch was due to loss of PI(4,5)P<sub>2</sub>, thereby revealing that PI(4,5)P<sub>2</sub> is required for TMEM16A to conduct  $\text{Cl}^-$  currents. Because PI(4,5)P<sub>2</sub> is just one of eight cell membrane phosphoinositides that share a common backbone but differ in phosphate group number and location on the inositol ring, I sought to determine which features of PI(4,5)P<sub>2</sub> enabled the lipid-channel interaction. I found that PI(4,5)P<sub>2</sub> recovered the most current compared to the other phosphoinositides, and phosphoinositides containing at least one phosphate group on position 4 were capable of recovering intermediate levels of current. The extent of recovery was dependent on whether or not the phospholipid included a phosphate at position 4 rather than the number of

negatively charged phosphates. In a separate line of experimentation, I determined that the rate of current rundown was influenced by the concentration of  $\text{Ca}^{2+}$  applied to excised patches in a way that activates a  $\text{Ca}^{2+}$ -sensitive phospholipase C (PLC) to then deplete  $\text{PI}(4,5)\text{P}_2$ . Taken together, my data reveal that  $\text{PI}(4,5)\text{P}_2$  regulates TMEM16A, and that the phosphate at position 4 is key in this interaction. Overall, my work revealed key mechanisms in how signals other than intracellular  $\text{Ca}^{2+}$  alter opening and closing of these critical channels. Expanding our understanding of TMEM16A's regulatory mechanisms may lay the foundation for developing novel therapeutics for TMEM16A-associated diseases.

## Table of Contents

List of Abbreviations .....	xiii
Preface.....	xvi
<b>1.0 Introduction.....</b>	<b>1</b>
<b>1.1 Ion transport proteins .....</b>	<b>2</b>
1.1.1 Transporters .....	2
1.1.2 ATP-powered pumps (ATPases).....	2
1.1.3 Ion channels.....	3
<b>1.2 TMEM16A discovery, physiology and structure-function .....</b>	<b>4</b>
1.2.1 Importance of TMEM16A in physiology .....	4
1.2.2 TMEM16A discovery.....	6
1.2.3 TMEM16A structure-function.....	7
<b>1.3 TMEM16A regulation.....</b>	<b>8</b>
1.3.1 Ion channel regulation .....	8
1.3.2 TMEM16 family regulation .....	10
1.3.3 TMEM16A gating .....	12
<b>1.4 <i>Xenopus laevis</i> oocytes as a model for TMEM16A studies .....</b>	<b>14</b>
<b>1.5 Dissertation aims .....</b>	<b>14</b>
<b>1.6 Figures .....</b>	<b>15</b>
<b>2.0 Materials and Methods.....</b>	<b>22</b>
<b>2.1 Reagents.....</b>	<b>22</b>

<b>2.2 Solutions .....</b>	<b>22</b>
<b>2.2.1 Oocyte wash and storage solution.....</b>	<b>22</b>
<b>2.2.2 Inside-out patch clamp solutions .....</b>	<b>23</b>
<b>2.3 Animals.....</b>	<b>23</b>
<b>2.4 Experimental methods .....</b>	<b>24</b>
<b>2.4.1 Inside-out patch clamp .....</b>	<b>24</b>
<b>2.5 Quantification and statistical analysis .....</b>	<b>25</b>
<b>2.5.1 Inside-out patch data analysis.....</b>	<b>25</b>
<b>2.6 Figures .....</b>	<b>26</b>
<b>3.0 TMEM16A Gating is Regulated by PI(4,5)P<sub>2</sub> .....</b>	<b>28</b>
<b>3.1 Introduction .....</b>	<b>28</b>
<b>3.2 Results.....</b>	<b>30</b>
<b>3.2.1 TMEM16A currents recorded from excised inside-out patches decay .....</b>	<b>30</b>
<b>3.2.2 PI(4,5)P<sub>2</sub> recovered TMEM16A currents in inside-out excised patches.....</b>	<b>31</b>
<b>3.2.3 Scavenging PI(4,5)P<sub>2</sub> sped TMEM16A current rundown.....</b>	<b>33</b>
<b>3.2.4 Slowing PI(4,5)P<sub>2</sub> depletion slowed TMEM16A rundown .....</b>	<b>34</b>
<b>3.3 Discussion .....</b>	<b>36</b>
<b>3.3.1 PI(4,5)P<sub>2</sub> regulates TMEM16A gating.....</b>	<b>36</b>
<b>3.3.2 PI(4,5)P<sub>2</sub> dephosphorylation promotes current rundown.....</b>	<b>37</b>
<b>3.3.3 Controversial TMEM16A-PI(4,5)P<sub>2</sub> relationship .....</b>	<b>38</b>
<b>3.3.4 Mechanism of PI(4,5)P<sub>2</sub> regulation of TMEM16A .....</b>	<b>39</b>
<b>3.3.5 Physiological implications of TMEM16A's regulation by PI(4,5)P<sub>2</sub> .....</b>	<b>40</b>
<b>3.3.6 Summary.....</b>	<b>41</b>

3.4 Figures and Tables .....	42
<b>4.0 The Rate of TMEM16A Current Rundown Depends on Intracellular Ca<sup>2+</sup> .....</b>	<b>51</b>
4.1 Introduction .....	51
4.2 Results.....	53
4.2.1 PI(4,5)P <sub>2</sub> does not recover TMEM16A currents completely.....	53
4.2.2 Phosphate at position 4 of the inositol ring is key in PI(4,5)P <sub>2</sub> 's interaction with TMEM16A .....	54
4.2.3 The <i>Xenopus</i> voltage sensing phosphatase does not completely inhibit TMEM16A currents .....	58
4.2.4 Lowering applied intracellular Ca <sup>2+</sup> concentration slows current rundown .....	59
4.2.5 Complete Ca <sup>2+</sup> substitution slows TMEM16A current rundown.....	61
4.2.6 Inhibition of phospholipase C (PLC) slows rundown.....	62
4.3 Discussion .....	64
4.3.1 Phosphate position is key in mediating TMEM16A-PI(4,5)P <sub>2</sub> interaction ..	64
4.3.2 Ca <sup>2+</sup> concentration determines the rate of TMEM16A current rundown...	66
4.3.3 Mechanism of TMEM16A regulation and the Ca <sup>2+</sup> -TMEM16A-PI(4,5)P <sub>2</sub> relationship .....	68
4.3.4 Other mechanisms regulating TMEM16A gating.....	69
4.3.5 Summary.....	69
4.4 Figures and Tables .....	70
<b>5.0 Overall Discussion.....</b>	<b>79</b>
<b>5.1 Overview of dissertation research.....</b>	<b>79</b>

<b>5.2 Research implications for the PI(4,5)P<sub>2</sub> regulation of TMEM16A .....</b>	<b>79</b>
<b>5.3 Research implications for the Ca<sup>2+</sup> regulation of TMEM16A.....</b>	<b>80</b>
<b>5.4 Unanswered questions about TMEM16A regulation.....</b>	<b>80</b>
<b>5.5 Dissertation research conclusions .....</b>	<b>82</b>
<b>Bibliography .....</b>	<b>83</b>

## List of Tables

<b>Table 3-1. Altering PI(4,5)P<sub>2</sub> altered the rate of rundown.....</b>	<b>44</b>
<b>Table 4-1. Ca<sup>2+</sup> activates PLC to speed patch rundown.....</b>	<b>73</b>

## List of Figures

<b>Figure 1-1. TMEM16A's role in physiology .....</b>	<b>16</b>
<b>Figure 1-2. Schematic depicting the activation of a Ca<sup>2+</sup>-activated Cl<sup>-</sup> channel (CaCC).....</b>	<b>17</b>
<b>Figure 1-3. Homology model of mouse TMEM16A and structure of chicken Bestrophin 1</b>	<b>18</b>
<b>Figure 1-4. Human TMEM16 family phylogenetic tree .....</b>	<b>19</b>
<b>Figure 1-5. Homology model of mouse TMEM16A aligned with <i>Nectria haematococca</i> TMEM16.....</b>	<b>20</b>
<b>Figure 1-6. Schematic depicting TMEM16A gating .....</b>	<b>21</b>
<b>Figure 2-1. Inside-out patch clamp technique.....</b>	<b>27</b>
<b>Figure 3-1. Structure of phosphatidyl 4,5-bisphosphate (PI(4,5)P<sub>2</sub>) .....</b>	<b>42</b>
<b>Figure 3-2. TMEM16A Ca<sup>2+</sup>-evoked Cl<sup>-</sup> currents rundown in excised inside-out patches..</b>	<b>43</b>
<b>Figure 3-3. Rate of TMEM16A Ca<sup>2+</sup>-evoked Cl<sup>-</sup> current rundown not determined by peak currents .....</b>	<b>45</b>
<b>Figure 3-4. PI(4,5)P<sub>2</sub> analog or natural PI(4,5)P<sub>2</sub> with Ca<sup>2+</sup> recovered TMEM16A conducted currents following rundown.....</b>	<b>47</b>
<b>Figure 3-5. PI(4,5)P<sub>2</sub> and Ca<sup>2+</sup> are both required for TMEM16A conducted currents .....</b>	<b>48</b>
<b>Figure 3-6. Scavenging PI(4,5)P<sub>2</sub> sped TMEM16A current rundown in excised inside-out patches.....</b>	<b>49</b>
<b>Figure 3-7. Enabling rephosphorylation or inhibiting phosphatases slowed current decay in excised inside-out patches.....</b>	<b>50</b>
<b>Figure 4-1. Phosphate position is key mediating TMEM16A-PI(4,5)P<sub>2</sub> interaction.....</b>	<b>72</b>

<b>Figure 4-2. XI-VSP speeds TMEM16A current rundown but does not abolish TMEM16A currents .....</b>	<b>74</b>
<b>Figure 4-3. Different concentrations of Ca<sup>2+</sup> result in different TMEM16A current profiles .....</b>	<b>75</b>
<b>Figure 4-4. Lowering Ca<sup>2+</sup> slows current rundown .....</b>	<b>76</b>
<b>Figure 4-5. Substituting Ca<sup>2+</sup> with other divalents slows current rundown.....</b>	<b>77</b>
<b>Figure 4-6. Inhibiting PLC slows current rundown .....</b>	<b>78</b>

## List of Abbreviations

ABC: ATP-binding cassette

ADP: Adenosine diphosphate

AMP: Adenosine monophosphate

ANO1: Anoctamin 1

Anti-PI(4,5)P<sub>2</sub>: Anti-phosphatidylinositol 4,5-bisphosphate

ATP: Adenosine triphosphate

ATPases: ATP-powered pumps

BEST1: Bestrophin 1

βGP: β-glycerophosphate

CaCC: Ca<sup>2+</sup>-activated Cl<sup>-</sup> channel

CLCA1: Cl<sup>-</sup> channel accessory 1

CNS: Central nervous system

Cryo-EM: cryogenic electron microscopy

DAG: Diacylglycerol

diC8-PI(3,4,5)P<sub>3</sub>: Dioctanoyl phosphatidylinositol 3,4,5-trisphosphate

diC8-PI(3,4)P<sub>2</sub>: Dioctanoyl phosphatidylinositol 3,4-bisphosphate

diC8-PI(3,5)P<sub>2</sub>: Dioctanoyl phosphatidylinositol 3,5-bisphosphate

diC8-PI(3)P: Dioctanoyl phosphatidylinositol 3-monophosphate

diC8-PI(4,5)P<sub>2</sub>: Dioctanoyl phosphatidylinositol 4,5-bisphosphate

diC8-PI(4)P: Dioctanoyl phosphatidylinositol 4-monophosphate

diC8-PI(5)P: Dioctanoyl phosphatidylinositol 5-monophosphate

DOG1: Discovered on gastrointestinal stromal tumors protein 1

Dr-VSP: *Danio rerio* voltage sensing phosphatase

DRG: Dorsal root ganglion

EC<sub>50</sub>: Half maximal effective concentration

EGFR: Epidermal growth factor receptor

ER: Endoplasmic reticulum

GABA: Gamma-aminobutyric acid

GDD: Gnathodiaphyseal dysplasia

HEK293: Human embryonic kidney 293

IP<sub>3</sub>: inositol triphosphate

Kir: K<sup>+</sup> inward rectifier channel

mTMEM16A: mouse TransMEMbrane 16A

OR2- Oocyte ringers solution 2

ORAOV2: Oral cancer overexpressed protein 2

PGY1: Permeability glycoprotein 1

PI(4,5)P<sub>2</sub>: phosphatidylinositol 4,5-bisphosphate

PIP<sub>3</sub>: Phosphatidylinositol 3,4,5-trisphosphate

PKC: Protein kinase C

PLC: Phospholipase C

PTEN: Phosphatase and tensin homolog

SERCA: Sarcoendoplasmic reticulum Ca<sup>2+</sup>- ATPase

TAOS2: Tumor-amplified and overexpressed sequence 2

TM6: Transmembrane domain 6

TMEM16A: TransMEMbrane 16A

TMEM16B: TransMEMbrane 16B

TMEM16C: TransMEMbrane 16C

TMEM16D: TransMEMbrane 16D

TMEM16E: TransMEMbrane 16E

TMEM16F: TransMEMbrane 16F

TMEM16G: TransMEMbrane 16G

TMEM16H: TransMEMbrane 16H

TMEM16J: TransMEMbrane 16J

TMEM16K: TransMEMbrane 16K

XI-VSP: *Xenopus laevis*-voltage sensing phosphatase

## Preface

First and foremost, I want to thank God. In as much as I would ever love to take credit for my successes thus far, I could not explain my journey here without believing in such a High power. Next, I would like to thank Dr. Anne E. Carlson, whose endless support for me created opportunities beyond what the pages to follow could ever capture. I would also like to thank Anne for her enthusiasm for me as a scientist. I cannot emphasize enough just what a momentum such as her does for a new scientist trying to find her way. I will today and for the rest of my life be thankful for the all-in-one blueprint you have given me so that I can become a person to proud of, a scientist and a woman in science. I would also like to thank the Carlson lab crew: Rachel, Katie, Joel, Dominique and the talented undergraduates. There were no dull moments just endless chatter and forward-moving science, which I will miss immensely. Thank you all for helping me grow.

To my committee, Dr. Jeffrey Brodsky, Dr. Debbie Chapman, Dr. Gerry Hammond and Dr. Kirill Kiselyov, thank you for your guidance and support throughout my graduate career. Your contributions have been instrumental in making my project what it is today. Additionally, I would like to thank the Department of Biological Sciences and Transport journal club for striving to teach me diverse science. Moreover, I want to thank the department for giving me a family to grow with. This includes Cathy Barr who helped me navigate through the program.

Next, I want to thank my family for being the building blocks for the human I have become and am becoming. To my grandmother, Lister Mulenga, whose work ethic transcends time and knows no excuse, thank you for being triumphant in the battle of hard work. To my mother, Robinah, you have put many things aside to be my companion on so many adventures and that is a testament to how supportive you are of me. I cannot imagine what you have had to do to make

my world a better place even when it offset yours. To my Baba, Kwame, who has taken every word I have spoken and written to be as valuable as treasure, showing me every day that I have and will always have a seat at the table. You taught me to nourish my mind and use it like it was the coolest superpower ever had.

To all my siblings, there is no life without you. The laughter and trouble created together or singlehandedly were the building blocks of my childhood. My need to remember all the iconic blunders may be the reason that my memory trained enough to have come this far. Thank you for your hand in raising me. Even today, all the stories you tell about my childhood are a testament to your presence and I cannot thank you enough for that.

To my friends, Akua, Ariane, Briand, Deepa, Diane, Oyindamola, Sandra and Selamile, thank you for propelling me in the directions of my dreams. I am grateful that you hold me accountable to my dreams so that I never stop dreaming and chasing. I am also thankful that you chose me to be a part of your lives. I cannot thank you enough for the shoulders, tears (both happy and sad) and your commitment to making sure that my journey is never lonely, forgotten or burdensome.

To Blaise, my partner in fun and life, thank you for the patience you exercise with me as I become the person I want to be. There is not a day that I question your support for me. I am excited to continue making memories with you despite us never agreeing on important issues such as which outfits are doing too much or LeBron James's move to Laker Nation.

## 1.0 Introduction

Ion signaling is fundamental to cellular function in all tissues and essential for survival in living organisms. This is true for organisms ranging from bacteria whose ability to adapt to different ionic environments is key to their survival [1] to humans whose neuronal firings rely on ionic gradients for proper brain function [2, 3]. In fact, our ability to experience the world relies on ion signaling. To feel the excruciating pain of knocking a toe against a bed post or hear the beautiful sound of Whitney Houston's "I'm every woman" exploding into a room, ion transport must take place. To respond to these sensory stimuli accurately, one can imagine that cells must tightly regulate ion transport. Cells do so by building concentration gradients that are kept in homeostatic balance. Shifting ionic gradients allows for ion signaling that can be translated into us sensing our environments, the body's physiologic functions and some voluntary actions. Even though ion signaling is crucial for our existence and that of other organisms, maintaining optimal cellular ion concentrations is difficult given the ion-impermeable lipid bilayers that surround cells.

To traverse this barrier, cells have proteins embedded in these lipid bilayers to traffic ions across membranes. The three common classes of ion transport proteins are transporters, adenosine triphosphate (ATP)-powered pumps (ATPases) and ion channels [4] which can be in membranes of the cell and/or a cell's internal organelles. These transport proteins play an important role in controlling the timing and direction of ion transport and ultimately, ion signaling. Following the appropriate signals, transport proteins can determine how fast an ion is transported and for how long. Additionally, each ion has an electrochemical potential or driving force [5] determining how hard it is to add more of that ion to a particular space. This results in transport proteins either working with or working against the ionic driving forces. Therefore, cells must also regulate the

transport proteins. With proper regulation, each transport protein plays distinct but instrumental roles that at times can even be collaborative.

## **1.1 Ion transport proteins**

### **1.1.1 Transporters**

Transporters, sometimes referred to as carriers, move a variety of ions across the membrane [4]. Transporters are classified into three groups: uniporters, symporters and antiporters. Uniporters transport a single molecule such as glucose or amino acids down their concentration gradient [4]. By contrast, symporters and antiporters couple the movement of one type of ion or molecule against its concentration gradient with the transport of a different ion down its concentration gradient [4]. The couplings of different ion transports can happen in the same direction as is observed in symporters or it can happen the in the opposite direction as is observed in antiporters [4]. An example of this family of proteins include ATP-binding cassette (ABC) transport proteins such as the multidrug resistance permeability glycoprotein 1 (PGY1) known to confer resistance to a hydrophobic cancer treatment drug in tumor cells [6].

### **1.1.2 ATP-powered pumps (ATPases)**

ATPases use the energy derived from the hydrolysis of ATP to move ions or small molecules across membranes against their concentration gradients and/or electrical potentials [4]. Similar to antiporters and symporters, ATPases conduct coupled transport in that they

simultaneously hydrolyze ATP into adenosine diphosphate (ADP) with ion transport [4]. However, ATPases rely on ATP hydrolysis for energy whereas antiporters and symporters rely on the electrochemical gradient of the ions being transported [4]. Examples of this class of proteins include the gastric  $H^+/K^+$ -ATPase that maintains intestine acidity levels [7] or the sarcoendoplasmic reticulum  $Ca^{2+}$ -ATPase (SERCA) known to transport  $Ca^{2+}$  from the sarcoendoplasmic reticulum cytosol to the lumen in myocytes [8].

### **1.1.3 Ion channels**

Ion channels transport ions down their electrochemical gradients. Channels are precisely embedded in the membrane to create a hydrophilic pore that allows the rapid movement of ions [4]. Some channels are kept open more regularly than others whereas other ion channels require a signal that is either electrical or chemical for the channel to open its pore and allow ion movement [4]. The opening and closing of ion channels is referred to as gating. The ability of an electrical or chemical signal to open an ion channel makes that channel gated by that signal. For example an ion channel opened by changes in voltage is referred to as voltage gated and an ion channel opened by a ligand binding is called ligand gated [9]. Upon signal induction, ion channel kinetics are 1,000,000 times faster than ATPases or transporters [10]. They can transport many ions after receiving a single signal. Interestingly, many now think of ion channels and transporters as quite similar and only distinguished by their kinetics [11]. Ion channels are able to function because transporters (as well as ATPases) create the concentration gradients driving ions through open channels [12]. Whether the ion channels are voltage-gated, ligand-gated, stretch- or heat-activated [12], ion channels are not just essential for physiologic function, they are the spark of life. They are working even at this very moment to generate the electrical signals needed to get through this

page-turner from having relayed the idea of turning the page to the muscle movement used to accomplish this task. An example star player of this class of proteins is TransMEMbrane member 16A (TMEM16A), a widely expressed Cl<sup>-</sup> channel that we cannot live without, and the channel I will discuss in this dissertation.

## **1.2 TMEM16A discovery, physiology and structure-function**

### **1.2.1 Importance of TMEM16A in physiology**

TMEM16A is an evolutionarily conserved ion channel expressed in many cell types. Species including the zebrafish *Danio rerio*, armadillo *Dasypus novemcinctus*, African clawed frog *Xenopus laevis*, and humans *Homo sapiens* have TMEM16A. TMEM16A is widely expressed in different cell types including smooth muscle cells of the cardiovascular system [13], dorsal root ganglion (DRG) neurons [14], airway epithelial cells [15] and renal epithelial cells [16]. In each of these cells, TMEM16A plays a fundamental role in the physiologic processes carried out by these cells.

In the cardiovascular system, TMEM16A regulates vascular smooth muscle tone [13, 17]. Because vascular tone determines blood vessel caliber, a healthy cardiovascular system requires properly functioning TMEM16A channels. Properly functioning TMEM16A channels enable blood vessels that are constantly undergoing series of vasoconstrictions and vasodilations to respond to our physiological needs such as a fight or flight response with controlled opening and closing of TMEM16A [17]. However, when TMEM16A channels are constitutively open this causes excessive vasoconstriction (Figure 1-1A). Excessive vasoconstriction or hypertension is

itself a gateway and a mortality increasing factor for other cardiovascular diseases such as coronary heart disease and stroke [18]. Therefore, properly functioning TMEM16A protects us against cardiovascular disease.

In DRG neurons, TMEM16A-conducted currents signal nociception. DRG neurons have a higher intracellular  $\text{Cl}^-$  concentration that helps maintain their resting potential at approximately -60 mV [19, 20]. Upon TMEM16A activation,  $\text{Cl}^-$  exits the neuron to depolarize the membrane to approximately -20 mV (Figure 1-1B). [20]. This depolarization by TMEM16A is thought to be stimulated by the signaling of the G-coupled protein receptor for the peptide bradykinin [21] whose signaling is triggered by pain upon heat or mechanical stimulation. Therefore, TMEM16A channels play a protective role in inflammatory responses.

TMEM16A is also protective against inflammatory airway diseases. In tracheal and bronchial epithelia, TMEM16A supports the  $\text{Cl}^-$  secretion necessary for basal mucosal regulation (Figure 1-1C) [22]. In the absence of TMEM16A in such epithelial cells, mucous secretion is reduced [23]. Insufficient amounts of mucous leads to inflammatory airway diseases such as asthma and cystic fibrosis [24]. The mucous layer is maintained by the extracellular fluid or airway mucous serum which is a complex constituting mucins and glycoproteins, that kept at optimal levels, manage pH, cell permeability and inflammatory mediator response [24]. The levels of this extracellular fluid is in turn regulated by TMEM16A-conducted  $\text{Cl}^-$  [24]. When TMEM16A channels open,  $\text{Cl}^-$  concentration increases in the extracellular fluid. This increase in extracellular  $\text{Cl}^-$  upregulates mucous production and leads to the swelling of the mucous layer (Figure 1-1C). When TMEM16A channels close, the extracellular fluid decreases and this leads to a reduction in the mucous layer (Figure 1-1C). Interestingly, TMEM16A overexpression results in excessive

mucus secretion which can also be obstructive to the airway [25]. The role of TMEM16A in physiology described just touches the surface on the importance of TMEM16A.

TMEM16A regulates other proteins as well such as epidermal growth factor receptor (EGFR) [26]. TMEM16A promotes EGFR phosphorylation and activates EGFR signaling cascades [27]. The physiological importance for correct TMEM16A function cannot be underscored enough given not only its role in debilitating diseases, but its potential for therapy in these different diseases. TMEM16A could be a suitable target to treat the diseases associated with excessive vasoconstriction or inflammatory airways, however, a complete understanding of TMEM16A function and regulation is the first step toward achieving this goal.

### **1.2.2 TMEM16A discovery**

TMEM16A like other transmembrane member proteins was identified in the human genome project [28]. As suggested by its name, amino acid signatures within its sequence revealed that it was likely found in cellular membranes. Unbeknownst at the time, TMEM16A was already disease associated and called DOG1 (discovered on gastrointestinal stromal tumors protein 1) [29, 30], ORAOV2 (oral cancer overexpressed protein 2) [31], and TAOS2 (tumor-amplified and overexpressed sequence 2) [32].

Finally, in 2008, TMEM16A, the protein associated with cancer, was classified. Three independent labs characterized TMEM16A as a *bone fide*  $\text{Ca}^{2+}$ -activated  $\text{Cl}^-$  channel (CaCC) using three independent experimental approaches [33-35]. Notably, for about 20 years prior, scientists had known that proteins in some cell types could be activated by  $\text{Ca}^{2+}$  and result in  $\text{Cl}^-$  currents [36-39] (Figure 1-2). For example, human bronchial cells had been shown to conduct  $\text{Ca}^{2+}$ - activated  $\text{Cl}^-$  in response to interleukin [40] and *Xenopus laevis* eggs were also shown to

conduct  $\text{Ca}^{2+}$ - activated  $\text{Cl}^-$  currents in response to fertilization [41, 42]. As such, many sought to identify the channel conducting these currents.

To classify TMEM16A, Caputo et al. (2008) employed a global gene expression analysis of membrane proteins that took advantage of interleukin's ability to induce  $\text{Ca}^{2+}$ - activated  $\text{Cl}^-$  currents in bronchial epithelia cells. Using si-RNA against membrane protein hits, they uncovered that TMEM16A was responsible for conducting  $\text{Ca}^{2+}$ -activated  $\text{Cl}^-$  currents in bronchial epithelia cells [33]. Another group, Yang et al. (2008) scoured public databases for proteins with unknown functions with at least two transmembrane domains and wide tissue expression. TMEM16A fit these criteria. Upon identifying TMEM16A, they cloned and expressed mouse retinal TMEM16A in human embryonic kidney (HEK)293 cells and observed  $\text{Ca}^{2+}$ - activated  $\text{Cl}^-$  currents [35]. Lastly, Schroeder et al. (2008) applied an expression cloning approach where they injected the *X. laevis* oocyte total cDNA into axolotl oocytes that lack endogenous  $\text{Ca}^{2+}$ -activated  $\text{Cl}^-$  currents. Once they successfully measured  $\text{Ca}^{2+}$ -activated  $\text{Cl}^-$  currents in axolotl oocytes, they fractioned and subsectioned the *X. laevis* oocyte total cDNA until they identified the subsection that resulted in  $\text{Ca}^{2+}$ - activated  $\text{Cl}^-$  currents and then searched the public databases for the identity of TMEM16A [34]. Interestingly, in earlier studies TMEM16A was initially referred to as anoctamin 1 for being an anion channel predicted to have eight transmembrane domains [35]. Later studies would then return to calling it TMEM16A based on its classification as a transmembrane member protein of unknown function from the human genome project [43].

### **1.2.3 TMEM16A structure-function**

TMEM16A is presently described as a homodimer made of two subunits each with ten transmembrane domains [44-48]. Each subunit acts independently and contains a  $\text{Cl}^-$  conducting

pore and two  $\text{Ca}^{2+}$  binding pockets [44-47]. Interestingly, the two  $\text{Ca}^{2+}$  binding sites are embedded in the plasma membrane [44-46]. This unique quality of TMEM16A [45, 46] and some TMEM16 family members [44] is perhaps linked to its gating properties. When  $\text{Ca}^{2+}$  binds TMEM16A, this induces a conformational rearrangement that enables the  $\text{Cl}^-$  pore to open and allow  $\text{Cl}^-$  to pass through. Each  $\text{Ca}^{2+}$ -binding site in the TMEM16A channel can accommodate two  $\text{Ca}^{2+}$  and it appears as though the channel gates differently depending on whether one or two  $\text{Ca}^{2+}$  are bound [44-46].

The structure of TMEM16A is unlike other CaCCs such as bestrophin 1 (BEST1) (Figure 1-3). The  $\text{Ca}^{2+}$  binding sites of TMEM16A formed by amino acid E698, E701, E702 and E705 (mTMEM16A a, c and abc splice variants) are embedded in the plasma membrane [49, 50]. On the other hand, BEST1's  $\text{Ca}^{2+}$  binding sites formed by amino acids E300, D302 and D303 are located on the intracellular side where they form a  $\text{Ca}^{2+}$  clasp [51]. Additionally, TMEM16A structures have no identifiable pore, but BEST1 has a visible pore shown in the bottom-up view (Figure 1-3). Despite more than a decade of intensive studies, we are still uncovering the unique structure-function relationship of TMEM16A.

## **1.3 TMEM16A regulation**

### **1.3.1 Ion channel regulation**

In just a blink of an eye, the body must redirect most of a person's blood to the heart and vital organs for a fight or flight response ignited by a threat. TMEM16A channels must then cause vasoconstriction to force blood to vital organs following adrenaline release [17]. With such an

important role and many others unmentioned, a major question that arises is how TMEM16A channels know when it is appropriate to open and close to match our physiological needs. Therefore, I ask how is TMEM16A regulated? Remembering that excessive constriction is associated with hypertension, TMEM16A must have regulatory mechanisms in place. Even though it is known that TMEM16A is activated by  $\text{Ca}^{2+}$ , I am interested in determining how TMEM16A is regulated in the hope of targeting TMEM16A for therapy in conditions where TMEM16A is associated with disease.

Cells employ several mechanisms to regulate ion channels and therefore, their excitability. Ion channels can be regulated by ligand-binding, pressure changes, voltage fluxes, cellular volume changes, post-translational modifications, pH changes, protein interactions, protein degradation and fatty acid interactions [4]. The importance of each of these mechanisms to a channel's regulation depends on the physiological role of the channel. For example, the ligand gated ion channel gamma-aminobutyric acid type A ( $\text{GABA}_A$ ) requires the binding of the neurotransmitter GABA which binds an extracellular loop on the channel and activates  $\text{GABA}_A$  so that  $\text{Cl}^-$  flows into the cell and hyperpolarizes the neuron membrane [52] during a process such as learning [4]. This hyperpolarization inhibits glutamate signaling in the central nervous system (CNS) [52]. Tightly regulated  $\text{GABA}_A$  activity is required to enable correct CNS function. On the other hand, the  $\text{K}^+$  voltage gated inwardly rectifying ion channels (Kir1-7) are gated by the inner membrane abundant fatty acid phosphatidylinositol 4,5-bisphosphate ( $\text{PI}(4,5)\text{P}_2$ ), and depending on the Kir subfamily, the Kirs are either constitutively active, G protein-gated, ATP-sensitive or cellular metabolism-sensitive [53]. Once activated by changes in voltage, Kir channels allow  $\text{K}^+$  into the cell to repolarize cell membranes. A tight regulation of Kir is required to enable correct function in in the CNS, muscular system and neuromuscular system [54].

Kir channels and GABA<sub>A</sub> are just a few of the 285 known ion channels of the human genome whose mechanisms have been studied [55]. Learning how such ion channels are regulated has been instrumental in drug design. For example, by knowing that K<sup>+</sup> regulates the kidney's electrolyte and water balance, and influences blood pressure, a drug and a small molecule inhibitor (MK-7145) was designed to block Kir1.1. MK-7145 treats hypertension and heart failure [56, 57] but manifests symptoms of Bartter's syndrome [58]. Bartter's syndrome is an inheritable disease caused by a defect in the loop of Henle's thick ascending limb that causes hypokalemia or low potassium levels [58]. An ideal drug would not manifest Bartter's syndrome. Thus, it is important to understand the fine details of an ion channel's regulation. My goal is to characterize the signaling mechanisms regulating TMEM16A channels. Elucidating the regulatory mechanisms gating TMEM16A could result in effective therapeutic drugs for TMEM16A associated diseases and those of similar TMEM16 family whose regulation will be discussed next.

### **1.3.2 TMEM16 family regulation**

The mammalian TMEM16 family is composed of the ten members TMEM16A-K (excluding I) that share 37 to 77% sequence similarity to TMEM16A [59]. The regulation of TMEM16C-K excluding TMEM16F are poorly understood. TMEM16C, TMEM16D, TMEM16G and TMEM16K are phosphatidylserine scramblases lacking Ca<sup>2+</sup>-evoked Cl<sup>-</sup> currents [60]. TMEM16E, also known as GDD1 for its role in the bone-related late-onset disease gnathodiaphyseal dysplasia (GDD), does not conduct Ca<sup>2+</sup>-evoked Cl<sup>-</sup> currents nor does it show phosphatidylserine scramblase activity [61]. This might be due to TMEM16E's inability to traffic to the plasma membrane [61]. Similarly, TMEM16J does not localize to the plasma membrane and is instead located at plasma membrane-endoplasmic reticulum (ER) junctions where it acts as a

tether allowing for the ER  $\text{Ca}^{2+}$  sensor STIM1 and the plasma membrane  $\text{Ca}^{2+}$  influx channel Orai1 to form complexes at PI(4,5) $\text{P}_2$ -rich compartments [62].

TMEM16B and TMEM16F conduct ions at the plasma membrane. TMEM16B is the most similar to TMEM16A (Figure 1-4). Not only does it have the highest sequence similarity (77%), it is also a CaCC [63-66]. Thus, TMEM16B is activated by  $\text{Ca}^{2+}$  to enable the passage of  $\text{Cl}^-$  through its pore. It is expressed at the plasma membranes of retinal photoreceptors and olfactory sensory neurons [64, 66]. To date, studies determining how TMEM16B is gated have suggested that in addition to  $\text{Ca}^{2+}$ , TMEM16B gating is modulated by permeant anions and phosphatidyl 4,5-bisphosphate (PI(4,5) $\text{P}_2$ ) [67, 68]. The bigger and more permeant anion thiocyanate requires a lower concentration of  $\text{Ca}^{2+}$  to pass through TMEM16B channels than  $\text{Cl}^-$  does [67, 68]. The other component regulating TMEM16B gating, PI(4,5) $\text{P}_2$ , is a minor component at the plasma membrane and its water soluble analogue (diC8-PI(4,5) $\text{P}_2$ ) was shown to inhibit TMEM16B  $\text{Ca}^{2+}$ -evoked  $\text{Cl}^-$  currents when applied to TMEM16B channels expressed in HEK293 cells [68]. Conversely, depletion of PI(4,5) $\text{P}_2$  via the activation of the *Danio rerio* voltage sensing phosphatase (Dr-VSP) resulted in greater TMEM16B  $\text{Ca}^{2+}$ -evoked  $\text{Cl}^-$  currents [68].

TMEM16F is quite different from TMEM16A both in sequence and in activity (Figure 1-4 and Figure 1-5). Although our initial understanding of TMEM16A was based on the fungus *Nectria haematococca* TMEM16 (nhTMEM16) scramblase which was the first crystal structure purified for this family of proteins [44], TMEM16A and TMEM16F only share 56% sequence similarity. Nevertheless, from nhTMEM16, we learned that TMEM16A and other TMEM16 proteins share similar structure and have  $\text{Ca}^{2+}$  binding sites located in the plasma membrane [44]. Consistently, mutating TMEM16A  $\text{Ca}^{2+}$  binding sites based on nhTMEM16  $\text{Ca}^{2+}$  binding sites reduced TMEM16A  $\text{Ca}^{2+}$  sensitivity [44]. Additionally, TMEM16F also conducts ions although

whether it is a cation or anion conducting channel remains controversial. However, all agree that TMEM16F's scramblase and ion conduction are  $\text{Ca}^{2+}$ -dependent [69-72]. TMEM16F gating is also regulated by  $\text{PI}(4,5)\text{P}_2$  which is believed to interact with the residues involved in scrambling [73]. In contrast to TMEM16B,  $\text{diC8-PI}(4,5)\text{P}_2$  potentiates TMEM16F currents and the depletion of  $\text{PI}(4,5)\text{P}_2$  was shown to reduce TMEM16F  $\text{Ca}^{2+}$ -evoked currents [73].

### 1.3.3 TMEM16A gating

Using a combination of structural and regulatory information from the TMEM16 family, we have begun to understand how TMEM16A channel activity is finely tuned. Based on the similarities TMEM16A shares with TMEM16B and TMEM16F, it is possible TMEM16A binds  $\text{PI}(4,5)\text{P}_2$  similarly to TMEM16B and TMEM16F. Previous studies suggest that TMEM16A gating is influenced by alternative splicing [74], volume [74, 75], acid [76], cholesterol [77, 78], heat [79], and phosphoinositides [80-83]. My aim was to characterize physiologically relevant modulators of TMEM16A. Taken together, previous studies indicate that  $\text{Ca}^{2+}$  is necessary to evoke TMEM16A-conducted  $\text{Cl}^-$  currents. However,  $\text{Ca}^{2+}$  is a widely utilized signaling molecule involved in diverse signaling cascades separate from TMEM16A. This puts into question how TMEM16A channels are regulated to ensure that they are only activated when needed. Therefore, I sought to determine the signaling mechanisms that alter TMEM16A gating. To address my aims, I used the endogenous *Xenopus laevis* TMEM16A channels to study its regulation.

TMEM16A structures have provided important clues about TMEM16A gating. Firstly, cryogenic electron microscopy (Cryo-EM) findings supported the general architecture of TMEM16A extrapolated from the nhTMEM16 crystal structure suggesting that indeed it is much like the nhTMEM16 scramblase but contains differences in the ion pore [7]. Second, Cryo-EM

focused on the ion conduction pore revealed the unique coupling of  $\text{Ca}^{2+}$  binding to pore opening [46]. Bound  $\text{Ca}^{2+}$  alters the electrostatic properties of the pore conduction pathway by triggering a rearrangement of  $\alpha$ -helix six or transmembrane 6 (TM6) [46]. Thirdly, nanodiscs obtained via single-particle electron cryo-microscopy revealed that not only is each monomer capable of binding two  $\text{Ca}^{2+}$ , but that in this state, the TMEM16A pore is closed [45], hinting that an additional component is required to open the  $\text{Cl}^-$  pore.

Functional studies have also provided important clues for TMEM16A gating. First, recordings of the  $\text{Ca}^{2+}$ -evoked  $\text{Cl}^-$  currents under conditions distinguishing each subunit of the dimer suggest that TMEM16A subunits activate independently of each other [47]. Mutations inhibiting an individual pore in one subunit did not reduce the conduction of the second subunit's  $\text{Cl}^-$  pore suggesting that the  $\text{Cl}^-$  pores also open independently of each other [48]. Second, TMEM16A gating properties dependent on  $\text{Ca}^{2+}$ , anion type and voltage are conferred by the  $\alpha$ -helix on TM6 [71]. This is explained by the idea that some residues contributing to the putative  $\text{Cl}^-$  pore and  $\text{Ca}^{2+}$ -binding site are located on TM6. Lastly, TMEM16A occupies different conformational states based on whether one or two  $\text{Ca}^{2+}$  bind each subunit (Figure 1-6) [44-46]. Taken together, these functional studies report that TMEM16A gating is regulated by  $\text{Ca}^{2+}$  whose occupancy on the dimer is required to open its pores. However, structural studies with complete  $\text{Ca}^{2+}$  occupancy reveal that TMEM16A channels are closed which gives rise to the hypothesis that additional cellular components, perhaps similar to those regulating TMEM16B and TMEM16F gating, are required to open TMEM16A.

## **1.4 *Xenopus laevis* oocytes as a model for TMEM16A studies**

Oocytes from the African clawed frog, *Xenopus laevis*, are a classic model cell for electrophysiologists. The oocytes, arrested in prophase I, are an excellent expression system that has been used by biophysicists to study ion channel function and regulation for decades [83-86].

The primary strength of the *X. laevis* oocytes for the purpose of my studies is that TMEM16A is endogenously and abundantly expressed in these cells [34]. Additionally, these oocytes provide a native environment to identify how TMEM16A gating is regulated. Notably, previous studies investigating TMEM16A regulation in exogenous systems have resulted in conflicting findings [81, 87].

Other benefits of the *X. laevis* model that make using them ideal for ion channel studies are as follows: 1) thousands of oocytes can be obtained surgically, 2) these oocytes are large (1.2-1.3 mm in diameter), and 3) they can easily be injected with cRNA to exogenously express desired proteins [88, 89]. In summary, *X. laevis* oocytes have been instrumental in the study of diverse ion channels and are one of the model cells used in the classification of TMEM16A as a CaCC.

## **1.5 Dissertation aims**

Although TMEM16A was classified as a CaCC in 2008 and structures have been resolved revealing information about the channel, TMEM16A's regulation has remained unclear. In particular, the components necessary for the channel to open are only beginning to be understood. Two aims of my dissertation were to uncover the signaling mechanism

mediating TMEM16A gating including: 1) the PI(4,5)P<sub>2</sub> regulation of TMEM16A, and 2) the multimodal Ca<sup>2+</sup> regulation of TMEM16A. The first of these aims was published in the Journal of Biological Chemistry and is described in chapter 3 [90]. The second of these aims will be submitted for publication also to Journal of Biological Chemistry and is described in chapter 4.

## **1.6 Figures**

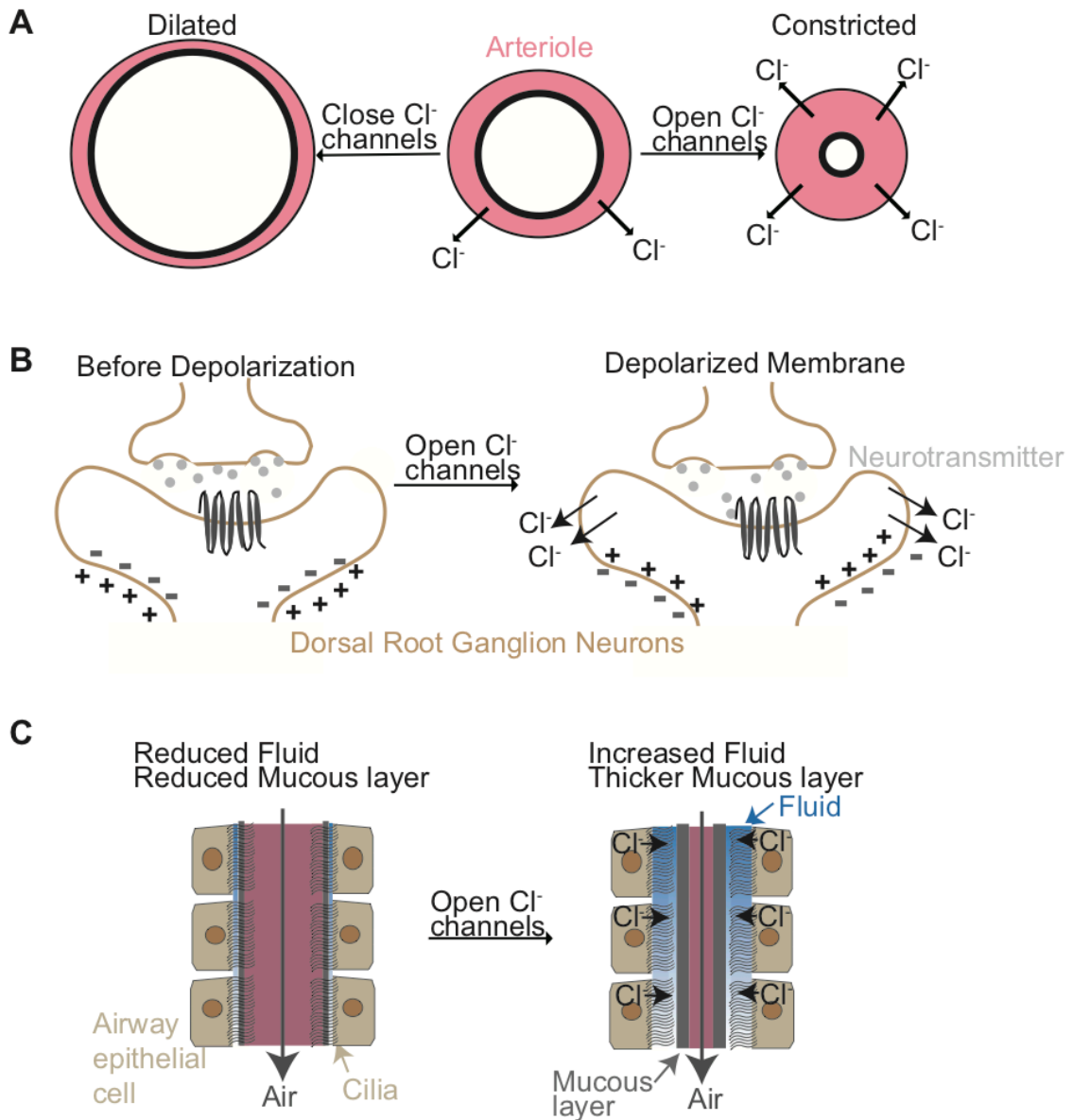


**Figure 1-1. TMEM16A's role in physiology**

TMEM16A is expressed in multiple cell types including A) smooth muscle, B) dorsal root ganglion (DRG) neurons and C) airway epithelial. A) In smooth muscle cells, TMEM16A channels open to constrict vessels and close to dilate them. B) In DRG neurons, TMEM16A channels open and result in the membrane depolarizing (firing) or becoming more positively charged following a stimulatory signal such as pain. C) In airway epithelial cells, the airway is kept moist by fluid that regulates the mucous layer. Opening TMEM16A channels dispenses Cl<sup>-</sup> into the fluid cavity and this causes water to flow into the cavity and increase fluid. This increase in fluid is necessary to maintain healthy and protective mucous levels.

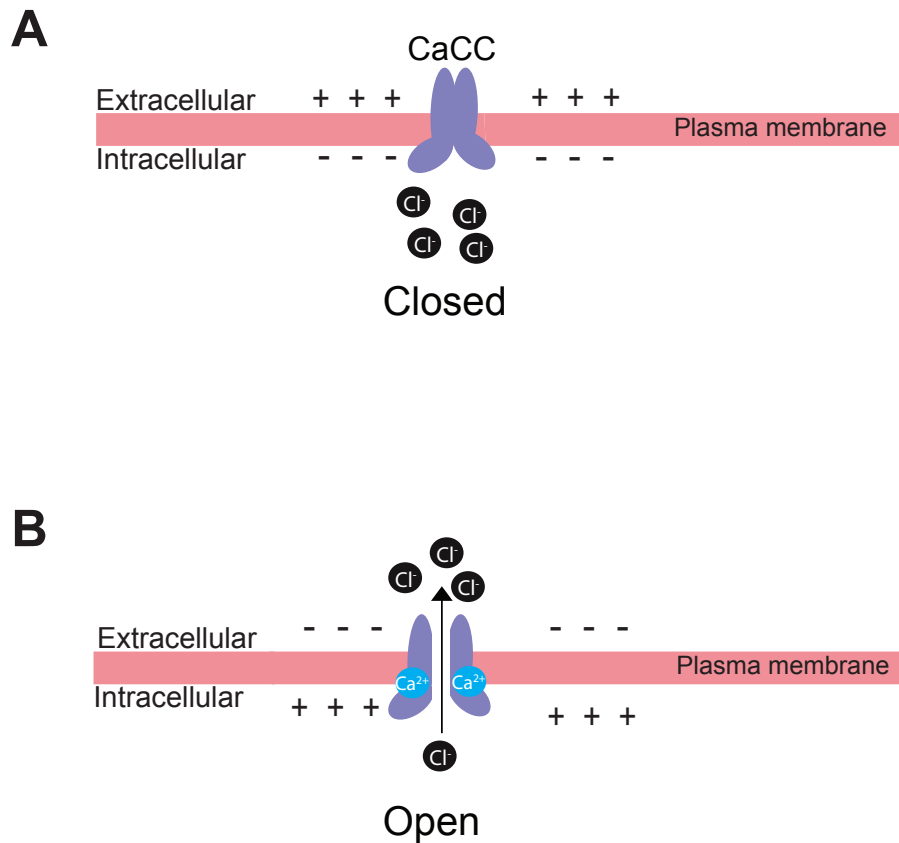


**Figure 1-2. Schematic depicting the activation of a Ca<sup>2+</sup>-activated Cl<sup>-</sup> channel (CaCC)**

CaCCs are embedded in the plasma membrane. (A) In the absence of Ca<sup>2+</sup>, CaCCs remain closed and the membrane potential is negative. (B) Upon an increase in intracellular Ca<sup>2+</sup>, Ca<sup>2+</sup> binds the CaCC Ca<sup>2+</sup> binding sites, enabling the Cl<sup>-</sup> pore to open. The open pore then allows the passage of Cl<sup>-</sup> and results in the membrane depolarizing.

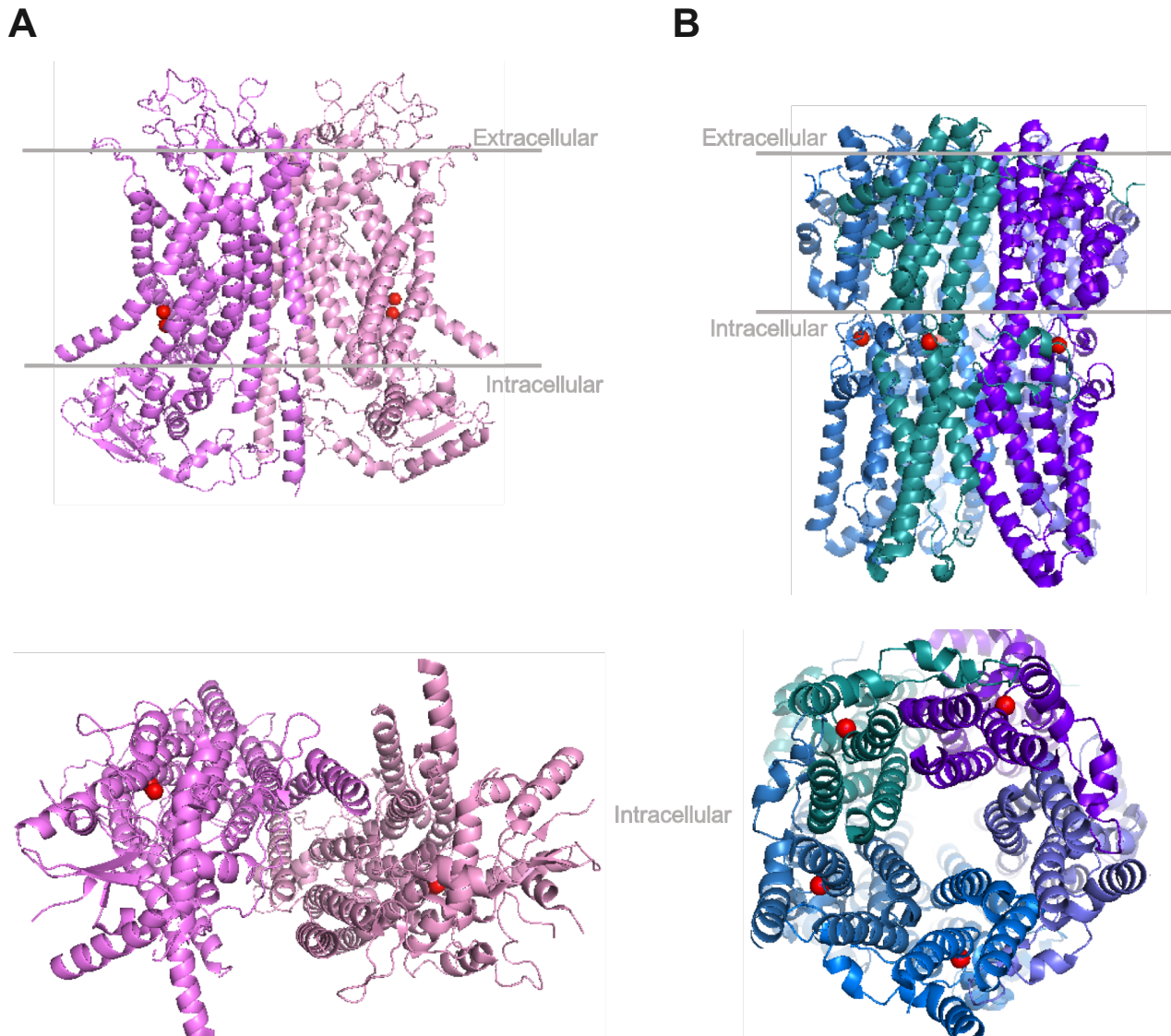


**Figure 1-3. Homology model of mouse TMEM16A and structure of chicken Bestrophin 1**

(A) TMEM16A (PDB:5OYB) consists of two identical subunits embedded in the membrane indicated by the lines. Each TMEM16A subunit has ten transmembrane domains, and an ion conduction pore which to date has not been resolved clearly. Notably, each subunit has two Ca<sup>2+</sup> binding sites embedded in the membrane. (B) Bestrophin 1 (BEST1) (PDB: 6N25) is made of five identical subunits spanning the membrane four times each. The subunits are arranged to form a central ion conduction pore which opens when Ca<sup>2+</sup> binds its intracellular sites found on each subunit. BEST1's Ca<sup>2+</sup> binding sites are not embedded in the membrane like TMEM16A's but are instead found on the intracellular side of the cell. Red spheres represent Ca<sup>2+</sup>.

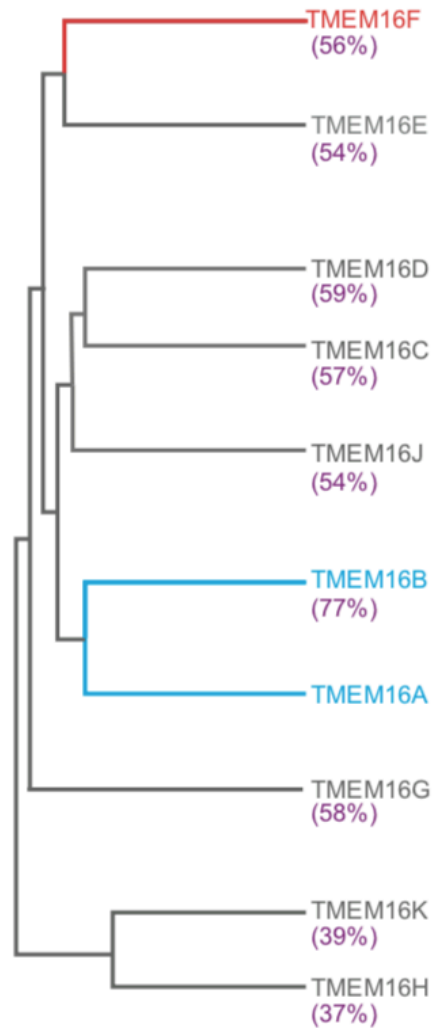


**Figure 1-4. Human TMEM16 family phylogenetic tree**

TMEM16A is just one of ten proteins in the TMEM16 family predicted to be ion channels or scramblases. TMEM16A is most closely related and similar to TMEM16B (blue) (77%). Colored grey are the family members whose functions remain to be understood. Although TMEM16F (orange) is not the most similar to TMEM16A (56%), its structural information has been instrumental in learning about TMEM16A. Percentages show similarity to TMEM16A. Blue shows CaCCs. Red shows channel/scramblase. The phylogenetic tree was generated using software : Dendroscope [91].

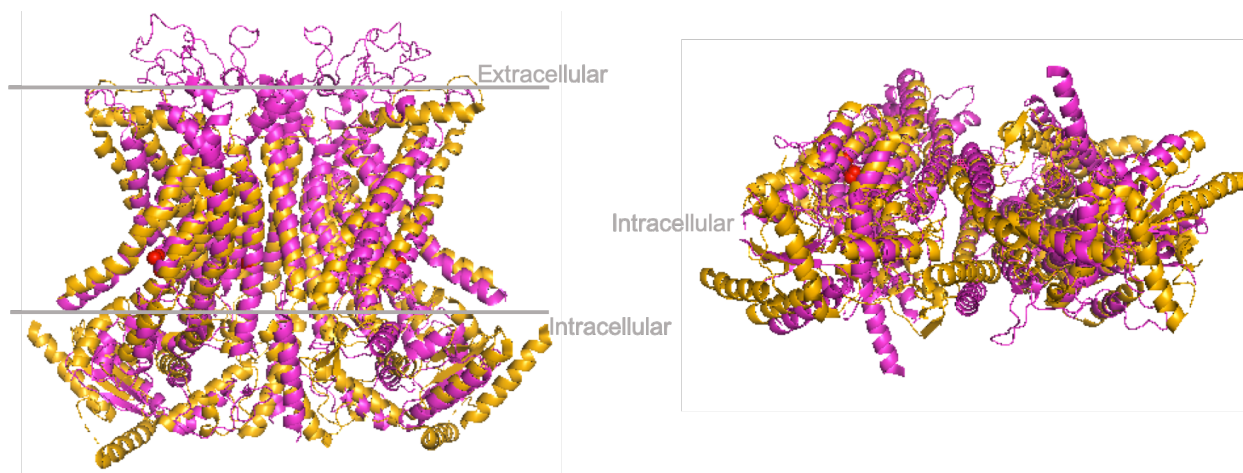


**Figure 1-5. Homology model of mouse TMEM16A aligned with *Nectria haematococca* TMEM16**

The scramblase nhTMEM16 (PDB: 6QM5) crystal structure (orange) was obtained in 2014. nhTMEM16 aligns closely with mouse mTMEM16A (magenta) and has been used to provide information about TMEM16A as previously discussed. Like TMEM16A, nhTMEM16 can bind four  $\text{Ca}^{2+}$  in similar regions as TMEM16A. However, some differences in structural arrangement can be seen as depicted in the bottom-up view or intracellular side (right).

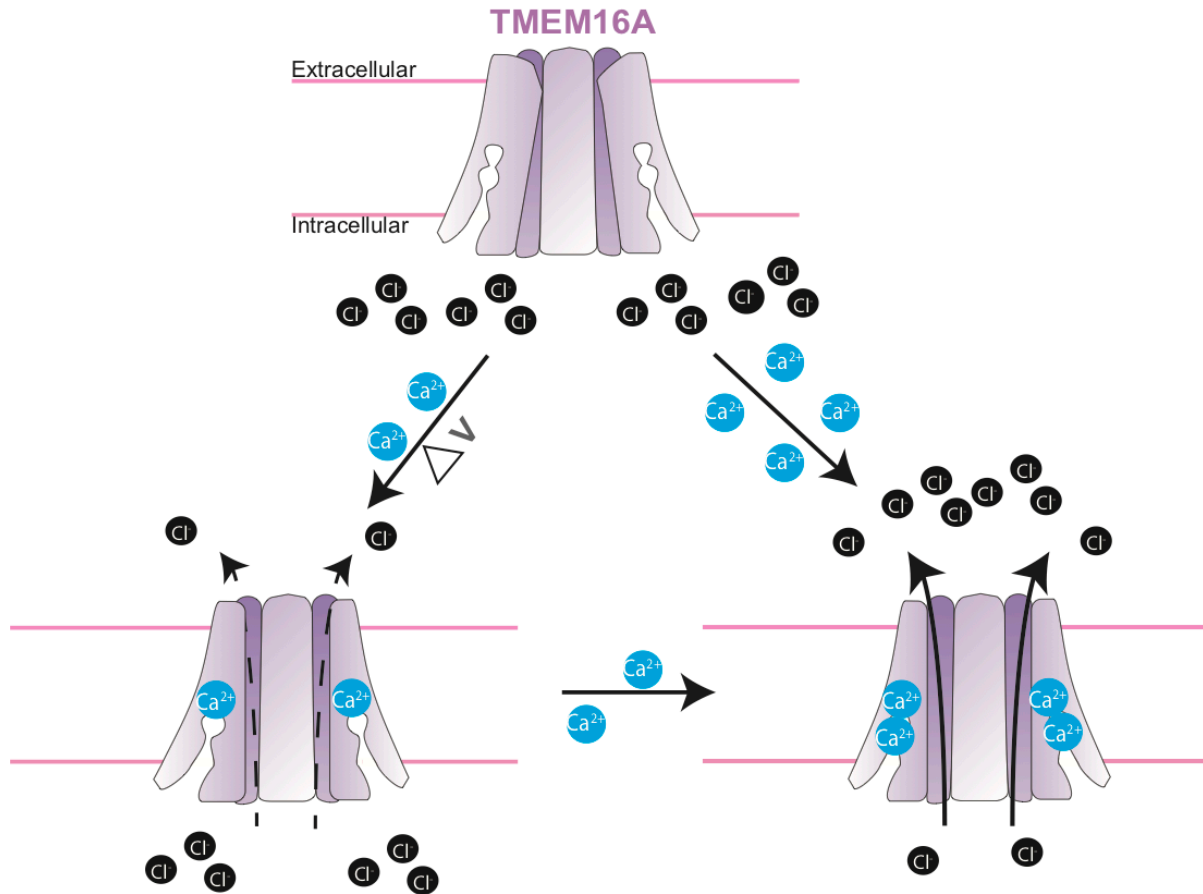


**Figure 1-6. Schematic depicting TMEM16A gating**

TMEM16A gating depends on the presence of Ca<sup>2+</sup> and voltage. At low concentrations of Ca<sup>2+</sup> where not all Ca<sup>2+</sup> binding sites are occupied, TMEM16A channels can allow Cl<sup>-</sup> passage in a voltage dependent manner. At high concentrations of Ca<sup>2+</sup> where most Ca<sup>2+</sup> binding sites are occupied, TMEM16A Cl<sup>-</sup> conductance does not depend on voltage and allows continuous Cl<sup>-</sup> passage.

## 2.0 Materials and Methods

### 2.1 Reagents

Diocanoyl phosphatidylinositol (diC8-PI), dioctanoyl 3-monophosphate diC8-PI(3)P, dioctanoyl 4-monophosphate diC8-PI(4)P, dioctanoyl 5-monophosphate diC8-PI(5)P, dioctanoyl phosphatidylinositol 3,4-bisphosphate (diC8-PI(3,4)P<sub>2</sub>), dioctanoyl phosphatidylinositol 4,5-bisphosphate (diC8-PI(4,5)P<sub>2</sub>), dioctanoyl phosphatidylinositol 3,5-bisphosphate (diC8-PI(3,5)P<sub>2</sub>), dioctanoyl phosphatidylinositol 3,4,5-trisphosphate (diC8-PIP<sub>3</sub>) and anti-phosphatidylinositol 4,5-bisphosphate IgM (anti-PI(4,5)P<sub>2</sub>; Echelon Cat#:Z-P045, Lot#: 080416) were obtained from Echelon Biosciences. MgCl<sub>2</sub>, CaCl<sub>2</sub> and NiCl<sub>2</sub> were purchased from Sigma-Aldrich. U-73343 and U-73122 were purchased from Tocris. Unless otherwise noted, all other reagents were purchased from Thermo Fisher Scientific.

### 2.2 Solutions

#### 2.2.1 Oocyte wash and storage solution

Oocyte wash and storage solution were made as follows: Oocyte Ringers 2 (OR2) (in mM): 82.5 NaCl, 2.5 KCl, 1 MgCl<sub>2</sub>, and 5 mM HEPES, pH 7.2. ND96 (in mM): supplemented with 5 mM sodium pyruvate and 100 mg/L gentamycin, pH 7.6 and filtered with a sterile, 0.2 µm polystyrene filter [92].

### 2.2.2 Inside-out patch clamp solutions

All excised inside-out patch clamp recordings were made in HEPES-buffered saline solution (in mM): 130 NaCl and 3 HEPES, pH 7.2, and filtered using a sterile, 0.2  $\mu\text{m}$  polystyrene filter. For  $\text{Ca}^{2+}$ -free recordings, this solution was supplemented with 200  $\mu\text{M}$  EGTA. For solutions used during  $\text{Ca}^{2+}$  application, the HEPES-buffered saline solution was supplemented with 100  $\mu\text{M}$  or 500  $\mu\text{M}$  or 2 mM  $\text{CaCl}_2$ . Where indicated 2 mM  $\text{CaCl}_2$  was substituted with 2 mM  $\text{NiCl}_2$  or  $\text{MgCl}_2$ .

## 2.3 Animals

Animal procedures were conducted using accepted standards of humane animal care and approved by the Animal Care and Use Committee at the University of Pittsburgh. *X. laevis* adult, oocyte-positive females were obtained commercially (RRID: NXR\_0.0031, NASCO, Fort Atkinson, WI) and housed at 18 °C with 12/12-hour light/dark cycle. Oocytes were collected from *X. laevis* females anesthetized by immersion in 1.0 g/L tricaine pH 7.4, for 30 minutes. Ovarian sacs containing the oocytes were surgically removed from the female, manually pulled apart, and incubated for 90 minutes in 1 mg/ml collagenase diluted in ND96 solution. Collagenase was removed by several OR2 rinses, and healthy oocytes were stored at 14°C in ND96 for up to 14 days.

## 2.4 Experimental methods

### 2.4.1 Inside-out patch clamp

Patch clamp recordings were made on *X. laevis* oocytes following the manual removal of the vitelline membrane. Current recordings were made in the excised inside-out configuration of the patch clamp technique with an EPC-10 USB patch clamp amplifier (HEKA Elektronik) [93]. Briefly, after formation of a gigaseal (greater than 1 G $\Omega$ ) on the oocyte membrane, inside-out patches were excised in HEPES-buffered saline solution without EGTA (where resistances decreased to 10-200 M $\Omega$  in solutions lacking EGTA but returned to at least 1 G $\Omega$  with EGTA application). Data were collected at a rate of 10 kHz. Glass pipettes were pulled from borosilicate glass (OD 1.5 mm, ID 0.86 mm; Warner Instruments), fire polished (Narshige microforge), and had a resistance of 0.4-1.5 M $\Omega$ . Lipids were applied to excised inside-out patches in a RC-28 chamber (Warner Instruments). All other solutions were applied using a VC-8 fast perfusion system (Warner Instruments). All inside-out patch recordings were initiated within 10 s of patch excision.

## 2.5 Quantification and statistical analysis

### 2.5.1 Inside-out patch data analysis

Currents recorded in the inside-out patch configuration were normalized for analysis such that peak currents recorded in Ca<sup>2+</sup> (or Ni<sup>2+</sup>) were equated to 1 and basal currents recorded in Ca<sup>2+</sup>- or divalent-free conditions were equated to 0.

Controls are plotted with dashed lines and represent an idealized averaged normalized current versus time calculated using the single exponential equation:

$$Y(x) = Y_0 \times e^{-\frac{x}{\tau}}$$

where Y(x), Y<sub>0</sub>, x, and τ represent the current at time x, initial current, time, and rate of current rundown, respectively. Briefly, current traces were collected and fitted with the single exponential equation above to derive the Y<sub>0</sub>, x, and τ per trace. For the Ca<sup>2+</sup> control and otherwise indicated control conditions, averaged plots of current rundown were plotted along with the normalized current versus time graphs and depicted as the predicted current traces displayed as dashed lines.

Analyzed kinetics data are displayed in Tukey box plot distributions where the box depicts 25-75% of the data range, the central line represents the median value and the whiskers span 10-90%. Additionally, to simplify comparison between the kinetics of current rundown recorded under experimental conditions to controls, the normalized current for each condition is plotted together with the averaged rundown for associated control either the 2 mM Ca<sup>2+</sup> or the indicated control.

To compare the magnitude of current recovered using the synthetic lipid analogs the fold change in current recovered was calculated by dividing the peak current after lipid addition by

baseline current. The peak current was defined as the maximum current recorded after lipid addition and the baseline current was defined as the steady-state current observed at the time of lipid addition. The equation used was:

$$\textit{Current recovered} = \frac{\textit{maximum current after lipid addition}}{\textit{baseline current at lipid addition}}$$

The baseline current was normalized to 1. All experiments include trials conducted on multiple days with oocytes collected from different females.

Two-tailed ANOVAs were used to assess differences between experiment conditions, followed by post-hoc t-tests to evaluate differences between particular experimental treatments.

## 2.6 Figures

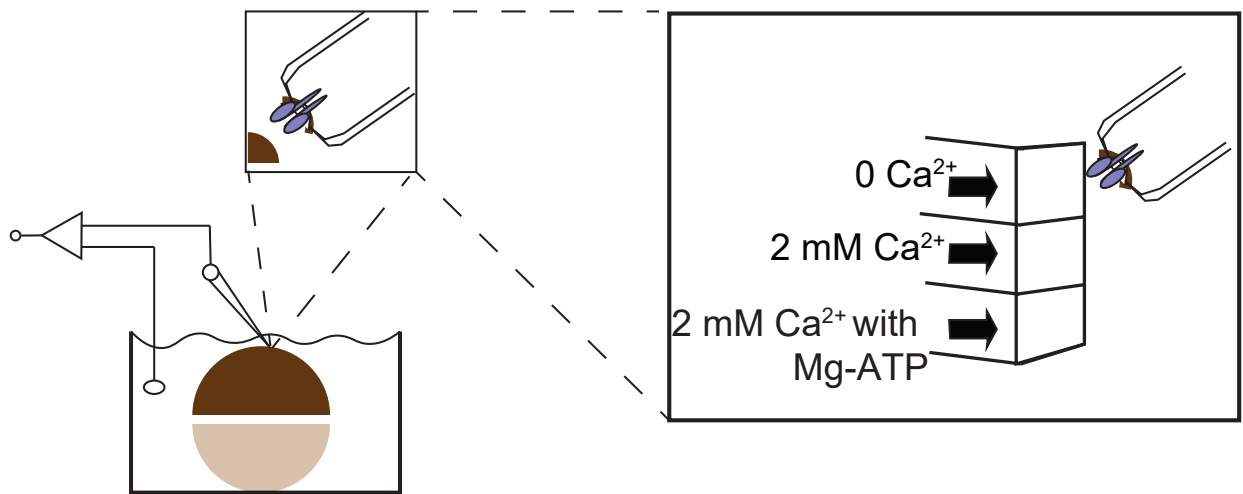


**Figure 2-1. Inside-out patch clamp technique**

Schematic of recordings made in the inside-out patch clamp configuration. A *Xenopus laevis* oocyte is placed in a bath solution lacking Ca<sup>2+</sup>. Two electrodes are also placed in the bath solution; one is a reference electrode and completes the circuit and the other is attached to a glass pipette for current recording. The glass pipette is placed on the oocyte membrane and suction is applied to pull a patch of membrane and form a GΩ seal, an indication that the pipette and the membrane are continuous. After formation of a seal, the pipette is slowly moved away from the oocyte to expose the membrane's intracellular side to the bath solution [94]. Next, the patch is placed at the rapid perfusion chamber where different solutions are applied while Cl<sup>-</sup> passage (current) through the patch is recorded.

### 3.0 TMEM16A Gating is Regulated by PI(4,5)P<sub>2</sub>

This chapter is an adaptation of the published article: © 2019 Tembo et al. [92] published the Journal of Biological Chemistry <https://doi.org/10.1074/jbc.RA118.007128>

#### 3.1 Introduction

TMEM16A is essential for diverse physiological processes such as smooth muscle contraction [95-97] and signal transduction [98, 99]. Disrupting TMEM16A function has serious implications exemplified by the perinatal lethality phenotype in TMEM16A-null mice [100]. Yet, how TMEM16A is functionally regulated is not well understood. As a key mediator in multiple physiological processes, this channel could be a target for novel therapeutics to treat chronic conditions such as hypertension.

Determining how TMEM16A controls physiological processes requires a more nuanced understanding of how cellular events and second messengers alter TMEM16A channel gating. To date, TMEM16A is known to be activated by elevated intracellular Ca<sup>2+</sup> which binds to a membrane-embedded domain located near a Cl<sup>-</sup> conducting pore [33-35, 45-48, 101]. The binding of Ca<sup>2+</sup> to its cognate domain on TMEM16A induces a conformational rearrangement of the  $\alpha$ -helix on TM6 that physically opens the anion conducting pore [46]. Each Ca<sup>2+</sup>-binding site on the TMEM16A channel can accommodate two Ca<sup>2+</sup> cations, and it appears as though the channel gates differently depending on whether one or two cations are bound [47, 48, 71]. Intriguingly, the recent cryo-EM structures of TMEM16A in a Ca<sup>2+</sup>-bound state revealed that the anion pore was not wide

enough for Cl<sup>-</sup> permeation suggesting that Ca<sup>2+</sup> alone is not sufficient to activate TMEM16A channels [45, 46]. Another signaling molecule that may regulate TMEM16A is the acidic phospholipid phosphatidyl 4,5-bisphosphate (PI(4,5)P<sub>2</sub>) [68, 71, 78, 81].

PI(4,5)P<sub>2</sub> is a minor component of the membrane (Figure 3-1), yet it is a master regulator of membrane function [102]. Importantly, PI(4,5)P<sub>2</sub> serves as the substrate for phospholipase C (PLC) cleavage to produce inositol triphosphate (IP<sub>3</sub>) and diacylglycerol (DAG); pathways that transduce extracellular signals to intracellular signaling events. However, PI(4,5)P<sub>2</sub> also serves as a signaling molecule in its own right by regulating endocytosis and exocytosis, actin polymerization, establishment of basolateral polarity, and regulation of ion channels [103]. A possible role for PI(4,5)P<sub>2</sub> in TMEM16A regulation has already been explored by other groups, however, the interpretation of how PI(4,5)P<sub>2</sub> alters TMEM16A currents remains disputed: one study reported that PI(4,5)P<sub>2</sub> inhibits TMEM16A [75], another states that it does not regulate the channel [98], and yet two others indicate that PI(4,5)P<sub>2</sub> promotes TMEM16A activity [68, 78, 81, 104]. I speculate that the disparity between the experimental interpretations may stem from the use of indirect methods.

The objective of this research was to determine whether the phospholipid PI(4,5)P<sub>2</sub> regulates TMEM16A channels. For these experiments, I made electrophysiology recordings from *Xenopus laevis* oocytes, cells that endogenously and abundantly express TMEM16A channels [34]. Using excised inside-out patch clamp together with methods that directly alter the available PI(4,5)P<sub>2</sub> content of the patch, I found that TMEM16A currents decayed following patch excision. By changing the available PI(4,5)P<sub>2</sub> content, I altered the kinetics of this rundown. Moreover, depleting the membrane PI(4,5)P<sub>2</sub> rendered TMEM16A channels unable to conduct current even

in saturating concentrations of intracellular  $\text{Ca}^{2+}$ . Together these findings establish that TMEM16A channels are potentiated by PI(4,5)P<sub>2</sub>.

## 3.2 Results

### 3.2.1 TMEM16A currents recorded from excised inside-out patches decay

To study TMEM16A currents, I made recordings of the endogenous channel in *X. laevis* oocytes using the inside-out configuration of the patch clamp technique. Notably, the prominent  $\text{Ca}^{2+}$ -activated current recorded from these cells is conducted by TMEM16A channels [34]. During 100-150 ms steps to -60 and +60 mV, I observed robust,  $\text{Ca}^{2+}$ -activated TMEM16A currents at both voltages (Figure 3-2A). Surprisingly, these currents decayed over time despite the continued presence of a saturating concentration of intracellular  $\text{Ca}^{2+}$  [45]. Figure 3-2A depicts typical currents recorded at -60 and +60 mV, at 30, 60, 120, and 180 s following 2 mM  $\text{Ca}^{2+}$  application. Loss of current from excised patches is a phenomenon known as *rundown* [105]. This can be observed also in Figure 3-2B depicting typical currents normalized to the highest currents recorded at -60 and +60 mV over time. I next sought to characterize the rundown of TMEM16A-conducted currents after patch excision.

I first explored whether the rundown of TMEM16A currents was voltage dependent. To do so, plots of the currents recorded during steps to -60 mV or +60 mV, versus time, were fit with single exponential functions, and enabled me to quantify the kinetics of rundown (Equation 1) (Figure 3-2C). In 15 independent experimental trials, the average rate of rundown was  $68.9 \pm 7.1$

s at -60 mV, and  $63.8 \pm 5.9$  s at +60 mV (Table 3-1 and Figure 3-2D). Similar kinetics measured at the two voltages reveal that the current decay is voltage independent.

To explore a possible relationship between the rate of rundown and the number of channels in an excised patch, I plotted the rate of current decay recorded at -60 mV versus the peak steady state current (Figure 3-3). In 15 independent trials, I found that there was no apparent relationship between these two metrics. These data represent a negative control suggesting that TMEM16A currents ran down regardless of pipette size or the number of channels opened by  $\text{Ca}^{2+}$  across the different trials.

### 3.2.2 PI(4,5)P<sub>2</sub> recovered TMEM16A currents in inside-out excised patches

Rundown of currents recorded in the inside-out configuration of the patch clamp technique is characteristic of channels regulated by PI(4,5)P<sub>2</sub> [103]. I therefore hypothesized that if TMEM16A current rundown occurred due to the depletion of PI(4,5)P<sub>2</sub> in excised patches, exogenous PI(4,5)P<sub>2</sub> application should recover TMEM16A currents following their decay. To test this hypothesis, I applied a water-soluble analog of PI(4,5)P<sub>2</sub> [106-109], dioctanoyl-PI(4,5)P<sub>2</sub> (diC8-PI(4,5)P<sub>2</sub>), to inside-out patches excised from *X. laevis* oocytes (Figure 3-4A). For these experiments, I recorded TMEM16A-conducted currents at -60 mV before and during the application of 2 mM  $\text{Ca}^{2+}$ . Once the  $\text{Ca}^{2+}$ -activated currents ran down to a steady state, I applied 100  $\mu\text{M}$  diC8-PI(4,5)P<sub>2</sub> [68] in the presence of 2 mM  $\text{Ca}^{2+}$ . Figure 3-4B depicts an example plot of TMEM16A-conducted currents recorded at -60 mV versus time, before and during 100  $\mu\text{M}$  diC8-PI(4,5)P<sub>2</sub> application in the presence of  $\text{Ca}^{2+}$ . In seven independent trials, I observed that 100  $\mu\text{M}$  diC8-PI(4,5)P<sub>2</sub> application recovered an average 38% of the peak current. Because I did not

observe full TMEM16A current recovery with 100  $\mu\text{M}$  diC8-PI(4,5)P<sub>2</sub>, I explored whether this was due to the short fatty acid tail or the concentration of diC8-PI(4,5)P<sub>2</sub> applied. I first conducted a similar experiment where I applied 100  $\mu\text{M}$  natural PI(4,5)P<sub>2</sub> (Figure 3-4C and D). Surprisingly, I observed that natural PI(4,5)P<sub>2</sub> recovered an average of 23% of the peak current, which was less than the current recovered by 100  $\mu\text{M}$  diC8-PI(4,5)P<sub>2</sub>. I proceeded with further experimentation only using the diC8-PI(4,5)P<sub>2</sub>. Next, I sought to estimate the concentration-response for diC8-PI(4,5)P<sub>2</sub>. I conducted additional TMEM16A current recovery experiments using 10  $\mu\text{M}$  diC8-PI(4,5)P<sub>2</sub> (Figure 3-4E) and 30  $\mu\text{M}$  diC8-PI(4,5)P<sub>2</sub> (Figure 3-4F). I observed that 10  $\mu\text{M}$  or 30  $\mu\text{M}$  diC8-PI(4,5)P<sub>2</sub> incompletely recovered the current compared to 100  $\mu\text{M}$  diC8-PI(4,5)P<sub>2</sub> (Figure 3-4G). Altogether, the data suggest that PI(4,5)P<sub>2</sub> recovers TMEM16A currents and that the currents are recovered in a concentration-dependent manner.

After demonstrating that PI(4,5)P<sub>2</sub> recovers TMEM16A currents, I sought to further characterize the relationship between PI(4,5)P<sub>2</sub> and TMEM16A. I tested whether 100  $\mu\text{M}$  diC8-PI(4,5)P<sub>2</sub> (Figure 3-5A) was sufficient to recover TMEM16A current following rundown, or if diC8-PI(4,5)P<sub>2</sub> and Ca<sup>2+</sup> were both required. Application of diC8-PI(4,5)P<sub>2</sub> in the absence of Ca<sup>2+</sup> had a nominal effect on TMEM16A, with a recovery of  $1.1 \pm 0.1$ -fold (N= 5, Figure 3-5B and C). These data demonstrate that although Ca<sup>2+</sup> activates TMEM16A, PI(4,5)P<sub>2</sub> is required for these channels to conduct Cl<sup>-</sup> currents. Moreover, PI(4,5)P<sub>2</sub> potentiates TMEM16A currents only in the presence of intracellular Ca<sup>2+</sup>.

The diC8-PI(4,5)P<sub>2</sub> compound could theoretically regulate TMEM16A channels by interactions mediated by its lipid tail group or its phosphoinositol head group (Figure 3-1). Thus, I tested the hypothesis that the dioctanoyl-phosphoinositol (diC8-PI) backbone (Figure 3-5A) alone was sufficient to recover current. Following TMEM16A current rundown, I applied 100  $\mu\text{M}$

diC8-PI with  $\text{Ca}^{2+}$  and quantified the proportion of current recovered. Figure 3-5D shows an example plot of TMEM16A currents recorded at -60 mV versus time, before and during diC8-PI application. In six separate trials, I observed that 100  $\mu\text{M}$  diC8-PI application nominally altered the TMEM16A currents, recovering  $1.4 \pm 0.2$ -fold current, which was significantly lower than the  $3.6 \pm 0.5$ -fold current recovered by diC8-PI(4,5) $\text{P}_2$  with  $\text{Ca}^{2+}$ , but not significantly different from the current recovered by diC8-PI(4,5) $\text{P}_2$  in the absence of  $\text{Ca}^{2+}$  (Figure 3-5B). This result demonstrates that without the phosphorylated head groups, diC8-PI was unable to recover TMEM16A currents, thereby suggesting that the phosphates on the inositol head-group mediate the TMEM16A-PI(4,5) $\text{P}_2$  interaction.

### **3.2.3 Scavenging PI(4,5) $\text{P}_2$ sped TMEM16A current rundown**

My finding that diC8-PI(4,5) $\text{P}_2$  restored TMEM16A currents following rundown suggested that rundown may be the result of PI(4,5) $\text{P}_2$  depletion in excised patches. Thus, I reasoned that I should be able to speed rundown by applying compounds that compete with TMEM16A for binding to PI(4,5) $\text{P}_2$ . I tested this hypothesis by quantifying the rate of TMEM16A current decay during application of two compounds known to scavenge PI(4,5) $\text{P}_2$ : a PI(4,5) $\text{P}_2$ -targeting antibody (anti-PI(4,5) $\text{P}_2$ ) [110] or neomycin [111, 112] (Figure 3-6A). I began these experiments by recording TMEM16A currents at -60 mV before and during treatment with 2 mM  $\text{Ca}^{2+}$  applied with 15  $\mu\text{g/ml}$  anti-PI(4,5) $\text{P}_2$ . In four independent trials, I observed that TMEM16A current ran down with an average rate of  $48.6 \pm 7.4$  s in the presence of anti-PI(4,5) $\text{P}_2$  compared to  $68.9 \pm 7.3$  s from patches treated with 2 mM  $\text{Ca}^{2+}$  alone (N = 15) (Figure 3-6B and C, Table 3-1).

In a parallel series of experiments, I quantified the rate of TMEM16A current rundown in the presence of the PI(4,5)P<sub>2</sub> scavenger neomycin. Neomycin is an antibiotic that also scavenges PI(4,5)P<sub>2</sub> when applied to the intracellular membrane at high concentrations [111]. Figure 3-5D depicts an example plot of the TMEM16A currents recorded at -60 mV versus time, before and during 2 mM Ca<sup>2+</sup> and 50 mM neomycin application. In five independent trials, neomycin sped current rundown from 68.9 ± 7.3 s to 32.0 ± 8.8 s (Figure 3-6B).

Altogether, I observed that both anti-PI(4,5)P<sub>2</sub> and neomycin application sped TMEM16A rundown (Figure 3-6). Moreover, the rate of rundown was not significantly different in the presence of either anti-PI(4,5)P<sub>2</sub> or neomycin (Figure 3-6B and Table 3-1) consistent with the hypothesis that each compound was acting by scavenging PI(4,5)P<sub>2</sub> rather than exerting nonspecific effects on the channel. Together, these data support the hypothesis that PI(4,5)P<sub>2</sub> is required for TMEM16A to conduct Cl<sup>-</sup> currents.

### **3.2.4 Slowing PI(4,5)P<sub>2</sub> depletion slowed TMEM16A rundown**

Phosphatases and kinases work together to maintain stable levels of PI(4,5)P<sub>2</sub> in whole cells (Figure 3-7A) [102]. In excised patches, however, membrane-anchored kinases lack access to the ATP required to fuel phosphorylation and regeneration of PI(4,5)P<sub>2</sub> [102, 103]. Consequently, continued activity of phosphatases without counter-acting kinases leads to PI(4,5)P<sub>2</sub> dephosphorylation. I reasoned that if TMEM16A currents decayed in excised patches due to the dephosphorylation of PI(4,5)P<sub>2</sub>, then enabling rephosphorylation or inhibiting phosphatases should slow current loss. I tested the hypothesis by determining whether enabling rephosphorylation of PI(4,5)P<sub>2</sub> with application of magnesium-adenosine triphosphate (Mg-ATP) [113, 114] would slow TMEM16A current rundown in excised inside-out patches. As a control for

these experiments, I first recorded TMEM16A currents at -60 mV before and during the application of magnesium adenosine monophosphate (Mg-AMP), which can bind to, but not activate, kinases. Thus, Mg-AMP application should not affect current rundown. Indeed, I observed no difference in current rundown between Mg-AMP and control condition of 2 mM  $\text{Ca}^{2+}$  (Figure 3-7B and 3-7C). I then recorded TMEM16A currents at -60 mV before and during application of 2 mM  $\text{Ca}^{2+}$  with 1.5 mM Mg-ATP. An example plot of normalized current versus time is shown in Figure 3-7D. I observed that in the presence of 1.5 mM Mg-ATP and 2 mM  $\text{Ca}^{2+}$ , TMEM16A currents ran down over a longer time course, with a time constant of  $143.4 \text{ s} \pm 17.2 \text{ s}$  (N=5) (Fig 3-7D and Table 3-1).

Next, I reasoned that if phosphatase-mediated  $\text{PI}(4,5)\text{P}_2$  depletion causes TMEM16A current rundown in excised patches then inhibiting phosphatase activity would also slow rundown. I tested this hypothesis by quantifying the kinetics of current rundown in the presence of  $\text{Ca}^{2+}$  and the general phosphatase inhibitor sodium  $\beta$ -glycerophosphate pentahydrate ( $\beta\text{GP}$ ) [115]. Figure 3-7E depicts an example plot of TMEM16A-conducted currents recorded at -60 mV versus time, before and during application of 50 mM  $\beta\text{GP}$  and 2 mM  $\text{Ca}^{2+}$ . In five independent trials, I observed that TMEM16A currents ran down slower in the presence of the phosphatase inhibitor, with a time constant of  $166 \text{ s} \pm 14.7 \text{ s}$  (N=5) (Fig 3-7E and Table 3-1). Together, these data suggest that TMEM16A currents rundown in excised patches as the result of  $\text{PI}(4,5)\text{P}_2$  depletion via its dephosphorylation. Moreover, these data are consistent with the hypothesis that the phosphates found on the inositol head group of  $\text{PI}(4,5)\text{P}_2$  are responsible for the interaction between TMEM16A and  $\text{PI}(4,5)\text{P}_2$ .

### 3.3 Discussion

By recording TMEM16A currents while modifying the membrane PI(4,5)P<sub>2</sub> content, here I demonstrate that these channels require both Ca<sup>2+</sup> and PI(4,5)P<sub>2</sub> to conduct current. A possible role for PI(4,5)P<sub>2</sub> in TMEM16A regulation was initially suggested by rundown of these currents recorded from *X. laevis* oocytes despite the continued presence of a saturating concentration of Ca<sup>2+</sup> (Figure 3-2). Rundown results from the removal of a membrane patch from the cytosol that includes ATP [102]. This ATP is required to fuel the phospholipid kinases which rephosphorylate the phospholipids present in the membrane [102]. As such, current rundown in excised patches is a hallmark of channels regulated by PI(4,5)P<sub>2</sub>.

#### 3.3.1 PI(4,5)P<sub>2</sub> regulates TMEM16A gating

Application of the soluble PI(4,5)P<sub>2</sub> analog, diC8-PI(4,5)P<sub>2</sub>, recovered TMEM16A conducted currents following rundown, but only when applied with Ca<sup>2+</sup> (Figure 3-3 and 3-4). Not all TMEM16A current was recovered with diC8-PI(4,5)P<sub>2</sub> application. 100 μM diC8-PI(4,5)P<sub>2</sub> applied without Ca<sup>2+</sup> had a nominal effect on TMEM16A currents revealing that both Ca<sup>2+</sup> and PI(4,5)P<sub>2</sub> are required for the phospholipid to potentiate these channels. I speculate that the incomplete recovery with 100 μM diC8-PI(4,5)P<sub>2</sub> applied with Ca<sup>2+</sup> may reflect a slow rate of PI(4,5)P<sub>2</sub> integration into the membrane. This is consistent with my observation that the current recovery was diminished when longer acyl chains were applied to patches (Figure 3-5). Alternatively, the incomplete recovery may reflect the role of a Ca<sup>2+</sup> dependent recovery of PI(4,5)P<sub>2</sub>. PI(4,5)P<sub>2</sub> recovery can be more pronounced at lower Ca<sup>2+</sup> than at higher Ca<sup>2+</sup> [68]. This complex relationship between PI(4,5)P<sub>2</sub> and Ca<sup>2+</sup> needs to be explored further in my system.

Phospholipid-mediated recovery of TMEM16A currents following rundown requires phosphorylation of the inositol ring. Accordingly, I found that 100  $\mu$ M diC8-PI, the phospholipid lacking the negatively charged phosphate head groups, was unable to recover TMEM16A currents (Figure 3-5). In contrast to the recent report that suggests that the neutral acyl chain of fatty acids is sufficient to regulate TMEM16A [78], my findings suggest that TMEM16A potentiation by PI(4,5)P<sub>2</sub> requires the presence of phosphate heads which are lacking in lipids like oleic acid or cholesterol. My results do not preclude the possibility that fatty acids change PI(4,5)P<sub>2</sub> membrane content, but they do suggest that just a fatty acid tail or backbone like that from PI(4,5)P<sub>2</sub> is not sufficient for channel potentiation.

My data suggested that TMEM16A current rundown in the excised patch was caused by PI(4,5)P<sub>2</sub> depletion. I therefore reasoned that scavenging PI(4,5)P<sub>2</sub> present in the patch should speed TMEM16A current rundown. Indeed, application of either PI(4,5)P<sub>2</sub>-scavenging compounds, anti-PI(4,5)P<sub>2</sub> or neomycin, sped TMEM16A current rundown (Figure 3-6). Other groups have shown that anti-PI(4,5)P<sub>2</sub> and neomycin effectively scavenged PI(4,5)P<sub>2</sub> without disrupting ion conductance during single channel recordings [116] or in excised macropatches expressing the inwardly rectifying K<sup>+</sup> channels [117, 118]. These data are consistent with the depletion of PI(4,5)P<sub>2</sub> causing current rundown.

### **3.3.2 PI(4,5)P<sub>2</sub> dephosphorylation promotes current rundown**

PI(4,5)P<sub>2</sub> depletion occurs in excised patches due to the continued activity of membrane-associated phosphatases which dephosphorylate the inositol head group without the activity of the counter-acting kinases. If TMEM16A current rundown in excised patches is the result of PI(4,5)P<sub>2</sub> dephosphorylation, I predicted that by enabling kinases to rephosphorylate the lipid or by

inhibiting phosphatase activity, I ought to be able to slow current rundown. Indeed, providing patches with Mg-ATP to fuel membrane-anchored kinases to make PI(4,5)P<sub>2</sub>, resulted in TMEM16A currents that ran down significantly more slowly compared to control recordings (Figure 3-7). While it is possible that Mg-ATP could bind to and alter the activity of other proteins in the excised patches, in the context of the other data included in this chapter it is likely that Mg-ATP is fueling kinases needed to rephosphorylate PI(4,5)P<sub>2</sub>. In a parallel series of experiments, the broad-spectrum phosphatase inhibitor βGP [115] similarly slowed rundown by at least 3-fold. Together, these data demonstrate that the dephosphorylation of the inositol head group of PI(4,5)P<sub>2</sub> with patch excision, leads to TMEM16A current decay. These data provide additional support that the phosphates on the inositol head group mediate the PI(4,5)P<sub>2</sub> potentiation of TMEM16A.

### 3.3.3 Controversial TMEM16A-PI(4,5)P<sub>2</sub> relationship

My data directly demonstrate that PI(4,5)P<sub>2</sub> and Ca<sup>2+</sup> are both required for TMEM16A activation, yet previous studies of phospholipid regulation of this channel came to varied conclusions. Although agreeably demonstrating that PI(4,5)P<sub>2</sub> modifies TMEM16A current in native rat isolated pulmonary cells, one study reported a *decrease* in whole cell Ca<sup>2+</sup>-activated Cl<sup>-</sup> currents with the application of diC8-PI(4,5)P<sub>2</sub> via a pipette solution [81]. This study found that including the PI(4,5)P<sub>2</sub> scavenger polylysine in the pipette solution *increased* TMEM16A currents and therefore concluded that PI(4,5)P<sub>2</sub> *inhibits* TMEM16A currents [81]. Using HEK293 cells exogenously expressing mouse TMEM16A, another group reported that neither siRNA-mediated knockdown of phosphatase and tensin homolog (PTEN), nor wortmannin application, altered TMEM16A currents [104]. Because both treatments should reduce PI(4,5)P<sub>2</sub> content by diminishing the dephosphorylation of phosphatidylinositol 3,4,5-triphosphate (PIP<sub>3</sub>) into

PI(4,5)P<sub>2</sub>, this report concluded that PI(4,5)P<sub>2</sub> does not regulate TMEM16A [104]. The final two studies on the subject also used TMEM16A transfected HEK293 cells to conclude that mouse TMEM16A is potentiated by PI(4,5)P<sub>2</sub> [68, 78]. One group reported that although TMEM16A-mediated currents did not rundown in excised inside-out patches, application of diC8-PI(4,5)P<sub>2</sub> increased the current [68]. In this same study, activation of a co-expressed voltage-sensing phosphatase reduced, but did not abolish, TMEM16A currents [68]. A final study reported that fatty acids, including PI(4,5)P<sub>2</sub>, potentiate TMEM16A conducted currents [78]. My data, by contrast, indicate that the lipid tail alone is unable to regulate TMEM16A currents. A possible explanation for the difference between my data and the finding that other fatty acids potentiate TMEM16A is that stearic acids, including those used during these particular experiments, can associate with PI(4,5)P<sub>2</sub> [119]. Consequently, stearic acids could alter membrane PI(4,5)P<sub>2</sub> and therefore alter TMEM16A-conducted currents. I sought to resolve these seemingly conflicting results by recording from natively expressed TMEM16A channels in *X. laevis* oocytes to determine if PI(4,5)P<sub>2</sub> regulates TMEM16A gating. Using direct experimental methods, here I demonstrate that TMEM16A requires both membrane PI(4,5)P<sub>2</sub> and intracellular Ca<sup>2+</sup> to conduct currents in *X. laevis* oocytes.

### **3.3.4 Mechanism of PI(4,5)P<sub>2</sub> regulation of TMEM16A**

Despite my demonstration that TMEM16A gating is regulated by PI(4,5)P<sub>2</sub>, the exact mechanism involved is yet to be determined. PI(4,5)P<sub>2</sub> regulates other ion channels by diverse mechanisms [103]. For example, PI(4,5)P<sub>2</sub> may regulate TMEM16A currents by acting on an accessory protein, exemplified by PI(4,5)P<sub>2</sub> binding to KCNE1 to regulate currents conducted by the voltage-gated potassium channel KCNQ1 [120]. Alternatively, PI(4,5)P<sub>2</sub> can form electrostatic

interactions between a cluster of positive charges on a channel and the negative charges on the phosphoinositol head of PI(4,5)P<sub>2</sub> as has been observed for transient receptor potential vanilloid 5 (TRPV5) [121], inward-rectifier K<sup>+</sup> (Kir2.2) [122] and G protein-gated K<sup>+</sup> (GIRK2) [123]. Unlike KCNQ1, no accessory protein has been revealed for TMEM16A. Although Cl<sup>-</sup> channel accessory 1 (CLCA1) has been identified as an accessory protein for TMEM16A channels [124], neither this protein nor the RNA are found in mature *X. laevis* eggs, or the fertilization-incompetent oocytes [125-127]. My data, however, does not preclude an indirect mechanism for PI(4,5)P<sub>2</sub> regulation of TMEM16A by another accessory protein for TMEM16A. I speculate that TMEM16A and PI(4,5)P<sub>2</sub> may form electrostatic interactions similar to those revealed by the TRPV5, Kir2.2 and GIRK2 PI(4,5)P<sub>2</sub>-bound structures.

Electrostatic interactions mediate PI(4,5)P<sub>2</sub> binding to the closely-related cation channel, TMEM16F [73]. The putative PI(4,5)P<sub>2</sub> binding site in TMEM16F is comprised of positively charged residues and neutralizing these residues perturbed PI(4,5)P<sub>2</sub>'s ability to potentiate TMEM16F currents [73]. It is possible that a conserved domain mediates PI(4,5)P<sub>2</sub> interactions with all TMEM16 family proteins including TMEM16A channels. Although the binding domain may be shared, the effects on proteins will most certainly differ. For example, the Ca<sup>2+</sup> activated Cl<sup>-</sup> channel TMEM16B, is inhibited by PI(4,5)P<sub>2</sub> [68]. Yet, a shared PI(4,5)P<sub>2</sub> regulation amongst TMEM16 family proteins is perhaps not surprising given that this protein family includes several lipid scramblases whose physiologic function requires their interaction with charged lipids.

### **3.3.5 Physiological implications of TMEM16A's regulation by PI(4,5)P<sub>2</sub>**

A requirement for PI(4,5)P<sub>2</sub> in TMEM16A activation is intriguing because the PI(4,5)P<sub>2</sub> cleavage into IP<sub>3</sub> to signal Ca<sup>2+</sup> release from the ER would seemingly oppose the ability of

increased  $\text{Ca}^{2+}$  to activate the channel. Yet, independent studies have revealed that an  $\text{IP}_3$ -evoked  $\text{Ca}^{2+}$ -release from the ER opens TMEM16A channels to signal diverse physiologic processes including signaling contraction of lymphatic vessels [128, 129] to activation of the fast polyspermy block [126, 130]. I propose that in systems that use an  $\text{IP}_3$  pathway to activate TMEM16A channels, the amount of  $\text{PI}(4,5)\text{P}_2$  cleaved in order to generate  $\text{IP}_3$  matters greatly. For example, stimuli that evoke the cleavage of only a moderate amount of  $\text{PI}(4,5)\text{P}_2$  to increase  $\text{IP}_3$  and evoke a  $\text{Ca}^{2+}$  release from the ER will ultimately signal the opening of more TMEM16A channels compared to other stimuli that signal the cleavage of most of the membrane  $\text{PI}(4,5)\text{P}_2$  to increase  $\text{IP}_3$  and evoke an even larger  $\text{Ca}^{2+}$  release from the ER. Perhaps TMEM16A discriminates its own  $\text{Ca}^{2+}$  signal from  $\text{Ca}^{2+}$  signaling cascades that exclude it by seeking interactions with  $\text{PI}(4,5)\text{P}_2$  at the plasma membrane. Moreover, these studies reveal that the physiologic mechanisms underlying TMEM16A opening are more complicated than simply the presence or absence of intracellular  $\text{Ca}^{2+}$ , thereby enabling TMEM16A to play diverse roles in different cell types.

### **3.3.6 Summary**

Understanding how the channel is regulated lays the conceptual framework for drugging this interaction in disease. In hypertension, the over-constriction of vessels can be alleviated by inhibiting  $\text{Ca}^{2+}$ -activated- $\text{Cl}^-$  channels like TMEM16A [131]. In cystic fibrosis, a condition arising from a dysfunctional  $\text{Cl}^-$  channel, increasing TMEM16A activity could rescue the defects caused by poor  $\text{Cl}^-$  transport [132]. By understanding the interaction between  $\text{PI}(4,5)\text{P}_2$  and TMEM16A, drugs targeting the  $\text{PI}(4,5)\text{P}_2$ -TMEM16A interaction site can be designed to either inhibit TMEM16A activity with the benefit of lowering blood pressure or increase its activity to promote  $\text{Cl}^-$  transport.

### 3.4 Figures and tables

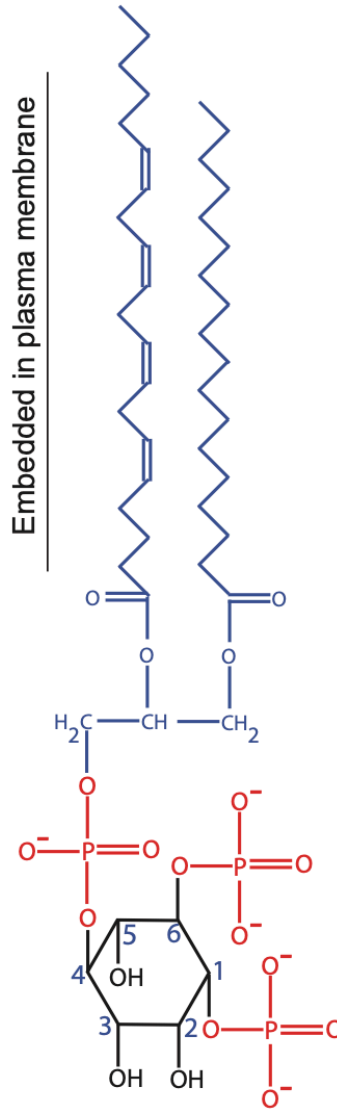


**Figure 3-1. Structure of phosphatidyl 4,5-bisphosphate (PI(4,5)P<sub>2</sub>)**

PI(4,5)P<sub>2</sub> is a fatty acid embedded in the inner leaflet of the plasma membrane. It is made of a fatty acid tail (blue), a phosphate group attaching the inositol head to the fatty acid tail and negatively charged phosphate groups at positions 4 and 5 of the inositol head.

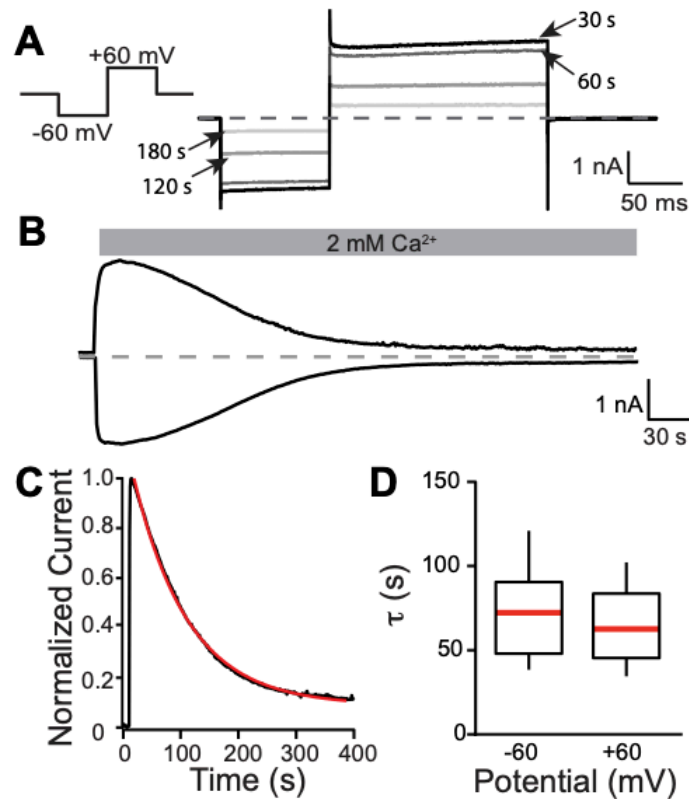


**Figure 3-2. TMEM16A  $\text{Ca}^{2+}$ -evoked  $\text{Cl}^-$  currents rundown in excised inside-out patches**

Inside-out patch clamp recordings were conducted on macropatches excised from *X. laevis* oocytes. (A) Example currents recorded during 100-150 ms steps to -60 and +60 mV, at indicated times following patch excision. (B) Representative plot of current measured at -60 (bottom) or +60 mV (top) versus time, after patch excision. 2 mM  $\text{Ca}^{2+}$  was applied at 10 s as denoted by the grey bar. The dashed grey line represents 0 nA. (C) Normalized plot of current measured at -60 mV versus time, fit with a single exponential (red line). (D) Box plot distribution of the rate of current decay ( $\tau$ ), measured by fitting plots of relative current versus time with single exponentials ( $N = 15$ ). The central line denotes the median, the box denotes the distribution of 25-75 % of the data, and the whiskers represent 10-90% of the data. The  $\tau$  at +60 mV and -60 mV were not significantly different ( $P=0.29$ ) as determined by t-test.

**Table 3-1. Altering PI(4,5)P<sub>2</sub> altered the rate of rundown**

<b>Condition</b>	<b>Concentration</b>	<b>Tau, <math>\tau</math> (s)</b>	<b>Number of trials</b>
Control		68.9 $\pm$ 7.1	N = 15
Anti-PI(4,5)P <sub>2</sub>	15 $\mu$ g/mL	48.6 $\pm$ 7.4	N = 4
Neomycin	50 mM	32.0 $\pm$ 8.8	N = 5
Mg-AMP	1.5 mM	57.7 $\pm$ 12.6	N = 5
Mg-ATP	1.5 mM	143.4 $\pm$ 17.2	N = 5
$\beta$ GP	50 mM	168 $\pm$ 14.7	N = 5

The mean  $\pm$  SEM for the indicated measurements taken from excised inside-out patches. The  $\tau$  was obtained by fitting plots of the currents versus time with single exponential functions.

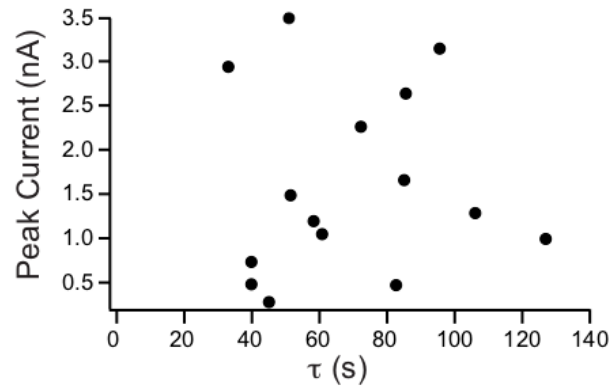


**Figure 3-3. Rate of TMEM16A Ca<sup>2+</sup>-evoked Cl<sup>-</sup> current rundown not determined by peak currents**

Nominal TMEM16A Ca<sup>2+</sup>-evoked Cl<sup>-</sup> currents were plotted against their rates of current rundown in excised inside-out patches from *X. laevis* oocytes (N=15).

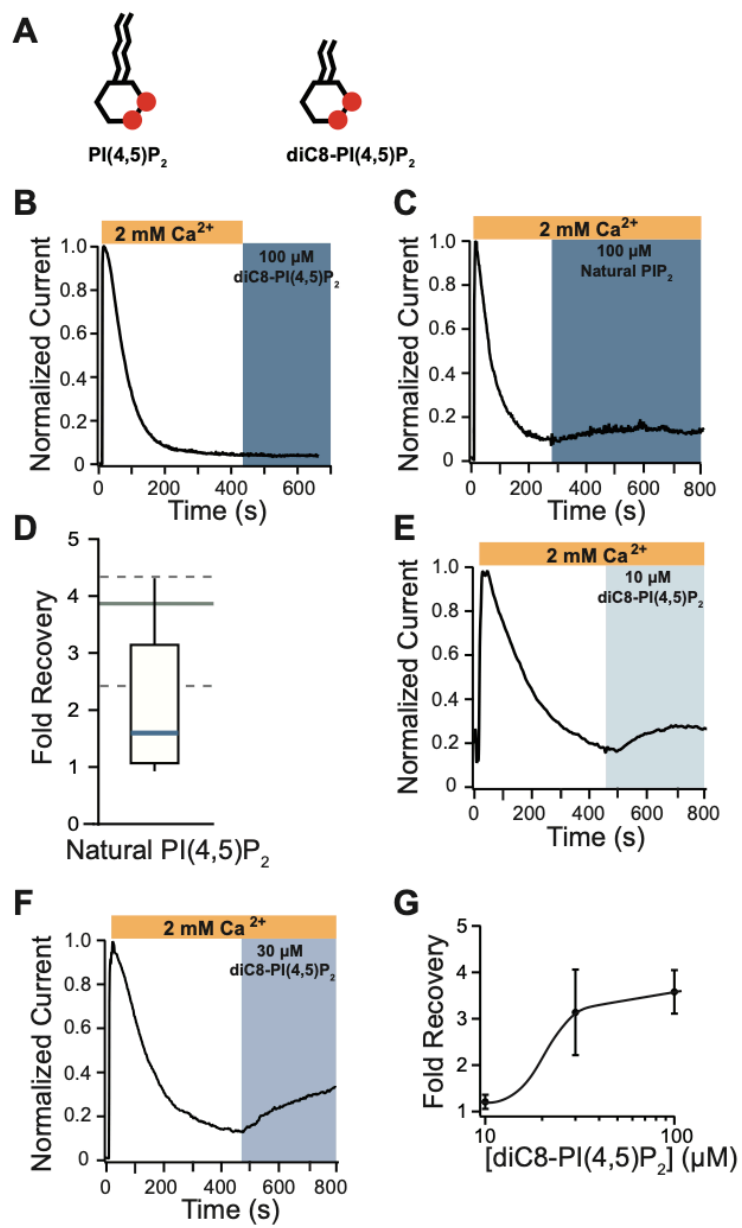


**Figure 3-4. PI(4,5)P<sub>2</sub> analog or natural PI(4,5)P<sub>2</sub> with Ca<sup>2+</sup> recovered TMEM16A conducted currents following rundown**

The soluble synthetic analog of PI(4,5)P<sub>2</sub> (diC8-PI(4,5)P<sub>2</sub>) or natural PI(4,5)P<sub>2</sub> was applied to excised inside-out patches once current had stably rundown. Currents were recorded at -60 mV. (A) Schematic depiction of natural PI(4,5)P<sub>2</sub> and diC8-PI(4,5)P<sub>2</sub>. (B) Representative plot of normalized currents versus time, before and during application of 100 μM diC8-PI(4,5)P<sub>2</sub> with 2 mM Ca<sup>2+</sup>. (C) Representative plot of normalized currents versus time, before and during application of 100 μM natural PI(4,5)P<sub>2</sub> with added Ca<sup>2+</sup> (N=6). (D) Box plot distribution of the fold current recovered after the application of natural PI(4,5)P<sub>2</sub> with added Ca<sup>2+</sup> (N=6). Representative plots of normalized currents versus time, before and during application of 10 μM diC8-PI(4,5)P<sub>2</sub> with added Ca<sup>2+</sup> (E) and 30 μM diC8-PI(4,5)P<sub>2</sub> with added Ca<sup>2+</sup> (F). Fold current recovered by natural PI(4,5)P<sub>2</sub> with added Ca<sup>2+</sup> compared to 100 μM diC8-PI(4,5)P<sub>2</sub> was not significantly different (*P*=0.06) as determined by t-test. (G) Plot of the average fold of current recovered by diC8-PI(4,5)P<sub>2</sub> at 10, 30 and 100 μM diC8-PI(4,5)P<sub>2</sub> addition in the presence of 2 mM Ca<sup>2+</sup>. The fold change in current recovered was calculated as change in current upon application of diC8-PI(4,5)P<sub>2</sub> with Ca<sup>2+</sup>. The grey lines denote the box plot distribution of fold current recovered from patches recorded with 100 μM diC8-PI(4,5)P<sub>2</sub> with Ca<sup>2+</sup> application, where the solid grey line represents the median value and the dashed lines represent the control data distribution from 25-75%.

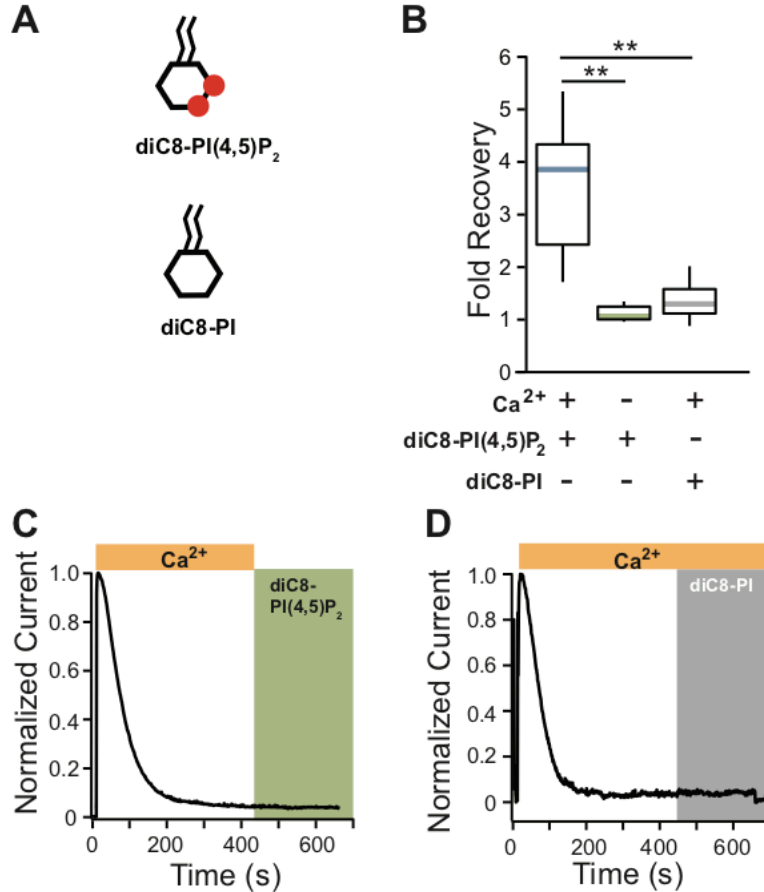


**Figure 3-5. PI(4,5)P<sub>2</sub> and Ca<sup>2+</sup> are both required for TMEM16A conducted currents**

diC8-PI(4,5)P<sub>2</sub> and PI (diC8-PI) were applied to excised inside-out patches once current had stably rundown. Currents were recorded at -60 mV. (A) Schematic depiction of the diC8 analogs used. (B) Box plot distribution of the fold current recovered after the application of diC8-PI(4,5)P<sub>2</sub> with Ca<sup>2+</sup>, diC8-PI(4,5)P<sub>2</sub> without Ca<sup>2+</sup>, and diC8-PI with Ca<sup>2+</sup>. The fold change in current recovered was calculated as change in current upon application of diC8-PI(4,5)P<sub>2</sub> with Ca<sup>2+</sup> (N=7) or diC8-PI(4,5)P<sub>2</sub> without Ca<sup>2+</sup> (N=5), diC8-PI (N=6) addition to the peak current observed after each synthetic analog addition. Representative plots of normalized currents versus time, before and during application of 100 μM diC8-PI(4,5)P<sub>2</sub> with no added Ca<sup>2+</sup> (C), 100 μM diC8-PI with 2 mM Ca<sup>2+</sup> (D). \*\* denotes  $P < 0.01$  and \* denotes  $P < 0.05$  as determined by t-test. Fold current recovered by diC8-PI(4,5)P<sub>2</sub> without Ca<sup>2+</sup> compared to diC8-PI was not significantly different ( $P=0.20$ ).

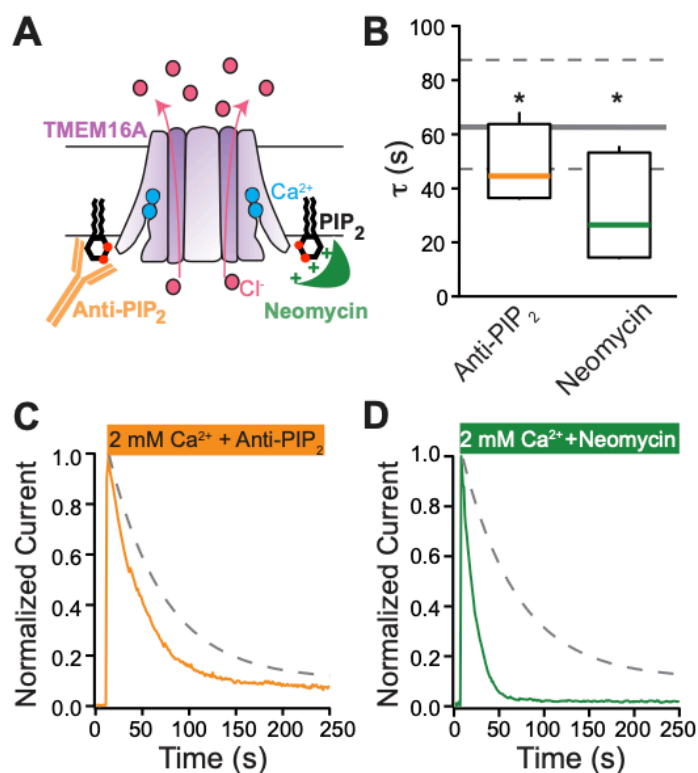


**Figure 3-6. Scavenging PI(4,5)P<sub>2</sub> sped TMEM16A current rundown in excised inside-out patches**

(A) Schematic depicting membrane-embedded TMEM16A with the PI(4,5)P<sub>2</sub> scavengers, anti-PI(4,5)P<sub>2</sub> or neomycin. (B) Box plot distribution of the rate of rundown observed from currents recorded at -60 mV from inside-out patches exposed to 2 mM Ca<sup>2+</sup> with 15  $\mu$ g/mL anti-PI(4,5)P<sub>2</sub> (N=4) or 50mM neomycin (N=5). The rate of current rundown was obtained by fitting the plots of the current versus time with a single exponential. The grey lines denote the box plot distribution of the rate of rundown measured from patches recorded under control conditions of 2 mM Ca<sup>2+</sup>-only application, where the solid grey line represents the median value and the dashed lines represent the control data distribution from 25-75%. Representative plots of Ca<sup>2+</sup>-evoked Cl<sup>-</sup> currents recorded at -60 mV, versus time, from inside-out patches in the presence of 2 mM Ca<sup>2+</sup> with 15  $\mu$ g/mL anti-PI(4,5)P<sub>2</sub> (C) or 50mM neomycin (D); both conditions sped current rundown when compared to the control denoted by the grey dashed line. \* denotes  $P < 0.05$  determined by t-test.

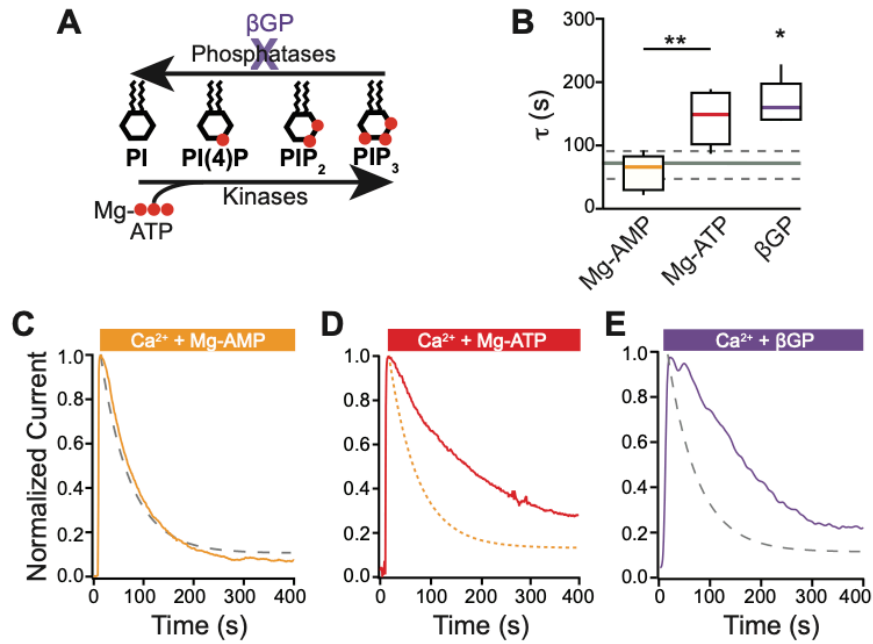


**Figure 3-7. Enabling rephosphorylation or inhibiting phosphatases slowed current decay in excised inside-out patches**

(A) Schematic depicting the role of phosphatases and kinases in generating various phosphoinositide species. (B) The box plot distribution of the rate of rundown ( $\tau$ ) observed from currents recorded at  $-60$  mV from inside-out patches exposed to  $2$  mM  $\text{Ca}^{2+}$  with  $1.5$  mM Mg-AMP ( $N=5$ ),  $2$  mM  $\text{Ca}^{2+}$  with  $1.5$  mM Mg-ATP ( $N=6$ ), and  $2$  mM  $\text{Ca}^{2+}$  with  $50$  mM sodium  $\beta$ -glycerophosphate pentahydrate ( $\beta$ GP) ( $N=6$ ). Single exponentials were fitted to current traces to obtain the rate of current rundown. Solid grey line denotes median rate of rundown measured from patches recorded under the control conditions of  $2$  mM  $\text{Ca}^{2+}$ -only application, and the dashed lines represent the control data distribution from 25-75%. Representative plots of normalized currents versus time made before and during application of  $1.5$  mM Mg-AMP with  $2$  mM  $\text{Ca}^{2+}$  (compared to  $2$  mM  $\text{Ca}^{2+}$ -only application with the grey dashed line) (C),  $1.5$  mM Mg-ATP with  $2$  mM  $\text{Ca}^{2+}$  (compared to  $1.5$  mM Mg-AMP with the orange dashed line) (D), and  $50$  mM  $\beta$ GP with  $2$  mM  $\text{Ca}^{2+}$  (compared to  $2$  mM  $\text{Ca}^{2+}$ -only application with the grey dashed line) (E). \*\* denotes  $P < 0.01$  and \* denotes  $P < 0.05$  when compared to  $2$  mM  $\text{Ca}^{2+}$ -only application or between indicated pairs determined by t-test.

## 4.0 The Rate of TMEM16A Current Rundown Depends on Intracellular Ca<sup>2+</sup>

This chapter is an adaptation of 2020 Tembo et al. to be submitted to the Journal of Biological Chemistry.

### 4.1 Introduction

Cl<sup>-</sup> channels contribute substantially to the regulation of excitable cells [128, 129, 133]. The ability of cellular membranes to shift between positive and negative potentials enables our neurons to relay information and our heart to beat. Thus, homeostatic ionic environments are key for proper functioning of excitable cells whose greater physiological roles are achieved through changes in membrane potential. A crucial protein regulating membrane potential is the Ca<sup>2+</sup>-activated Cl<sup>-</sup> channel TransMEMbrane 16A (TMEM16A). The disruption of TMEM16A leads to perinatal lethality in mice, revealing a critical role for TMEM16A in the quality of life [100]. TMEM16A is a key component regulating important physiological roles including smooth muscle contraction [79, 95, 97] and dorsal root ganglion signal transduction [79, 134]. TMEM16A channels are also as key players in diseases such as hypertension and cancer [128, 129, 133, 135].

Now that we have established a role for TMEM16A across different cell types and disease, an area needing further study is how these channels are regulated. Understanding TMEM16A regulation will lay the conceptual framework for the development of TMEM16A-based therapy. TMEM16A requires its ligand, Ca<sup>2+</sup>, and its cofactor, phosphatidylinositol 4,5-bisphosphate (PI(4,5)P<sub>2</sub>), which when present together promote the open conformation of TMEM16A [68, 78,

90, 136, 137]. In the absence of either  $\text{Ca}^{2+}$  or  $\text{PI}(4,5)\text{P}_2$ , the  $\text{Cl}^-$  pore of TMEM16A is impermeable to  $\text{Cl}^-$  [45, 46, 71]. The structure of TMEM16A has revealed that the homodimer has two  $\text{Ca}^{2+}$  binding pockets per subunit whose ability to bind  $\text{Ca}^{2+}$  is voltage dependent at low concentrations of  $\text{Ca}^{2+}$ . Each  $\text{Cl}^-$  pore was initially thought to be gated by just the binding of  $\text{Ca}^{2+}$  suggesting that  $\text{Ca}^{2+}$  occupancy alone would result in TMEM16A channels opening [47, 48]. However, with evidence that: (1)  $\text{PI}(4,5)\text{P}_2$  is a required to open TMEM16A channels, (2) fewer than two bound  $\text{Ca}^{2+}$  per dimer can activate TMEM16A in a voltage dependent manner, and (3) each pore operates independently, the regulation of TMEM16A gating has become complex.

$\text{Ca}^{2+}$  and  $\text{PI}(4,5)\text{P}_2$  are both required for TMEM16A to conduct  $\text{Cl}^-$  currents.  $\text{Ca}^{2+}$  signaling cascades can increase intracellular  $\text{Ca}^{2+}$  levels to 300-400 nM in smooth muscle cells [138] or 3-400  $\mu\text{M}$  in *Xenopus laevis* oocytes [139]. Given that reported half maximal effective concentration for mouse TMEM16A (mTMEM16A) exogenously expressed in human embryonic (HEK)293 cells is 800 nM-1.0  $\mu\text{M}$  [46, 50], it is possible that TMEM16A has a mechanism in place that allows the channel to distinguish between various signaling cascades. As previously shown, part of TMEM16A's regulation involves  $\text{PI}(4,5)\text{P}_2$  [90].  $\text{PI}(4,5)\text{P}_2$  makes up 1-3% of the plasma membrane and is tightly regulated by a series of phosphoinositol kinases and phosphatases [140, 141]. Local  $\text{PI}(4,5)\text{P}_2$  concentrations can even be higher where it is needed [142]. For example at intracellular vesicle docking sites on the plasma membrane of neurons,  $\text{PI}(4,5)\text{P}_2$  is estimated to be 3-6% of the cell surface area [143]. It is possible that TMEM16A is in close proximity to  $\text{PI}(4,5)\text{P}_2$  most of the time especially in cells where it is endogenously expressed. Constant  $\text{PI}(4,5)\text{P}_2$  abundance and regular  $\text{Ca}^{2+}$  signaling cascades could mean that a tight regulation is needed either directly acting on TMEM16A itself or  $\text{Ca}^{2+}$  or  $\text{PI}(4,5)\text{P}_2$ .

The objective of the research reported in this chapter was to determine how TMEM16A activity is tightly regulated by  $\text{Ca}^{2+}$  and  $\text{PI}(4,5)\text{P}_2$ . Specifically, I examined how  $\text{PI}(4,5)\text{P}_2$  and  $\text{Ca}^{2+}$  alter the opening and closing of TMEM16A channels. For these experiments, I conducted inside-out patch clamp recordings on the endogenous TMEM16A channel in *Xenopus laevis* oocytes. In examining how  $\text{PI}(4,5)\text{P}_2$  gates TMEM16A, I found that the phosphate at position 4 of  $\text{PI}(4,5)\text{P}_2$  is key in mediating the TMEM16A- $\text{PI}(4,5)\text{P}_2$  interaction. In examining how  $\text{Ca}^{2+}$  gates TMEM16A, I found that altering  $\text{Ca}^{2+}$  concentration altered the speed of current rundown. Specifically, I found that lower concentrations of  $\text{Ca}^{2+}$  or  $\text{Ca}^{2+}$  substitutions resulted in slowed TMEM16A current rundown. Next, I determined that inhibiting PLCs significantly slowed current rundown during the application of a general PLC inhibitor but not its analog. Taken together, my data provide insight on how  $\text{PI}(4,5)\text{P}_2$  and  $\text{Ca}^{2+}$  regulate TMEM16A channels in *X. laevis* oocytes.

## 4.2 Results

### 4.2.1 $\text{PI}(4,5)\text{P}_2$ does not recover TMEM16A currents completely

TMEM16A is activated by 2 mM  $\text{Ca}^{2+}$  and within seconds of application, the current peaks and then slowly runs down in excised inside-out patches of *X. laevis* (Figure 4-1A). Consistent with Figure 3-2, TMEM16A currents recorded in 2 mM  $\text{Ca}^{2+}$  during 100-150 ms steps to -60 mV and +60 mV are recovered by dioctanoyl-phosphatidyl 4,5-bisphosphate (diC8- $\text{PI}(4,5)\text{P}_2$ ) (Figure 4-1B). Interestingly, diC8- $\text{PI}(4,5)\text{P}_2$  did not recover currents completely (Figure 3-2) even though Figure 3-3 suggested that the phosphates on the inositol head of diC8- $\text{PI}(4,5)\text{P}_2$  were necessary

and sufficient to recover TMEM16A  $\text{Ca}^{2+}$ -evoked  $\text{Cl}^-$  currents. Thus I sought to understand the relationship between TMEM16A current recovery and the phosphates on diC8-PI(4,5)P<sub>2</sub>.

#### **4.2.2 Phosphate at position 4 of the inositol ring is key in PI(4,5)P<sub>2</sub>'s interaction with TMEM16A**

I tested the hypothesis that application of an analog of PI(4,5)P<sub>2</sub> with more phosphates and therefore an increased negative charge on the inositol head would recover TMEM16A currents following rundown. To do so, I applied a water-soluble analog of phosphatidyl 3,4,5-trisphosphate (diC8-PIP<sub>3</sub>) to excised inside-out patches after current had stably rundown. I recorded TMEM16A-conducted currents at -60 mV before and during application of 100  $\mu\text{M}$  diC8-PIP<sub>3</sub> (at the same concentration that I observed the greatest TMEM16A current recovery for diC8-PI(4,5)P<sub>2</sub>). In five independent trials, I observed that 100  $\mu\text{M}$  diC8-PIP<sub>3</sub> application recovered an average of  $2.8 \pm 0.4$ -fold current (Figure 4-1C) which was not more than the  $3.6 \pm 0.5$ -fold recovery by diC8-PI(4,5)P<sub>2</sub>. Figure 4-1D depicts an example plot of TMEM16A-conducted currents recorded at -60 mV versus time before and during diC8-PIP<sub>3</sub> application. Because the current recovered by diC8-PIP<sub>3</sub> was not greater or equal to the current recovered by diC8-PI(4,5)P<sub>2</sub>, these data suggest that negative charge carried by the phosphate groups alone is insufficient in regulating TMEM16A currents.

Given that diC8-PIP<sub>3</sub> resulted in less current recovery than diC8-PI(4,5)P<sub>2</sub>, I reasoned that either the third phosphate in the inositol ring introduced steric hinderance inositol ring in TMEM16A-PI(4,5)P<sub>2</sub> interaction or that PIP<sub>3</sub> must first be dephosphorylated to interact TMEM16A. Thus, I next examined whether charge alone was sufficient to recover TMEM16A currents or if phosphate position mattered for TMEM16A current recovery. I began by testing the

idea that having two phosphates (two negatively charged groups and not greater) on the inositol head was sufficient for recovering TMEM16A currents. To explore this possibility, I sought to determine if application of other phosphoinositides containing two negatively charged phosphates on the inositol ring would recover  $\text{Ca}^{2+}$ -evoked TMEM16A  $\text{Cl}^-$  currents. I applied a water-soluble analog of phosphatidyl 3,4-bisphosphate (diC8-PI(3,4)P<sub>2</sub>) to excised inside-out patches after current had stably rundown. I recorded TMEM16A-conducted currents at -60 mV before and while applying 100  $\mu\text{M}$  diC8-PI(3,4)P<sub>2</sub>. In five independent trials, I observed that 100  $\mu\text{M}$  diC8-PI(3,4)P<sub>2</sub> application recovered an average of  $2.8 \pm 0.9$ -fold current (Figure 4-1C). The currents recovered were similar to those observed by the application of diC8-PI(4,5)P<sub>2</sub>. Figure 4-1E depicts an example plot of TMEM16A-conducted currents recorded at -60 mV versus time before and during diC8-PI(3,4)P<sub>2</sub> application.

Surprisingly, TMEM16A-conducted currents recorded at -60 mV before and during application of 100  $\mu\text{M}$  diC8-PI(3,5)P<sub>2</sub> recovered  $1.1 \pm 0.1$ -fold current in five independent trials (Figure 4-1C). This level of current recovered was substantially smaller than the currents recovered by the equally charged species diC8-PI(4,5)P<sub>2</sub> and diC8-PI(3,4)P<sub>2</sub>. Figure 4-1F depicts an example plot of TMEM16A-conducted currents recorded at -60 mV versus time before and during diC8-PI(3,5)P<sub>2</sub> application. The current recovered by diC8-PI(3,5)P<sub>2</sub> was less than the current recovered by both diC8-PI(4,5)P<sub>2</sub> and diC8-PI(3,4)P<sub>2</sub>. These data also suggest that the negative charge alone does not account for the TMEM16A-PI(4,5)P<sub>2</sub> interaction. Both diC8-PI(3,5)P<sub>2</sub> and diC8-PI(3,4)P<sub>2</sub> carry the same number of phosphates and charge as diC8-PI(4,5)P<sub>2</sub>, yet diC8-PI(3,5)P<sub>2</sub> and diC8-PI(3,4)P<sub>2</sub> are unable to recover currents equal to diC8-PI(4,5)P<sub>2</sub>. However, diC8-PI(3,4)P<sub>2</sub> did recover currents similar to diC8-PI(4,5)P<sub>2</sub>. Perhaps in addition to having two negatively charged phosphates on the inositol head, TMEM16A prefers the two phosphates occupy

specific positions on the inositol head. Specifically, the phosphoinositides diC8-PI(3,4)P<sub>2</sub> and diC8-PI(4,5)P<sub>2</sub> that recovered TMEM16A conducted currents had a phosphate at position 4, but diC8-PI(3,5)P<sub>2</sub> which lacks a phosphate at position 4 of the inositol head was unable to recover substantial TMEM16A conducted currents.

To more directly explore a possible relationship between phosphate position and TMEM16A current recovery, I recorded TMEM16A-conducted currents at -60 mV before and while applying water soluble analogs of the phosphoinositol monophosphates. I tested the hypothesis that phosphate position was mediating TMEM16A current recovery. I first assessed if the phosphate at position 4 was indeed important for TMEM16A to conduct Cl<sup>-</sup> currents. I applied the water-soluble analog of phosphatidyl 4-monophosphate (diC8-PI(4)P) to excised inside-out patches after current had stably rundown. I recorded TMEM16A-conducted currents at -60 mV before and during application of 100 μM diC8-PI(4)P. In nine separate trials, I observed that 100 μM diC8-PI(4)P application recovered  $2.1 \pm 0.2$ -fold current (Figure 4-1C). The currents recovered by diC8-PI(4)P were similar albeit smaller than the fold recovery observed when diC8-PI(4,5)P<sub>2</sub> was applied (Figure 4-1C) which was consistent with the idea that the 4 position was important for TMEM16A current recovery. Figure 4-1G depicts an example plot of TMEM16A-conducted currents recorded at -60 mV versus time before and during diC8-PI(4)P application. Albeit recovering less current than diC8-PI(4,5)P<sub>2</sub>, diC8-PI(4)P showed an intermediate recovery (lying between  $3.6 \pm 0.5$ -fold current recovered by diC8-PI(4,5)P<sub>2</sub> with Ca<sup>2+</sup> and  $1.4 \pm 0.2$ -fold current recovered by diC8-PI with Ca<sup>2+</sup> (Figure 4-1C)).

Next, I assessed if having phosphates at positions 3 and 5 of the inositol head would also result in TMEM16A current recovery. I applied the water-soluble analog of phosphatidyl 3-monophosphate (diC8-PI(3)P) to excised inside-out patches after current had stably rundown. I

recorded TMEM16A-conducted currents at -60 mV before and during application of 100  $\mu$ M diC8-PI(3)P and observed  $1.5 \pm 0.3$ -fold current recovery in five separate trials. Figure 4-1H depicts an example plot of TMEM16A-conducted currents recorded at -60 mV versus time before and during diC8-PI(3)P application. diC8-PI(3)P recovered less current than both diC8-PI(4,5)P<sub>2</sub> and diC8-PI(4)P. This was also true for diC8-PI(5)P. I also recorded TMEM16A-conducted currents at -60 mV before and during application of 100  $\mu$ M diC8-PI(5)P. In five separate trials I observed that diC8-PI(5)P only recovered  $1.3 \pm 0.1$ -fold current (Figure 4-1C). Figure 4-1I depicts an example plot of TMEM16A-conducted currents recorded at -60 mV versus time before and during diC8-PI(5)P application. I observed a lower fold recovery for diC8-PI(5)P than diC8-PI(4)P even though PI(4,5)P<sub>2</sub> is composed of phosphates at position 4 and 5. Notably, application of diC8-PI(3,5)P<sub>2</sub> (Figure 4-1C) did not recover substantial currents which was consistent with our observation here that neither diC8-PI(3)P nor diC8-PI(5)P recovered TMEM16A currents. Overall, the phosphoinositide data collected demonstrated that diC8-PI(4)P, diC8-PI(3,4)P<sub>2</sub> and diC8-PIP<sub>3</sub> recovered intermediate or similar current to diC8-PI(4,5)P<sub>2</sub>. Each of these phosphoinositides has a phosphate at position 4 of the inositol head.

Across all the phosphoinositides tested, I observed that having a phosphate at position 4 of the inositol head elevated the TMEM16A current recovered. These data suggest that TMEM16A interacts with PI(4,5)P<sub>2</sub> in a way relying on the phosphate at position 4 is to keep TMEM16A channels open.

### 4.2.3 The *Xenopus* voltage sensing phosphatase does not completely inhibit TMEM16A currents

My findings thus far suggested that the phosphate at position 4 was critical for the recovery of TMEM16A currents recorded following rundown. Next, I explored the importance of the phosphate at this position further. I reasoned that if the phosphate at position 4 was the most important for PI(4,5)P<sub>2</sub> regulation of TMEM16A then removal of the phosphate at position 5 should not substantially alter current. To test this hypothesis, I expressed the *Xenopus laevis* voltage sensing phosphatase (Xl-VSP) in excised patches (Figure 4-2A). After confirming VSP expression (Figure 4-2B) I proceeded to record TMEM16A Ca<sup>2+</sup>-evoked Cl<sup>-</sup> currents. In five independent trials, I recorded TMEM16A-conducted currents at -60 mV before and during the application of 2 mM Ca<sup>2+</sup> in patches while activating Xl-VSP at depolarizing potentials (+60 mV). I observed that the rate of current rundown in patches expressing Xl-VSP at the membrane was an average rate of 61.2 ± 3.0 s (Table 4-1) and was not significantly different compared to control current rundown which ran down at an average rate of 86.0 ± 1.6 s (Figure 4-2C). Figure 4-2D depicts an example plot of TMEM16A-conducted currents recorded at -60 mV versus time after activating Xl-VSP. Unlike others who reported a significant depletion in TMEM16A conducted currents after activating a VSP [68, 78], I observed a slight depletion of TMEM16A conducted currents. The lack of significant difference in the rate of TMEM16A current depletion by the VSP is consistent with the hypothesis that the phosphate at position 4 is important for TMEM16A regulation.

#### 4.2.4 Lowering applied intracellular $\text{Ca}^{2+}$ concentration slows current rundown

Despite finding that phosphate position is important in mediating TMEM16A-PI(4,5) $\text{P}_2$ , none of the phosphoinositides containing a phosphate at position 4 of the inositol head were able to completely recover TMEM16A currents. Aside from membrane phosphatases dephosphorylating PI(4,5) $\text{P}_2$  and thereby depleting it, I hypothesize that  $\text{Ca}^{2+}$  may be acting on the patch by a TMEM16A-independent mechanism to speed PI(4,5) $\text{P}_2$  decay in excised patches.

I then asked if current rundown was independent of the  $\text{Ca}^{2+}$  concentration. I sought to assess the rate of rundown using various concentrations of  $\text{Ca}^{2+}$  to test my hypothesis that  $\text{Ca}^{2+}$ -evoked TMEM16A  $\text{Cl}^-$  currents would rundown in lower concentrations of  $\text{Ca}^{2+}$ . I recorded TMEM16A currents during 100-150-ms steps to -60 mV and +60 mV. I observed that lowering the concentrations of  $\text{Ca}^{2+}$  affected my ability to activate the channel. For instance, 2 mM  $\text{Ca}^{2+}$  resulted in peak TMEM16A currents almost immediately after  $\text{Ca}^{2+}$  application (Figure 4-3A) but 20  $\mu\text{M}$   $\text{Ca}^{2+}$  did not activate TMEM16A channels (Figure 4-3B). By contrast 50  $\mu\text{M}$   $\text{Ca}^{2+}$  activated TMEM16A channels whose currents delayed to peak (Figure 4-3C). However, when I applied 100  $\mu\text{M}$   $\text{Ca}^{2+}$  (Figure 3D) or 500  $\mu\text{M}$   $\text{Ca}^{2+}$  (Figure 4-3E), I observed currents that peaked within seconds of  $\text{Ca}^{2+}$  application (Figure 3F). 100  $\mu\text{M}$  is a reported saturating concentration for mTMEM16A [136]. Interestingly, I found that even though 100  $\mu\text{M}$   $\text{Ca}^{2+}$  could activate xTMEM16A, these currents ran down at a rate of  $755 \pm 388$  s which is much slower than the control which ran down at a rate of  $86 \pm 7.6$  s (Figure 4-4A). Figure 4-4B depicts an example plot of normalized TMEM16A-conducted currents recorded at -60 mV versus time before and during 100  $\mu\text{M}$   $\text{Ca}^{2+}$  application.

As done with 100  $\mu\text{M}$ , I recorded TMEM16A currents during 100-150-ms steps to -60 mV and +60 mV. I found that at this concentration of  $\text{Ca}^{2+}$ , TMEM16A currents ran down at a rate of  $216.3 \pm 45$  s, which was faster than the currents recorded at 100  $\mu\text{M}$   $\text{Ca}^{2+}$ , but still ran down slower than the controls recorded during 2 mM  $\text{Ca}^{2+}$  application (Figure 4-4A). Figure 4-4C depicts an example plot of TMEM16A-conducted currents recorded at -60 mV versus time before and during 500  $\mu\text{M}$   $\text{Ca}^{2+}$  application. Despite TMEM16A currents running down at 100 and 500  $\mu\text{M}$   $\text{Ca}^{2+}$ , the rate of TMEM16A current rundown was slower than observed at 2 mM  $\text{Ca}^{2+}$  (Figure 4-4B). These data suggest that high  $\text{Ca}^{2+}$  concentrations speed TMEM16A current rundown.

To further evaluate the effect of the 2 mM  $\text{Ca}^{2+}$  on the rate of current rundown, I recorded TMEM16A conducted currents during 100-150-ms steps to -60 mV and +60 mV while alternating the application 2 mM  $\text{Ca}^{2+}$  and 0 mM  $\text{Ca}^{2+}$ . I reasoned that if 2 mM  $\text{Ca}^{2+}$  was speeding rundown then short applications of 2 mM  $\text{Ca}^{2+}$  could enable me to speed rundown during application intervals. I recorded TMEM16A currents during 100-150-ms steps to -60 mV and +60 mV before and during the alternating application of 2 mM  $\text{Ca}^{2+}$  and 0 mM  $\text{Ca}^{2+}$  during 10 s intervals. In four independent trials, I observed substantial current rundown. Figure 4-4D depicts an example plot of TMEM16A-conducted currents recorded at -60 mV versus time before and during alternating between 2 mM  $\text{Ca}^{2+}$  and 0 mM  $\text{Ca}^{2+}$  application. I evaluated the rate of current rundown by also fitting the traces with a single exponential. I observed that even short exposures to 2 mM  $\text{Ca}^{2+}$  sped current rundown so that it was  $47.1 \pm 4.9$  s which is slightly faster than observed for the 2 mM  $\text{Ca}^{2+}$  controls (Figure 4-4B). These data suggest that indeed the high concentration of  $\text{Ca}^{2+}$  is speeding current rundown.

#### 4.2.5 Complete $\text{Ca}^{2+}$ substitution slows TMEM16A current rundown

The finding that  $\text{PI}(4,5)\text{P}_2$  depletion resulted in TMEM16A current rundown, and that 2 mM  $\text{Ca}^{2+}$  sped rundown suggested that there could be a relationship between  $\text{PI}(4,5)\text{P}_2$  depletion and  $\text{Ca}^{2+}$  concentration. Lower concentrations of  $\text{Ca}^{2+}$  also have slower rates of rundown (Figure 4-4). Therefore, it is possible that  $\text{Ca}^{2+}$  itself is acting to speed  $\text{PI}(4,5)\text{P}_2$  depletion in inside-out excised patches.  $\text{Ca}^{2+}$  is a cell signaling molecule that can have vast effects on cell signaling that could be contributing to its ability to speed rundown. Thus, I reasoned that if  $\text{Ca}^{2+}$  was acting in a TMEM16A independent mechanism then a complete substitution of  $\text{Ca}^{2+}$  with other divalent cations that activate the channel should slow TMEM16A current rundown to illustrate a specific role for  $\text{Ca}^{2+}$  [50, 144, 145]. I tested this hypothesis by quantifying the rate of TMEM16A rundown during the application of the divalent cation  $\text{Ni}^{2+}$ . I began these experiments by recording TMEM16A-conducted currents before and during the application of 2 mM  $\text{Ni}^{2+}$ . In five independent trials, I observed that TMEM16A current ran down slower than the  $\text{Ca}^{2+}$  controls at an average rate of  $468.6 \pm 176$  s (Figure 4-5A). Figure 4-5B depicts an example plot of current versus time at -60 mV before and during the application of 2 mM  $\text{Ni}^{2+}$ . Substituting 2 mM  $\text{Ca}^{2+}$  with 2 mM  $\text{Ni}^{2+}$  slowed TMEM16A current rundown suggesting that  $\text{Ca}^{2+}$  not  $\text{Ni}^{2+}$  is capable of increasing  $\text{PI}(4,5)\text{P}_2$  depletion.

Altogether, I have observed that  $\text{Ni}^{2+}$  activated TMEM16A and slowed current rundown. At this concentration of  $\text{Ni}^{2+}$ , TMEM16A currents are observed within a few seconds of application of  $\text{Ni}^{2+}$  and begin to rundown shortly after peaking. However, unlike 2 mM  $\text{Ca}^{2+}$ ,  $\text{Ni}^{2+}$  slowed current rundown despite being applied at the same ionic concentration as  $\text{Ca}^{2+}$ . These data suggest that  $\text{Ca}^{2+}$  has unique effects on the patch that are not replicated by  $\text{Ni}^{2+}$ . Nevertheless, these data point to  $\text{Ca}^{2+}$  regulating TMEM16A currents in a  $\text{Ca}^{2+}$  concentration dependent way.

Together, these findings reveal that  $\text{Ca}^{2+}$  speeds current rundown in a channel-independent mode. This is consistent with my hypothesis that high  $\text{Ca}^{2+}$  concentrations speed TMEM16A current rundown, but how this relates TMEM16A channels closing is yet to be determined.

#### **4.2.6 Inhibition of phospholipase C (PLC) slows rundown**

One possible mechanism by which  $\text{Ca}^{2+}$  can speed  $\text{PI}(4,5)\text{P}_2$  depletion in excised patches is by activation of membrane anchored phospholipase C. Given that I previously reported that the addition of 2 mM  $\text{Ca}^{2+}$  supplemented with 1.5 mM Mg-ATP or 50 mM  $\beta\text{GP}$  slowed TMEM16A current rundown (Figure 3-5), it is likely that PI-4 and PI-5 phosphatases contribute to  $\text{PI}(4,5)\text{P}_2$  depletion in excised patches. However, the inability for 1.5 mM Mg-ATP or  $\beta\text{GP}$  to completely prevent TMEM16A current rundown suggested that another membrane component may also contribute to  $\text{PI}(4,5)\text{P}_2$  depletion.

$\text{Ca}^{2+}$  is a master signaling molecule playing an essential role in mediating responses to cellular signals, GPCRs and other cell receptors [146].  $\text{Ca}^{2+}$  also activates ion channels either by directly binding to them or binding adaptor proteins which in turn activate ion channels [147].  $\text{Ca}^{2+}$  also promotes phospholipase C (PLC) activity which results in the hydrolysis of  $\text{PI}(4,5)\text{P}_2$  into DAG and  $\text{IP}_3$  [148, 149].

I reasoned that 2 mM  $\text{Ca}^{2+}$  could activate some PLC isoforms to cause  $\text{PI}(4,5)\text{P}_2$  depletion to speed rundown of TMEM16A currents in excised patches (Figure 4-6A). To test this hypothesis, I recorded TMEM16A  $\text{Ca}^{2+}$ -evoked  $\text{Cl}^-$  currents during the application of 2 mM  $\text{Ca}^{2+}$  supplemented with the general PLC inhibitor U-73122 [150, 151]. I recorded TMEM16A  $\text{Ca}^{2+}$ -evoked  $\text{Cl}^-$  currents during the application of 2 mM  $\text{Ca}^{2+}$  supplemented with 1  $\mu\text{M}$  U-73122. I observed that in the presence of both 2 mM  $\text{Ca}^{2+}$  and U-73122, current rundown was slowed. In

five independent trials, the average rate of current rundown was  $253 \pm 83$  s (Figure 4-6B). Figure 6C depicts an example plot of current versus time at -60 mV before and during the application of 2 mM  $\text{Ca}^{2+}$  supplemented with 1  $\mu\text{M}$  U73122. These data suggest that a PLC contributes to the rate of TMEM16A current rundown by speeding it. Thus, not only can  $\text{Ca}^{2+}$  bind TMEM16A to activate it,  $\text{Ca}^{2+}$  can activate  $\text{Ca}^{2+}$  sensitive PLCs to attenuate TMEM16A activity at high concentrations in inside-out excised patches. Therefore, TMEM16A channels are regulated by  $\text{PI}(4,5)\text{P}_2$ , whose rate of depletion is dependent on the activity of a  $\text{Ca}^{2+}$ -sensitive PLC.

Next, I evaluated the effects of U-73343, the inactive analog of U-73122, on current rundown. I recorded TMEM16A  $\text{Ca}^{2+}$ -evoked  $\text{Cl}^-$  currents during the application of 2 mM  $\text{Ca}^{2+}$  supplemented with U-73343 [150, 151]. I observed that in the presence of both 2 mM  $\text{Ca}^{2+}$  and 1  $\mu\text{M}$  U-73343, TMEM16A currents ran down quite quickly. In four independent trials, the current rundown at a rate of  $128 \pm 38$  s which was not different from the controls that ran down at a rate of  $86 \pm 7.6$  s (Figure 4-6B). Figure 4-6D depicts an example plot of normalized current versus time at -60 mV before and during the application of 2 mM  $\text{Ca}^{2+}$  supplemented with 1  $\mu\text{M}$  U73343. Admittedly, U-73343 also slowed current rundown although this effect was not significant. Because the rate of current rundown was not significantly different from the control, I decided to use U-73343 as a control for U-73122. These data suggest that a PLC contributes to the rate of TMEM16A current rundown by speeding it. Thus, not only can  $\text{Ca}^{2+}$  bind TMEM16A to activate it,  $\text{Ca}^{2+}$  can activate  $\text{Ca}^{2+}$  sensitive PLCs to attenuate TMEM16A activity at high concentrations in inside-out excised patches. Therefore, TMEM16A channels are regulated by  $\text{PI}(4,5)\text{P}_2$ , whose rate of depletion is dependent on the activity of a  $\text{Ca}^{2+}$ -sensitive PLC.

### 4.3 Discussion

By recording TMEM16A currents in the presence of different phosphoinositides or altering  $\text{Ca}^{2+}$  concentrations, here I demonstrate that TMEM16A is tightly regulated via its need for the phosphate at the 4 position in  $\text{PI}(4,5)\text{P}_2$  and the activation of a  $\text{Ca}^{2+}$ -sensitive PLC in these inside-out excised patches. The requirement for both  $\text{PI}(4,5)\text{P}_2$  and  $\text{Ca}^{2+}$  was established [68, 78, 128] but the mechanism behind this  $\text{Ca}^{2+}$ -TMEM16A- $\text{PI}(4,5)\text{P}_2$  relationship was not clearly established. Here, I sought to determine  $\text{Ca}^{2+}$  and  $\text{PI}(4,5)\text{P}_2$ 's contributions to this relationship. TMEM16A's  $\text{Ca}^{2+}$  binding sites and their properties have already been determined [44, 47, 48, 50, 152-154]. Similarly,  $\text{PI}(4,5)\text{P}_2$  binding sites have proposed [136, 137]. Here, I uncover the characteristics of  $\text{PI}(4,5)\text{P}_2$  that mediate TMEM16A regulation and establish how  $\text{Ca}^{2+}$  acts to regulate the channel and  $\text{PI}(4,5)\text{P}_2$  in a channel independent mechanism.

#### 4.3.1 Phosphate position is key in mediating TMEM16A- $\text{PI}(4,5)\text{P}_2$ interaction

Application of soluble phosphoinositide analogs containing phosphates recovered TMEM16A conducted currents following rundown when applied in the presence of  $\text{Ca}^{2+}$ , and the extent of recovery was dependent on whether a phosphate was present at position 4 of the inositol head (Figure 4-1). Not all TMEM16A current was recovered, but greater TMEM16A current recovery was observed in the presence of phosphoinositides with a phosphate at position 4 of the phosphoinositide head than phosphoinositides lacking a phosphate at position 4 of the inositol head. The phosphoinositides that recovered TMEM16A currents, namely, diC8- $\text{PI}(4,5)\text{P}_2$ , diC8- $\text{PI}(3,4)\text{P}_2$  and diC8- $\text{PI}(3,4,5)\text{P}_3$  could be recovering currents due to their shorter vicinal distances between phosphates compared to  $\text{PI}(3,5)\text{P}_2$  where the phosphates are much farther apart. However,

diC8-PI(4)P recovered TMEM16A currents while lacking the benefits of phosphates being closer together. Instead, it is possible that the phosphate at position 4 may fit the two-step model proposed by others [137]. In this model, there are three PI(4,5)P<sub>2</sub> binding sites located on TMEM16A containing basic residues that when neutralized reduce PI(4,5)P<sub>2</sub> sensitivity [137]. Perhaps the phosphate at position 4 interacts more readily with one of these PI(4,5)P<sub>2</sub> binding sites due to spatial proximity, and this specific site could be responsible for opening TMEM16A channels by forcing the Cl<sup>-</sup> pore open while the other two phosphate sites just enhance the opening of a pore already made big enough to pass Cl<sup>-</sup> by the phosphate at position 4 on the inositol head.

Surprisingly, diC8-PI(4)P recovered substantial TMEM16A currents whereas diC8-PI(5)P did not. The currents recovered by these monophosphates were not additive for currents recovered by PI(4,5)P<sub>2</sub>. It is possible that without a phosphate at the 4 position of the inositol head, PI(5)P does not access phosphoinositide binding sites. Alternatively, PI(5)P's contribution to TMEM16A's interaction with PI(4,5)P<sub>2</sub> may be based on its negative charge and not its actual position. Having the additional negative charge on PI(4,5)P<sub>2</sub> may help the stay pore in an open conformation [45, 46]. PI(3)P recovered little currents.

TMEM16A prefers PI(4,5)P<sub>2</sub> and PI(4)P over PI [90]. This supports the hypothesis that PI(4,5)P<sub>2</sub> possibly carries out its interaction with TMEM16A by first interacting with the phosphate at position 4. XI-VSP (Figure 4-2) trended toward speeding rundown and not completely eliminating TMEM16A currents. This is consistent with the idea that the phosphate at the 4 position on PI(4,5)P<sub>2</sub> makes the provision for PI(4,5)P<sub>2</sub> to interact with TMEM16A. Similarly, activation of another voltage sensing phosphatase, Dr-VSP, in mouse TMEM16A (mTMEM16A) expressing HEK293 cells reportedly resulted in the reduction of mTMEM16A Ca<sup>2+</sup>-evoked Cl<sup>-</sup> currents [68, 78]. As I observed in my XI-VSP experiments, Dr-VSP was unable

to obliterate mTMEM16A  $\text{Ca}^{2+}$ -evoked  $\text{Cl}^-$  currents [68, 78]. It is possible that the ratio of VSP expressed versus the concentration of  $\text{PI}(4,5)\text{P}_2$  in any one of these cells used is not sufficient to completely get rid of TMEM16A currents. However, the finding that  $\text{PI}(4)\text{P}$  alone can recover TMEM16A currents favors the idea that even if the VSPs did dephosphorylate all the  $\text{PI}(4,5)\text{P}_2$ , they would leave just as much  $\text{PI}(4)\text{P}$  which on its own, can potentiate TMEM16A currents.

#### **4.3.2 $\text{Ca}^{2+}$ concentration determines the rate of TMEM16A current rundown**

With  $\text{PI}(4,5)\text{P}_2$  as making up 1-3% of the plasma membrane [141] and  $\text{Ca}^{2+}$  reaching concentrations as high as 400  $\mu\text{M}$  in *X. laevis* oocyte [138], TMEM16A channels must employ additional regulatory mechanisms to prevent unnecessary activation from distorting the many physiological roles it plays. I speculate that TMEM16A channels use a combination of regulatory mechanisms to help determine whether to open and pass  $\text{Cl}^-$ . In addition to requiring a phosphate at position 4 of the inositol head in phosphoinositides, TMEM16A channels need  $\text{Ca}^{2+}$  to become activated (Figure 4-1). However, how TMEM16A distinguishes between  $\text{Ca}^{2+}$  signals for other cellular functions versus its own has not been determined. Here, I show that different concentrations of  $\text{Ca}^{2+}$  produce different TMEM16A current profiles. High  $\text{Ca}^{2+}$  concentrations open TMEM16A channels quickly and result in the channels closing immediately after (Figure 4-3 and 4-4). Low  $\text{Ca}^{2+}$  concentrations open TMEM16A channels slowly and result in the channels closing slowly over time (Figure 4-4). From these data, I speculate that TMEM16A channels are regulated by  $\text{Ca}^{2+}$  concentration. In particular, the *X. laevis* oocyte which eventually matures into an egg [155], must have a tight regulation of TMEM16A channels since they are important channels in preventing embryonic lethality during the early stages of egg fertilization [156].

To better examine  $\text{Ca}^{2+}$ 's role in determining the rate of TMEM16A current rundown, I evaluated the effects of other divalents on TMEM16A current rundown. I found that  $\text{Ni}^{2+}$  slowed TMEM16A current rundown (Figure 4-5). Since  $\text{Ni}^{2+}$  activates TMEM16A and  $\text{Ni}^{2+}$  is a  $\text{Ca}^{2+}$ -independent mechanism of activating the channel, the data demonstrate that indeed TMEM16A current rundown is sped by high  $\text{Ca}^{2+}$  concentrations. These data also point to  $\text{Ca}^{2+}$  playing another role in the cell aside from activating TMEM16A.  $\text{Ca}^{2+}$  could be depleting  $\text{PI}(4,5)\text{P}_2$  in excised inside-out patches.  $\text{PI}(4,5)\text{P}_2$  can be depleted by its hydrolysis into  $\text{IP}_3$  and DAG by PLC in a  $\text{Ca}^{2+}$ -dependent manner [148, 149]. It is possible that  $\text{Ca}^{2+}$  promotes  $\text{PI}(4,5)\text{P}_2$  hydrolysis in the excised inside-out patches and in doing so, reduces the available  $\text{PI}(4,5)\text{P}_2$  able to form electrostatic interactions with the TMEM16A  $\text{PI}(4,5)\text{P}_2$  binding sites [136, 137]. This is consistent with the data showing that inhibiting PLCs with U-73122 slows current rundown (Figure 4-5).

Although the data presented suggest that  $\text{Ca}^{2+}$  can both activate TMEM16A and inhibit its activation by depleting  $\text{PI}(4,5)\text{P}_2$ , the exact mechanisms behind this two-tier regulation of TMEM16A has yet to be determined. A possible explanation for  $\text{Ca}^{2+}$ 's ability to speed current rundown at high concentrations of  $\text{Ca}^{2+}$  is that at high concentrations of  $\text{Ca}^{2+}$  there is enough  $\text{Ca}^{2+}$  to both activate TMEM16A and also PLCs [149]. Alternatively,  $\text{Ca}^{2+}$  at high concentrations could act like  $\text{Mg}^{2+}$ , which has been reported to scavenge  $\text{PI}(4,5)\text{P}_2$  by coordinating it via electrostatic interactions [157-160]. This phenomenon of charge shielding of  $\text{PI}(4,5)\text{P}_2$  has been reported for  $\text{Mg}^{2+}$  and  $\text{Ca}^{2+}$  [149]. Increasing the concentration of these divalents or polyamines carrying high positive charges results in reduced PLC activity for PLC subtypes  $\beta$ ,  $\delta$  and  $\gamma$  [149, 161]. However, at millimolar concentrations of these divalents, PLC activity is still as high as ~60% [149] for  $\text{PLC}\beta$  and  $\text{PLC}\gamma$ , which are the only subtypes of PLC expressed in *X. laevis* [125, 162, 163]. Therefore, it seems unlikely that  $\text{Ca}^{2+}$  is preventing  $\text{PI}(4,5)\text{P}_2$  hydrolysis at 2 mM  $\text{Ca}^{2+}$  in the

context of the fast rate of current rundown observed in my experiments. Moreover, U-73122 should not have slowed current rundown if PLCs did not play a role in speeding current rundown. The inactive analog of the PLC inhibitor, U-73343, slightly slowed current rundown but not significantly (Figure 4-5). These data suggest that a PLC is playing a role in speeding current rundown.

#### **4.3.3 Mechanism of TMEM16A regulation and the $\text{Ca}^{2+}$ -TMEM16A-PI(4,5) $\text{P}_2$ relationship**

TMEM16A seemingly combines inputs from PI(4,5) $\text{P}_2$ ,  $\text{Ca}^{2+}$  and membrane potential to determine channel conformation state. This multimodal regulation of TMEM16A seems to be a feature shared with other TMEM16 family members. TMEM16A shares voltage regulation with the CaCC TMEM16B [63, 64]. However, TMEM16B is instead inhibited by PI(4,5) $\text{P}_2$  rather than potentiated [7]. PI(4,5) $\text{P}_2$  regulates TMEM16F gating such that applying PI(4,5) $\text{P}_2$  results in increased TMEM16F currents [73] of the reported cation channel [164]. These differences in TMEM16 channel regulation suggest a complex regulation of TMEM16A channel activity.

Just like TMEM16F, TMEM16A interacts with PI(4,5) $\text{P}_2$  through electrostatic interactions [73]. TMEM16A contains positively charged amino acids that when mutated reduce TMEM16A's sensitivity to PI(4,5) $\text{P}_2$  or prevent TMEM16A's activation altogether [73, 136]. Even though PI(4,5) $\text{P}_2$  uses negative charges to allow this PI(4,5) $\text{P}_2$ -TMEM16A, my data have determined that just the negative charges on the phosphate groups alone are not sufficient to enable this interaction. Therefore, it is possible that specific residues on TMEM16A interacting with the phosphate at the position 4 of the inositol head control this interaction. Consistent with this idea, diC8-PIP<sub>3</sub>, PI(3,4) $\text{P}_2$  and PI(3,5) $\text{P}_2$  trended toward less current recovery than diC8-PI(4,5) $\text{P}_2$  (Figure 4-1).

#### 4.3.4 Other mechanisms regulating TMEM16A gating

At low  $\text{Ca}^{2+}$ ,  $\text{Ca}^{2+}$ 's ability to bind the channel is voltage dependent. Regardless, TMEM16A currents are greater at positive membrane potentials showing TMEM16A's voltage regulation [165]. When high  $\text{Ca}^{2+}$  is applied, both positive and negative membrane potentials result in robust TMEM16A currents and the voltage dependence is reduced [165]. Other than  $\text{Ca}^{2+}$ , TMEM16A channel activity is modified by alternative splicing [74] volume [74, 75], acid [76], cholesterol [77, 78], heat [79], and phosphoinositides [80-82]. These proposed mechanisms do not preclude the need for  $\text{Ca}^{2+}$  or  $\text{PI}(4,5)\text{P}_2$ . However, another proposed regulator, the  $\text{Ca}^{2+}$ -activated  $\text{Cl}^-$  channel regulator 1 (CLCA1) does not need  $\text{Ca}^{2+}$  or  $\text{PI}(4,5)\text{P}_2$  [124, 166]. CLCA1 reportedly regulates TMEM16A by preventing its internalization and degradation at the lysosome [124, 166].

Even in the presence of all these other modulators of TMEM16A, at a minimum, TMEM16A requires both  $\text{PI}(4,5)\text{P}_2$  and  $\text{Ca}^{2+}$  to conduct  $\text{Cl}^-$  currents [90]. These other inputs can modify the activity of TMEM16A by reducing it or increasing it, but they cannot by themselves result in TMEM16A conducted  $\text{Cl}^-$  currents.  $\text{Ca}^{2+}$  and  $\text{PI}(4,5)\text{P}_2$  interact with residues on TMEM16A and together force the necessary shifts in the TMEM16A channel parts that open the  $\text{Cl}^-$  pore that would otherwise remain too small for  $\text{Cl}^-$  passage [45, 46].

#### 4.3.5 Summary

TMEM16A activity underlies basic cellular activity including neuronal firing and heart contractions. As such TMEM16A dysfunction could be a threat against life. TMEM16A is capable of promoting life by preventing perinatal lethality during early development [100]. TMEM16A works to our benefit. However, when dysfunctional or overworking, as is the case in hypertension,

[131] or overexpressed, as is the case in cancer [167], TMEM16A becomes an adversary working to reduce our quality of life. By understanding how TMEM16A is regulated, we can target these regulatory mechanisms for therapy in disease conditions associated with TMEM16A. Before effective therapy can be designed a clear and complete picture of TMEM16A's regulation must be obtained.

#### **4.4 Figures and tables**

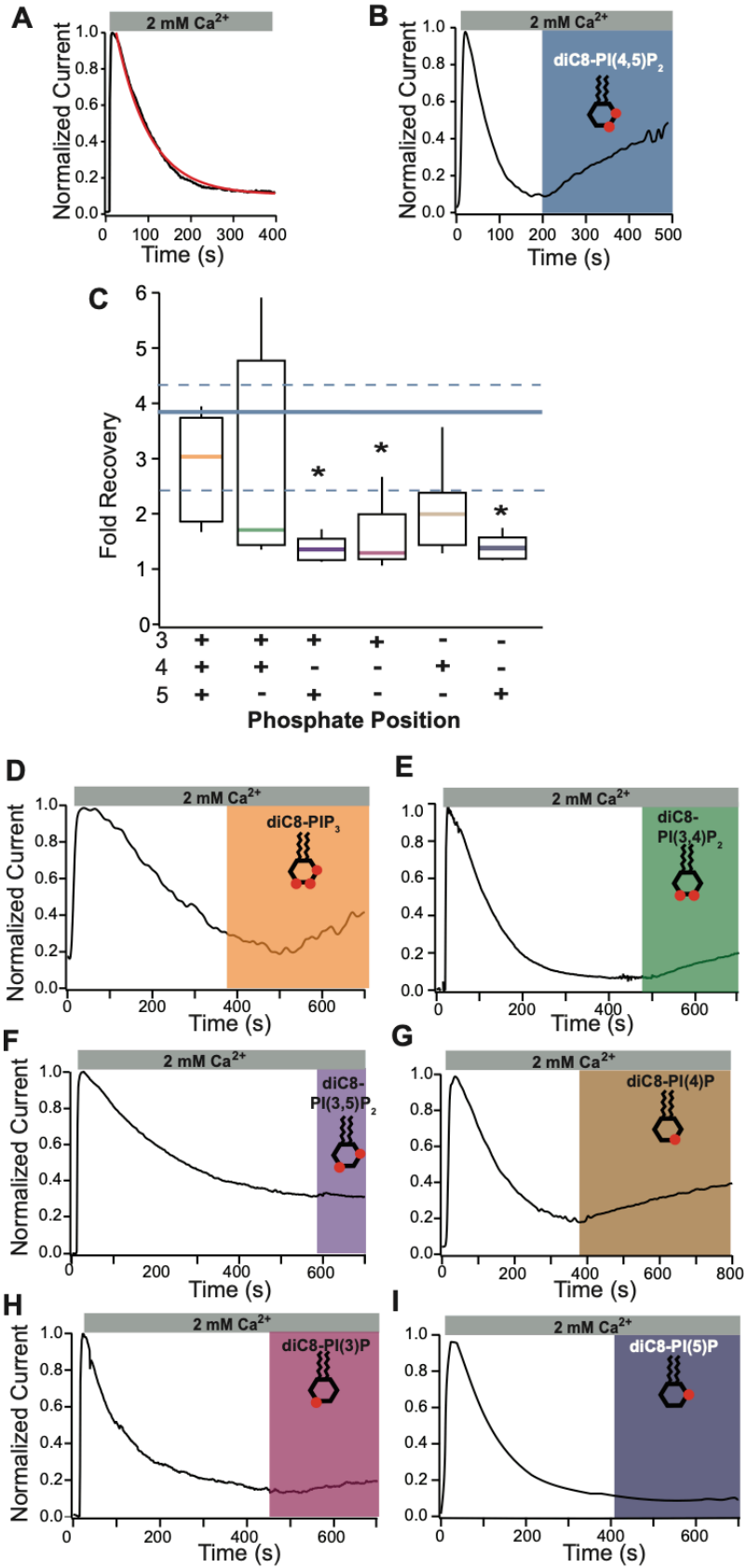


#### Figure 4-1. Phosphate position is key mediating TMEM16A-PI(4,5)P<sub>2</sub> interaction

Water-soluble analogs of the membrane phosphoinositides were applied to inside-out excised patches once current had stably rundown. Currents were recorded at -60 mV. (A) Representative plot of normalized current fit with a single exponential (red line) recorded during 100-150 ms steps to -60 versus time, after patch excision. 2 mM Ca<sup>2+</sup> was applied at 10 s as denoted by the grey bar. (B) Representative plot of normalized currents versus time, before and during application of 100 μM diC8-PI(4,5)P<sub>2</sub> with 2 mM Ca<sup>2+</sup>. (C) Box plot distribution of the fold current recovered after the application of 100 μM diC8-PI(3,4,5)P<sub>3</sub> with added Ca<sup>2+</sup> (N=5), 100 μM diC8-PI(3,4)P<sub>2</sub> with added Ca<sup>2+</sup> (N=5), 100 μM diC8-PI(3,4)P<sub>2</sub> with added Ca<sup>2+</sup> (N=5), 100 μM diC8-PI(3)P with added Ca<sup>2+</sup> (N=5), 100 μM diC8-PI(4)P with added Ca<sup>2+</sup> (N=9) and 100 μM diC8-PI(5)P with added Ca<sup>2+</sup> (N=5). The fold change in current recovered was calculated as change in current upon application of each phosphoinositide with Ca<sup>2+</sup>. The blue lines denote the box plot distribution of fold current recovered from patches recorded with 100 μM diC8-PI(4,5)P<sub>2</sub> with Ca<sup>2+</sup>, where the solid blue line represents the median value and the dashed lines represent the control data distribution from 25-75%. Representative plots of normalized currents versus time, before and during application of diC8-PIP<sub>3</sub> with added Ca<sup>2+</sup> (D), diC8-PI(3,4)P<sub>2</sub> with added Ca<sup>2+</sup> (E), diC8-PI(3,4)P<sub>2</sub> with added Ca<sup>2+</sup> (F), diC8-PI(4)P with added Ca<sup>2+</sup> (G), diC8-PI(3)P with added Ca<sup>2+</sup> (H) and diC8-PI(5)P with added Ca<sup>2+</sup> (I). \* indicates a *P* < 0.05 as determined by t-test.

**Table 4-1. Ca<sup>2+</sup> activates PLC to speed patch rundown**

<b>Condition</b>	<b>Concentration</b>	<b>Tau, <math>\tau</math> (s)</b>	<b>Number of trials</b>
Control (Ca <sup>2+</sup> )	2 mM	86 ± 7.6	N = 9
XI-VSP	---	61.2 ± 3.0	N = 5
Ca <sup>2+</sup>	100 $\mu$ M	755 ± 388	N = 5
Ca <sup>2+</sup>	500 $\mu$ M	216.3 ± 45	N = 5
Alternating 2 mM and 0 mM Ca <sup>2+</sup>	0 and 2 mM	47.1 ± 4.9	N = 4
Ni <sup>2+</sup>	2 mM	468.6 ± 176	N = 5
Mg <sup>2+</sup>	2 mM	---	N = 5
U-73343	1 $\mu$ M	128 ± 38	N = 4
U-73122	1 $\mu$ M	253 ± 83	N = 5

The mean ± SEM for the indicated measurements taken from excised inside-out patches. The  $\tau$  was obtained by fitting plots of the currents versus time with single exponential functions.

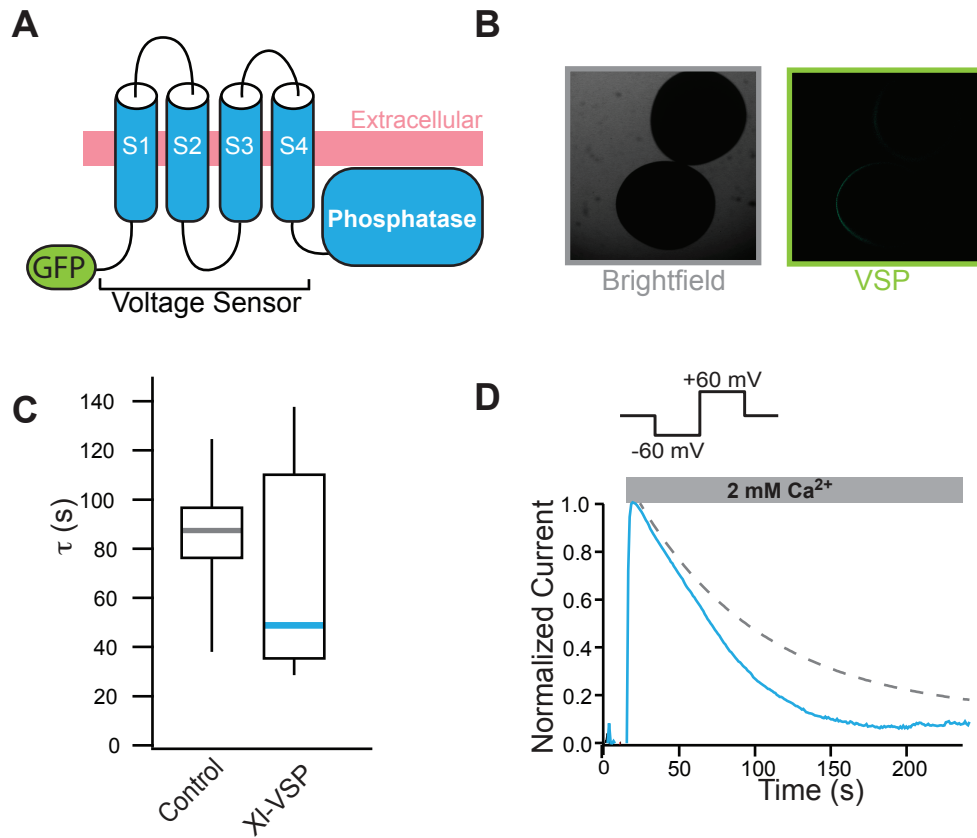


**Figure 4-2. XI-VSP speeds TMEM16A current rundown but does not abolish TMEM16A currents**

Inside-out patch clamp recordings were conducted on macropatches excised from *X. laevis* oocytes expressing XI-VSP. (A) Schematic depicting a VSP tagged with GFP. (B) Confocal images depicting VSP expression at the plasma membrane of an oocyte. (C) Box plot distribution of the rate of current decay ( $\tau$ ), measured by fitting plots of relative current versus time with single exponentials for the control (N=9) and VSP expressing (N=5). The central line denotes the median, the box denotes the distribution of 25-75 % of the data, and the whiskers represent 10-90 % of the data. (D) *Top*: voltage protocol used to activate the VSP. *Bottom*: representative plot of normalized currents versus time following VSP activation. The grey dashed line represents a predicted control representing the control traces.

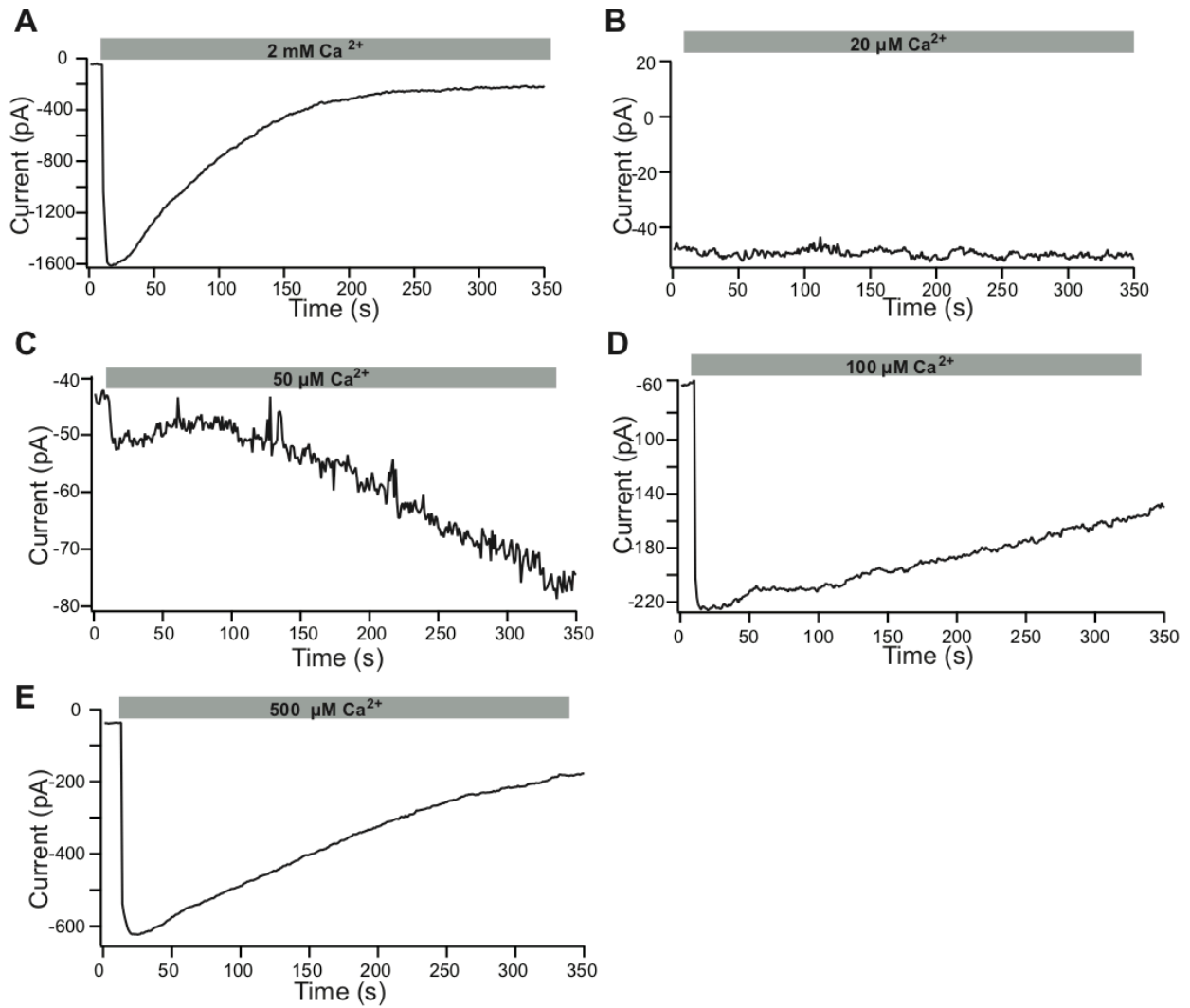


**Figure 4-3. Different concentrations of  $\text{Ca}^{2+}$  result in different TMEM16A current profiles**

Inside-out patch clamp recordings were conducted on macropatches excised from *X. laevis* oocytes during the application of  $\text{Ca}^{2+}$ . Representative nominal currents recorded during 100-150 ms steps to -60 mV before, during and after the application of  $\text{Ca}^{2+}$  at 2 mM (A), 20  $\mu\text{M}$  (B), 50  $\mu\text{M}$  (C), 100  $\mu\text{M}$  (D) and 500  $\mu\text{M}$  (E).

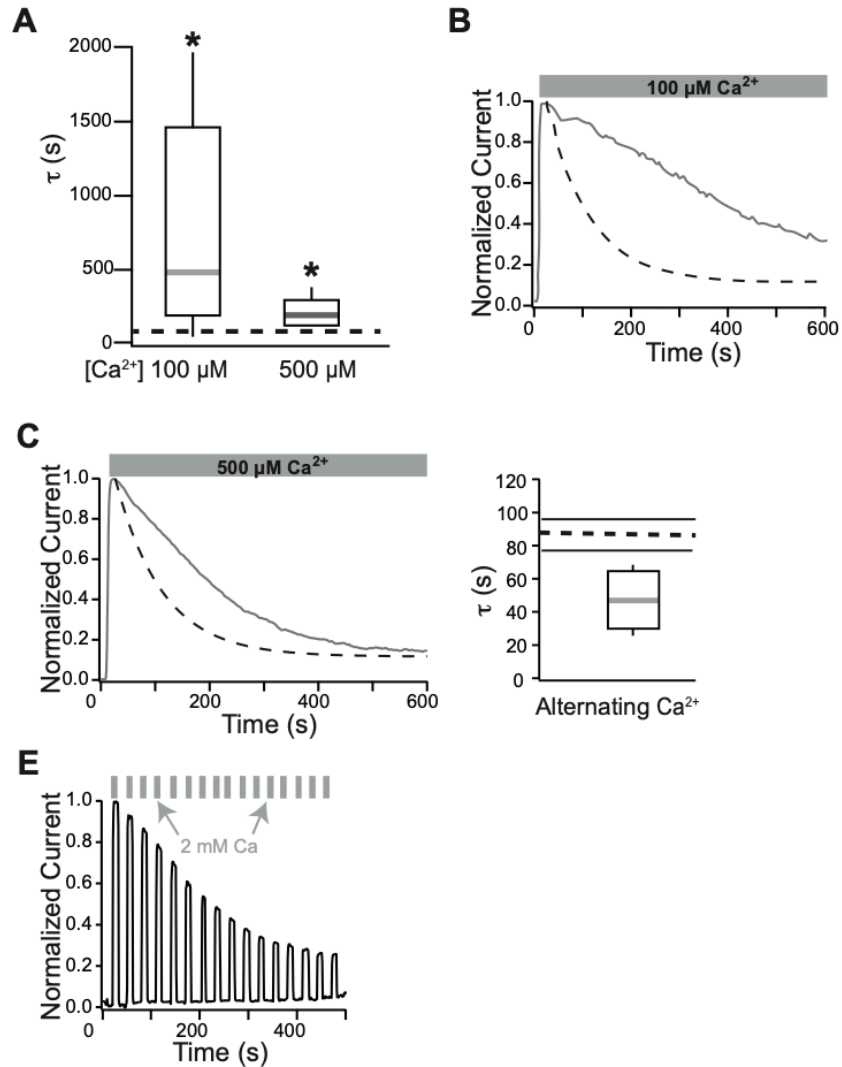


**Figure 4-4. Lowering  $\text{Ca}^{2+}$  slows current rundown**

Inside-out patch clamp recordings were conducted on macropatches excised from *X. laevis* oocytes during the application of varying concentrations of  $\text{Ca}^{2+}$ . (A) Box plot distribution of the rate of current decay ( $\tau$ ), measured by fitting plots of relative current versus time with single exponentials for the current recordings before, during and after the application of 100  $\mu\text{M}$   $\text{Ca}^{2+}$  (N=5), 500  $\mu\text{M}$   $\text{Ca}^{2+}$  (N=5) and alternating for 10s between 2 mM  $\text{Ca}$  and 0 mM  $\text{Ca}^{2+}$  (N=4). The dashed black line represents the median  $\tau$  for the control (N=9). Representative plot of normalized currents versus time before, during and after the application of 100  $\mu\text{M}$   $\text{Ca}^{2+}$  (B), 500  $\mu\text{M}$   $\text{Ca}^{2+}$  (C). (D) Box plot distribution of the rate of current decay ( $\tau$ ) current recordings before, during and after the application of alternating for 10s between 2 mM  $\text{Ca}$  and 0 mM. (E) Representative plot of normalized currents versus time before, during and after the application of alternating 10 s intervals of 2 mM  $\text{Ca}$  and 0 mM  $\text{Ca}^{2+}$ . \* indicates a  $P < 0.05$  as determined by t-test and compared to 2 mM  $\text{Ca}^{2+}$  control.

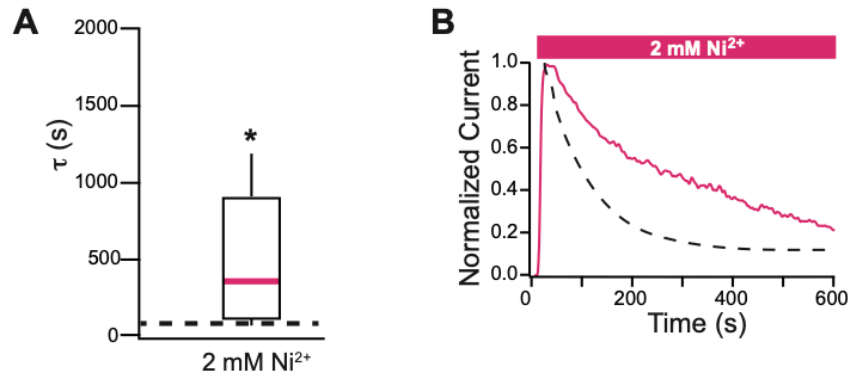


**Figure 4-5. Substituting  $\text{Ca}^{2+}$  with other divalents slows current rundown**

Inside-out patch clamp recordings were conducted on macropatches excised from *X. laevis* oocytes during the application of the divalents  $\text{Ni}^{2+}$  and  $\text{Mg}^{2+}$ . (A) Box plot distribution of the rate of current decay ( $\tau$ ), measured by fitting plots of relative current versus time with single exponentials for the current recordings before, during and after the application of 2 mM  $\text{Ni}^{2+}$  (N=6). The dashed black line represents the median  $\tau$  for the control (N=9). Representative plot of normalized currents versus time before, during and after the application of 2 mM  $\text{Ni}^{2+}$  (B) 2 mM  $\text{Mg}^{2+}$  (N=4) (C). \* indicates a  $P > 0.05$  compared to 2 mM  $\text{Ca}^{2+}$  control. \* indicates a  $P < 0.05$  compared to 2 mM  $\text{Ca}^{2+}$  control.  $P$ -values were determined by t-test.

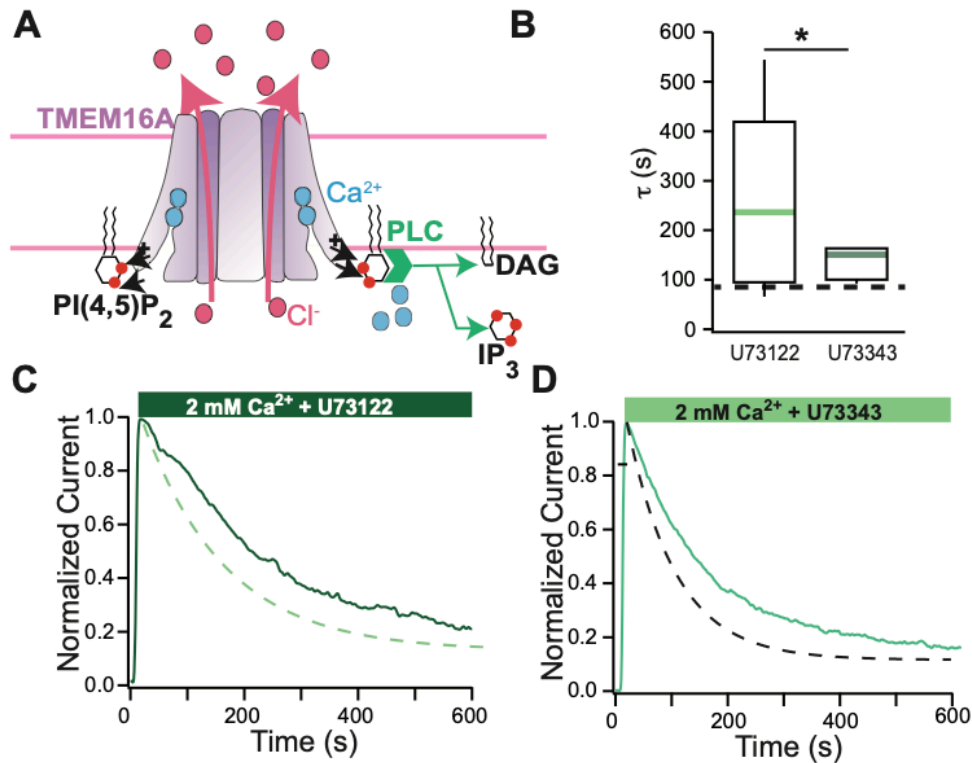


**Figure 4-6. Inhibiting PLC slows current rundown**

Inside-out patch clamp recordings were conducted on macropatches excised from *X. laevis* oocytes during the application of the general PLC inhibitor U-73122 and its inactive analog U-73343. (A) Schematic representing the  $Ca^{2+}$ -sensitive PLC mediated depletion of PI(4,5)P<sub>2</sub>. (B) Box plot distribution of the rate of current decay ( $\tau$ ), measured by fitting plots of relative current versus time with single exponentials for the current recordings before, during and after the application of 1  $\mu$ M U-73343 (N=4), and 1  $\mu$ M U-73122 (N=6). Representative plot of normalized currents versus time before, during and after the application 1  $\mu$ M U-73343 (C) and 1  $\mu$ M U-73122 (D). Grey dashed line represents controls recorded in 2 mM  $Ca^{2+}$ . Green dashed line represents recordings conducted in 1  $\mu$ M U-73343. \* indicates  $P < 0.05$  as determined by t-test.

## 5.0 Overall Discussion

In this section, I will summarize the research I have conducted for my dissertation as well as what this research offers to the scientific community. I will also propose experiments that could be a guide for future research.

### 5.1 Overview of dissertation research

For my dissertation, I investigated two main questions: 1) what are the signaling mechanisms regulating TMEM16A gating? and 2) how do PI(4,5)P<sub>2</sub> and Ca<sup>2+</sup> regulate TMEM16A gating? To answer these questions, I employed electrophysiology techniques that directly measured the activity of *Xenopus* TMEM16A in the oocytes of the African clawed frog, *Xenopus laevis*. Briefly, I have shown that TMEM16A requires both PI(4,5)P<sub>2</sub> and Ca<sup>2+</sup> to conduct Cl<sup>-</sup> currents. I have also shown that TMEM16A-evoked Cl<sup>-</sup> currents rundown and that the speed of rundown is dictated by Ca<sup>2+</sup>, suggesting a role for a Ca<sup>2+</sup>-sensitive PLC in the depletion of PI(4,5)P<sub>2</sub> which regulates TMEM16A gating.

### 5.2 Research implications for the PI(4,5)P<sub>2</sub> regulation of TMEM16A

In addition to managing the Cl<sup>-</sup> homeostasis required for the survival of most cells [133], TMEM16A is just as powerful at promoting disease. Since TMEM16A plays a role in promoting hypertension [135], a major gateway condition to cardiovascular and cerebrovascular disease

[101], and a factor contributing greater than 10 million preventable deaths every year [168], TMEM16A should be targeted for the development of novel forms of hypertensive therapy. However, targeting TMEM16A for therapy could have wide reaching consequences given that knocking out TMEM16A in mice is lethal [100]. Therefore, therapy could involve pharmaceutical targeting of TMEM16A's regulation. Now that I have demonstrated that PI(4,5)P<sub>2</sub> is required for TMEM16A activation and that the phosphate at position 4 on PI(4,5)P<sub>2</sub> is instrumental for this interaction, drugs can be designed to disrupt or enhance this interaction.

### **5.3 Research implications for the Ca<sup>2+</sup> regulation of TMEM16A**

Like PI(4,5)P<sub>2</sub>, Ca<sup>2+</sup> is also required to open TMEM16A channels. However, PI(4,5)P<sub>2</sub> is kept in homeostatic balance in the plasma membrane while Ca<sup>2+</sup> fluctuates relative to a cell's needs for signaling, therefore making it difficult to target the TMEM16A-Ca<sup>2+</sup> relationship without having off target effects. My research points to a Ca<sup>2+</sup>-sensitive PLC speeding TMEM16A rundown. The Ca<sup>2+</sup> modulation of the PLC can be used as a tool to alter PI(4,5)P<sub>2</sub>, DAG and IP<sub>3</sub> levels. This could be important in studying the regulation of other ion channels regulated by PI(4,5)P<sub>2</sub> using the excised inside-out patch technique.

### **5.4 Unanswered questions about TMEM16A regulation**

Future studies could focus on resolving the Cl<sup>-</sup> pore. Perhaps a first step would be to resolve a structure for TMEM16A in a Ca<sup>2+</sup> and PI(4,5)P<sub>2</sub> bound state so that a likely pore can be identified.

Studies have identified PI(4,5)P<sub>2</sub> [136, 137] and Ca<sup>2+</sup> [50] binding sites on TMEM16A but the Cl<sup>-</sup> pore has not been resolved. Perhaps, purifying TMEM16A channels containing a mutation that makes them constitutively active could help resolve the Cl<sup>-</sup> pore. TMEM16A gating is controlled by the shifting of the  $\alpha$ -helix on TM6 [46, 152]. This movement is enabled by a glycine hinge located at mTMEM16A G644 [46, 152]. G644P mutation results in constitutively active TMEM16A channels [46, 152] that I propose be used when resolving TMEM16A's Cl<sup>-</sup> pore.

High concentrations of Ca<sup>2+</sup> activate TMEM16A and the PLC that depletes PI(4,5)P<sub>2</sub>. A major question that requires additional study is how PI(4,5)P<sub>2</sub> can both encourage TMEM16A currents by forming electrostatic interactions [136, 137] and also be hydrolyzed to DAG and IP<sub>3</sub> (thereby depleting PI(4,5)P<sub>2</sub>, to activate TMEM16A) [163]. One explanation for this could be that in *X. laevis* oocytes, which mature into fertilization competent eggs [155], the egg is equipped with enough PI(4,5)P<sub>2</sub> to do both. This is supported by data showing that at fertilization PI(4,5)P<sub>2</sub> levels double [169]. By increasing PI(4,5)P<sub>2</sub> at the membrane, the egg may have enough PI(4,5)P<sub>2</sub> to both hydrolyze and to stay at the membrane to potentiate TMEM16A channels once the fast block is initiated. Since the membrane remains depolarized for at least 40 minutes [156], both Ca<sup>2+</sup> and PI(4,5)P<sub>2</sub> could be present. Alternatively, the channel may become inactive and the pumps that bring Cl<sup>-</sup> back could be unfunctional. To better understand TMEM16A regulation, I would like to evaluate if other cell types such as smooth muscle cells, known to express TMEM16A, would demonstrate a similar Ca<sup>2+</sup>-TMEM16A-PI(4,5)P<sub>2</sub> relationship in excised inside-out patches. Notably, other studies demonstrating that PI(4,5)P<sub>2</sub> potentiates TMEM16A have used exogenous expression systems such as HEK293 cells [68, 78] that do not have a reported physiological need comparable to the fast block in *X. laevis* eggs.

Lastly, the PLC in the oocyte whose activity is increased by  $\text{Ca}^{2+}$  has not been identified. The oocyte expresses PLC $\gamma$  and PLC $\beta$  subtypes [125, 162, 163], and the general PLC inhibitor U73122 is not specific for either subtype [151]. At this time, no potent inhibitors for specific PLC subtypes exist. Additional studies investigating which PLC(s) are involved in regulating TMEM16A could be informative. I propose to inject PLC subtype specific siRNAs in *X. laevis* oocytes and measure the rate of current rundown. It is possible that being able to distinguish between the PLCs could help reduce off target effects in the case that silencing one PLC subtype over the other slows current rundown.

## 5.5 Dissertation research conclusions

The overall goal of my dissertation has been to determine how a disease implicated channel is regulated using *X. laevis* oocytes as a model. Understanding how the well-established CaCC TMEM16A is regulated adds new insight into mechanisms of a proteins involved in debilitating diseases. Remembering that hypertension affects 1 billion people world-wide [168], this new research could have far reaching implications for how we think about and ultimately, how we treat diseases associated with TMEM16A.

## Bibliography

1. Martinac, B., Y. Saimi, and C. Kung, *Ion channels in microbes*. *Physiol Rev*, 2008. **88**(4): p. 1449-90.
2. Mattson, M.P., *Modification of ion homeostasis by lipid peroxidation: roles in neuronal degeneration and adaptive plasticity*. *Trends Neurosci*, 1998. **21**(2): p. 53-7.
3. Khanna, A., et al., *Disruption of ion homeostasis in the neuroglial unit underlies the pathogenesis of ischemic cerebral edema*. *Transl Stroke Res*, 2014. **5**(1): p. 3-16.
4. Lodish, H., et al., *Molecular Cell Biology*. 7th ed. 2012, New York: Freeman.
5. Alvarez-Leefmans, F.J. and E. Delpire, *Physiology and Pathology of Chloride Transporters and Channels in the Nervous System*. 2009: Academic Press.
6. Dean, M., Y. Hamon, and G. Chimini, *The human ATP-binding cassette (ABC) transporter superfamily*. *J Lipid Res*, 2001. **42**(7): p. 1007-17.
7. Abe, K., et al., *Inter-subunit interaction of gastric H<sup>+</sup>,K<sup>+</sup>-ATPase prevents reverse reaction of the transport cycle*. *Embo j*, 2009. **28**(11): p. 1637-43.
8. Ma, T.S., et al., *SR compartment calcium and cell apoptosis in SERCA overexpression*. *Cell Calcium*, 1999. **26**(1-2): p. 25-36.
9. Fröhlich, F., *Network Neuroscience*. 2016: Academic Press. 482.
10. Alberts, B., et al., *Molecular Biology of the Cell*. 4th ed. 2000, New York: Garland Science.
11. Ashcroft, F., D. Gadsby, and C. Miller, *Introduction. The blurred boundary between channels and transporters*. *Philos Trans R Soc Lond B Biol Sci*, 2009. **364**(1514): p. 145-7.
12. Purves, D., et al., *Neuroscience*. 2nd ed. Voltage-Gated Ion Channels. . 2001, Sunderland, MA: Sinauer Associates.
13. Wang, Q., et al., *Local coupling of TRPC6 to ANO1/TMEM16A channels in smooth muscle cells amplifies vasoconstriction in cerebral arteries*. *Am J Physiol Cell Physiol*, 2016. **310**(11): p. C1001-9.
14. Zhang, M., et al., *The association between the expression of PAR2 and TMEM16A and neuropathic pain*. *Mol Med Rep*, 2018. **17**(3): p. 3744-3750.

15. Huang, F., et al., *Studies on expression and function of the TMEM16A calcium-activated chloride channel*. Proc Natl Acad Sci U S A, 2009. **106**(50): p. 21413-8.
16. Svenningsen, P., et al., *TMEM16A is a Ca(2+) -activated Cl(-) channel expressed in the renal collecting duct*. Acta Physiol (Oxf), 2014. **212**(2): p. 166-74.
17. Manoury, B., A. Tamuleviciute, and P. Tammara, *TMEM16A/anoctamin 1 protein mediates calcium-activated chloride currents in pulmonary arterial smooth muscle cells*. J Physiol, 2010. **588**(Pt 13): p. 2305-14.
18. Benjamin, E.J., et al., *Heart Disease and Stroke Statistics-2017 Update: A Report From the American Heart Association*. Circulation, 2017. **135**(10): p. e146-e603.
19. Mao, S., et al., *Molecular and functional expression of cation-chloride cotransporters in dorsal root ganglion neurons during postnatal maturation*. J Neurophysiol, 2012. **108**(3): p. 834-52.
20. Takayama, Y. and M. Tominaga, *Involvement of TRPV1-ANO1 Interactions in Pain-Enhancing Mechanisms*. Adv Exp Med Biol, 2018. **1099**: p. 29-36.
21. Mizumura, K., et al., *Excitation and sensitization of nociceptors by bradykinin: what do we know?* Exp Brain Res, 2009. **196**(1): p. 53-65.
22. Hahn, A., et al., *Expression and function of Anoctamin 1/TMEM16A calcium-activated chloride channels in airways of in vivo mouse models for cystic fibrosis research*. Pflugers Arch, 2018. **470**(9): p. 1335-1348.
23. Benedetto, R., et al., *TMEM16A is indispensable for basal mucus secretion in airways and intestine*. Faseb j, 2019. **33**(3): p. 4502-4512.
24. Samet, J.M. and P.W. Cheng, *The role of airway mucus in pulmonary toxicology*. Environ Health Perspect, 1994. **102 Suppl 2**: p. 89-103.
25. Kunzelmann, K., et al., *TMEM16A in Cystic Fibrosis: Activating or Inhibiting?* Front Pharmacol, 2019. **10**: p. 3.
26. Bill, A., et al., *ANO1/TMEM16A interacts with EGFR and correlates with sensitivity to EGFR-targeting therapy in head and neck cancer*. Oncotarget, 2015. **6**(11): p. 9173-88.
27. Britschgi, A., et al., *Calcium-activated chloride channel ANO1 promotes breast cancer progression by activating EGFR and CAMK signaling*. Proc Natl Acad Sci U S A, 2013. **110**(11): p. E1026-34.
28. Lander, E.S., et al., *Initial sequencing and analysis of the human genome*. Nature, 2001. **409**(6822): p. 860-921.

29. Espinosa, I., et al., *A novel monoclonal antibody against DOG1 is a sensitive and specific marker for gastrointestinal stromal tumors*. Am J Surg Pathol, 2008. **32**(2): p. 210-8.
30. Berglund, E., et al., *Functional role of the Ca(2+)-activated Cl(-) channel DOG1/TMEM16A in gastrointestinal stromal tumor cells*. Exp Cell Res, 2014. **326**(2): p. 315-25.
31. Katoh, M. and M. Katoh, *Identification and characterization of human TP53I5 and mouse Tp53i5 genes in silico*. Int J Oncol, 2004. **25**(1): p. 225-30.
32. Huang, X., et al., *Comprehensive genome and transcriptome analysis of the 11q13 amplicon in human oral cancer and synteny to the 7F5 amplicon in murine oral carcinoma*. Genes Chromosomes Cancer, 2006. **45**(11): p. 1058-69.
33. Caputo, A., et al., *TMEM16A, a membrane protein associated with calcium-dependent chloride channel activity*. Science, 2008. **322**(5901): p. 590-4.
34. Schroeder, B.C., et al., *Expression cloning of TMEM16A as a calcium-activated chloride channel subunit*. Cell, 2008. **134**(6): p. 1019-29.
35. Yang, Y.D., et al., *TMEM16A confers receptor-activated calcium-dependent chloride conductance*. Nature, 2008. **455**(7217): p. 1210-5.
36. Parker, I. and R. Miledi, *A calcium-independent chloride current activated by hyperpolarization in Xenopus oocytes*. Proc R Soc Lond B Biol Sci, 1988. **233**(1271): p. 191-9.
37. Maricq, A.V. and J.I. Korenbrot, *Calcium and calcium-dependent chloride currents generate action potentials in solitary cone photoreceptors*. Neuron, 1988. **1**(6): p. 503-15.
38. Evans, M.G. and A. Marty, *Calcium-dependent chloride currents in isolated cells from rat lacrimal glands*. J Physiol, 1986. **378**: p. 437-60.
39. Barish, M.E., *A transient calcium-dependent chloride current in the immature Xenopus oocyte*. J Physiol, 1983. **342**: p. 309-25.
40. Galiotta, L.J., et al., *IL-4 is a potent modulator of ion transport in the human bronchial epithelium in vitro*. J Immunol, 2002. **168**(2): p. 839-45.
41. Webb, D.J. and R. Nuccitelli, *Fertilization potential and electrical properties of the Xenopus laevis egg*. Dev Biol, 1985. **107**(2): p. 395-406.
42. Hartzell, H.C., *Activation of different Cl currents in Xenopus oocytes by Ca liberated from stores and by capacitative Ca influx*. J Gen Physiol, 1996. **108**(3): p. 157-75.

43. Almen, M.S., et al., *Mapping the human membrane proteome: a majority of the human membrane proteins can be classified according to function and evolutionary origin*. BMC Biol, 2009. **7**: p. 50.
44. Brunner, J.D., et al., *X-ray structure of a calcium-activated TMEM16 lipid scramblase*. Nature, 2014. **516**(7530): p. 207-12.
45. Dang, S., et al., *Cryo-EM structures of the TMEM16A calcium-activated chloride channel*. Nature, 2017. **552**(7685): p. 426-429.
46. Paulino, C., et al., *Activation mechanism of the calcium-activated chloride channel TMEM16A revealed by cryo-EM*. Nature, 2017. **552**(7685): p. 421-425.
47. Jeng, G., et al., *Independent activation of distinct pores in dimeric TMEM16A channels*. J Gen Physiol, 2016. **148**(5): p. 393-404.
48. Lim, N.K., A.K. Lam, and R. Dutzler, *Independent activation of ion conduction pores in the double-barreled calcium-activated chloride channel TMEM16A*. J Gen Physiol, 2016. **148**(5): p. 375-392.
49. Yu, K., et al., *Explaining calcium-dependent gating of anoctamin-1 chloride channels requires a revised topology*. Circ Res, 2012. **110**(7): p. 990-9.
50. Tien, J., et al., *A comprehensive search for calcium binding sites critical for TMEM16A calcium-activated chloride channel activity*. Elife, 2014. **3**.
51. Kane Dickson, V., L. Pedi, and S.B. Long, *Structure and insights into the function of a Ca(2+)-activated Cl(-) channel*. Nature, 2014. **516**(7530): p. 213-8.
52. Olsen, R.W. and W. Sieghart, *GABA A receptors: subtypes provide diversity of function and pharmacology*. Neuropharmacology, 2009. **56**(1): p. 141-8.
53. Hibino, H., et al., *Inwardly rectifying potassium channels: their structure, function, and physiological roles*. Physiol Rev, 2010. **90**(1): p. 291-366.
54. Chen, R. and D.R. Swale, *Inwardly Rectifying Potassium (Kir) Channels Represent a Critical Ion Conductance Pathway in the Nervous Systems of Insects*. Sci Rep, 2018. **8**(1): p. 1617.
55. Skerratt, S.E. and C.W. West, *Ion channel therapeutics for pain*. Channels (Austin), 2015. **9**(6): p. 344-51.
56. Priest, B.T. and A. Pasternak, *The therapeutic potential of targeting the Kir1.1 (renal outer medullary K(+)) channel*. Future Med Chem, 2017. **9**(16): p. 1963-1977.

57. Tang, H., et al., *Discovery of MK-7145, an Oral Small Molecule ROMK Inhibitor for the Treatment of Hypertension and Heart Failure*. ACS Med Chem Lett, 2016. **7**(7): p. 697-701.
58. Hampton, C., et al., *The Renal Outer Medullary Potassium Channel Inhibitor, MK-7145, Lowers Blood Pressure, and Manifests Features of Bartter's Syndrome Type II Phenotype*. J Pharmacol Exp Ther, 2016. **359**(1): p. 194-206.
59. Hartzell, H.C., et al., *Anoctamin/TMEM16 family members are Ca<sup>2+</sup>-activated Cl<sup>-</sup> channels*. J Physiol, 2009. **587**(Pt 10): p. 2127-39.
60. Suzuki, J., et al., *Calcium-dependent phospholipid scramblase activity of TMEM16 protein family members*. J Biol Chem, 2013. **288**(19): p. 13305-16.
61. Tran, T.T., et al., *TMEM16E (GDD1) exhibits protein instability and distinct characteristics in chloride channel/pore forming ability*. J Cell Physiol, 2014. **229**(2): p. 181-90.
62. Jha, A., et al., *Anoctamin 8 tethers endoplasmic reticulum and plasma membrane for assembly of Ca(2+) signaling complexes at the ER/PM compartment*. Embo j, 2019. **38**(12).
63. Pifferi, S., M. Dibattista, and A. Menini, *TMEM16B induces chloride currents activated by calcium in mammalian cells*. Pflugers Arch, 2009. **458**(6): p. 1023-38.
64. Stohr, H., et al., *TMEM16B, a novel protein with calcium-dependent chloride channel activity, associates with a presynaptic protein complex in photoreceptor terminals*. J Neurosci, 2009. **29**(21): p. 6809-18.
65. Scudieri, P., et al., *The anoctamin family: TMEM16A and TMEM16B as calcium-activated chloride channels*. Exp Physiol, 2012. **97**(2): p. 177-83.
66. Pifferi, S., V. Cenedese, and A. Menini, *Anoctamin 2/TMEM16B: a calcium-activated chloride channel in olfactory transduction*. Exp Physiol, 2012. **97**(2): p. 193-9.
67. Betto, G., et al., *Interactions between permeation and gating in the TMEM16B/anoctamin2 calcium-activated chloride channel*. J Gen Physiol, 2014. **143**(6): p. 703-18.
68. Ta, C.M., et al., *Contrasting effects of phosphatidylinositol 4,5-bisphosphate on cloned TMEM16A and TMEM16B channels*. Br J Pharmacol, 2017. **174**(18): p. 2984-2999.
69. Juul, C.A., et al., *Anoctamin 6 differs from VRAC and VSOAC but is involved in apoptosis and supports volume regulation in the presence of Ca<sup>2+</sup>*. Pflugers Arch, 2014. **466**(10): p. 1899-910.

70. Kunzelmann, K., et al., *Molecular functions of anoctamin 6 (TMEM16F): a chloride channel, cation channel, or phospholipid scramblase?* Pflugers Arch, 2014. **466**(3): p. 407-14.
71. Peters, C.J., et al., *The Sixth Transmembrane Segment Is a Major Gating Component of the TMEM16A Calcium-Activated Chloride Channel.* Neuron, 2018.
72. Shimizu, T., et al., *TMEM16F is a component of a Ca<sup>2+</sup>-activated Cl<sup>-</sup> channel but not a volume-sensitive outwardly rectifying Cl<sup>-</sup> channel.* Am J Physiol Cell Physiol, 2013. **304**(8): p. C748-59.
73. Ye, W., et al., *Phosphatidylinositol-(4, 5)-bisphosphate regulates calcium gating of small-conductance cation channel TMEM16F.* Proc Natl Acad Sci U S A, 2018.
74. Ferrera, L., et al., *Regulation of TMEM16A chloride channel properties by alternative splicing.* J Biol Chem, 2009. **284**(48): p. 33360-8.
75. Bulley, S., et al., *TMEM16A/ANO1 channels contribute to the myogenic response in cerebral arteries.* Circ Res, 2012. **111**(8): p. 1027-36.
76. Chun, H., et al., *Protons inhibit anoctamin 1 by competing with calcium.* Cell Calcium, 2015. **58**(5): p. 431-41.
77. Sones, W.R., et al., *Cholesterol depletion alters amplitude and pharmacology of vascular calcium-activated chloride channels.* Cardiovasc Res, 2010. **87**(3): p. 476-84.
78. De Jesus-Perez, J.J., et al., *Phosphatidylinositol 4,5-bisphosphate, cholesterol, and fatty acids modulate the calcium-activated chloride channel TMEM16A (ANO1).* Biochim Biophys Acta, 2018. **1863**(3): p. 299-312.
79. Cho, H., et al., *The calcium-activated chloride channel anoctamin 1 acts as a heat sensor in nociceptive neurons.* Nat Neurosci, 2012. **15**(7): p. 1015-21.
80. Tian, Y., et al., *Control of TMEM16A by INO-4995 and other inositolphosphates.* Br J Pharmacol, 2013. **168**(1): p. 253-65.
81. Pritchard, H.A., et al., *Inhibitory role of phosphatidylinositol 4,5-bisphosphate on TMEM16A-encoded calcium-activated chloride channels in rat pulmonary artery.* Br J Pharmacol, 2014. **171**(18): p. 4311-21.
82. Ma, K., et al., *New Insights on the Regulation of Ca<sup>2+</sup> -Activated Chloride Channel TMEM16A.* J Cell Physiol, 2017. **232**(4): p. 707-716.
83. Papke, R.L. and C. Smith-Maxwell, *High throughput electrophysiology with Xenopus oocytes.* Comb Chem High Throughput Screen, 2009. **12**(1): p. 38-50.

84. Wagner, C.A., et al., *The use of Xenopus laevis oocytes for the functional characterization of heterologously expressed membrane proteins*. Cell Physiol Biochem, 2000. **10**(1-2): p. 1-12.
85. Weber, W.M., *Endogenous ion channels in oocytes of xenopus laevis: recent developments*. J Membr Biol, 1999. **170**(1): p. 1-12.
86. Meyerhof, W., et al., *Receptors for neuropeptides are induced by exogenous poly(A)<sup>+</sup> RNA in oocytes from Xenopus laevis*. Proc Natl Acad Sci U S A, 1988. **85**(3): p. 714-7.
87. Yang, T., W.A. Hendrickson, and H.M. Colecraft, *Preassociated apocalmodulin mediates Ca<sup>2+</sup>-dependent sensitization of activation and inactivation of TMEM16A/16B Ca<sup>2+</sup>-gated Cl<sup>-</sup> channels*. Proc Natl Acad Sci U S A, 2014. **111**(51): p. 18213-8.
88. Weber, W., *Ion currents of Xenopus laevis oocytes: state of the art*. Biochim Biophys Acta, 1999. **1421**(2): p. 213-33.
89. Sobczak, K., et al., *Endogenous transport systems in the Xenopus laevis oocyte plasma membrane*. Methods, 2010. **51**(1): p. 183-9.
90. Tembo, M., et al., *Phosphatidylinositol 4,5-bisphosphate (PIP<sub>2</sub>) and Ca(2+) are both required to open the Cl(-) channel TMEM16A*. J Biol Chem, 2019. **294**(33): p. 12556-12564.
91. Whitlock, J.M. and H.C. Hartzell, *A Pore Idea: the ion conduction pathway of TMEM16/ANO proteins is composed partly of lipid*. Pflugers Arch, 2016. **468**(3): p. 455-73.
92. Wallace, R.A., et al., *Protein incorporation by isolated amphibian oocytes. 3. Optimum incubation conditions*. J Exp Zool, 1973. **184**(3): p. 321-33.
93. Zhang, G. and J. Cui, *Patch-Clamp and Perfusion Techniques to Study Ion Channels Expressed in Xenopus Oocytes*. Cold Spring Harb Protoc, 2018.
94. Sakmann, B. and E. Neher, *Patch clamp techniques for studying ionic channels in excitable membranes*. Annu Rev Physiol, 1984. **46**: p. 455-72.
95. Hartzell, C., I. Putzier, and J. Arreola, *Calcium-activated chloride channels*. Annu Rev Physiol, 2005. **67**: p. 719-58.
96. Huang, F., X. Wong, and L.Y. Jan, *International Union of Basic and Clinical Pharmacology. LXXXV: calcium-activated chloride channels*. Pharmacological reviews, 2012. **64**(1): p. 1-15.
97. Pedemonte, N. and L.J. Galiotta, *Structure and function of TMEM16 proteins (anoctamins)*. Physiol Rev, 2014. **94**(2): p. 419-59.

98. Cho, H., et al., *The calcium-activated chloride channel anoctamin 1 acts as a heat sensor in nociceptive neurons*. Nature neuroscience, 2012. **15**(7): p. 1015-1021.
99. Deba, F. and B.F. Bessac, *Anoctamin-1 Cl<sup>-</sup> channels in nociception: activation by an N-aroylaminothiazole and capsaicin and inhibition by T16A[inh]-A01*. Molecular pain, 2015. **11**: p. 55-55.
100. Rock, J.R., C.R. Futtner, and B.D. Harfe, *The transmembrane protein TMEM16A is required for normal development of the murine trachea*. Dev Biol, 2008. **321**(1): p. 141-9.
101. *Correction to: Heart Disease and Stroke Statistics-2017 Update: A Report From the American Heart Association*. Circulation, 2017. **135**(10): p. e646.
102. Hilgemann, D.W. and R. Ball, *Regulation of cardiac Na<sup>+</sup>,Ca<sup>2+</sup> exchange and KATP potassium channels by PIP2*. Science, 1996. **273**(5277): p. 956-9.
103. Suh, B.C. and B. Hille, *PIP2 is a necessary cofactor for ion channel function: how and why?* Annu Rev Biophys, 2008. **37**: p. 175-95.
104. Tian, Y., et al., *Calmodulin-dependent activation of the epithelial calcium-dependent chloride channel TMEM16A*. Faseb j, 2011. **25**(3): p. 1058-68.
105. Egan, T.M., et al., *Properties and rundown of sodium-activated potassium channels in rat olfactory bulb neurons*. J Neurosci, 1992. **12**(5): p. 1964-76.
106. Balla, T., *Phosphoinositides: tiny lipids with giant impact on cell regulation*. Physiol Rev, 2013. **93**(3): p. 1019-137.
107. Gaidarov, I., et al., *A functional phosphatidylinositol 3,4,5-trisphosphate/phosphoinositide binding domain in the clathrin adaptor AP-2 alpha subunit. Implications for the endocytic pathway*. J Biol Chem, 1996. **271**(34): p. 20922-9.
108. Gamper, N. and M.S. Shapiro, *Regulation of ion transport proteins by membrane phosphoinositides*. Nat Rev Neurosci, 2007. **8**(12): p. 921-34.
109. Saleh, S.N., A.P. Albert, and W.A. Large, *Activation of native TRPC1/C5/C6 channels by endothelin-1 is mediated by both PIP3 and PIP2 in rabbit coronary artery myocytes*. J Physiol, 2009. **587**(Pt 22): p. 5361-75.
110. Hirono, M., et al., *Hair cells require phosphatidylinositol 4,5-bisphosphate for mechanical transduction and adaptation*. Neuron, 2004. **44**(2): p. 309-20.
111. Gabev, E., et al., *Binding of neomycin to phosphatidylinositol 4,5-bisphosphate (PIP2)*. Biochim Biophys Acta, 1989. **979**(1): p. 105-12.

112. Tang, Q.Y., et al., *Mutations in Nature Conferred a High Affinity Phosphatidylinositol 4,5-Bisphosphate-binding Site in Vertebrate Inwardly Rectifying Potassium Channels*. J Biol Chem, 2015. **290**(27): p. 16517-29.
113. Collins, A., A.V. Somlyo, and D.W. Hilgemann, *The giant cardiac membrane patch method: stimulation of outward Na(+)-Ca<sup>2+</sup> exchange current by MgATP*. J Physiol, 1992. **454**: p. 27-57.
114. Ono, K. and H.A. Fozzard, *Phosphorylation restores activity of L-type calcium channels after rundown in inside-out patches from rabbit cardiac cells*. J Physiol, 1992. **454**: p. 673-88.
115. Boskey, A.L., et al., *The mechanism of beta-glycerophosphate action in mineralizing chick limb-bud mesenchymal cell cultures*. J Bone Miner Res, 1996. **11**(11): p. 1694-702.
116. Xie, L.H., et al., *Phosphatidylinositol-4,5-bisphosphate (PIP<sub>2</sub>) regulation of strong inward rectifier Kir2.1 channels: multilevel positive cooperativity*. J Physiol, 2008. **586**(7): p. 1833-48.
117. Huang, C.L., S. Feng, and D.W. Hilgemann, *Direct activation of inward rectifier potassium channels by PIP<sub>2</sub> and its stabilization by Gbetagamma*. Nature, 1998. **391**(6669): p. 803-6.
118. Zhang, H., et al., *Activation of inwardly rectifying K<sup>+</sup> channels by distinct PtdIns(4,5)P<sub>2</sub> interactions*. Nat Cell Biol, 1999. **1**(3): p. 183-8.
119. Doignon, F., et al., *Requirement of Phosphoinositides Containing Stearic Acid To Control Cell Polarity*. Mol Cell Biol, 2015. **36**(5): p. 765-80.
120. Jalily Hasani, H., et al., *Effects of protein-protein interactions and ligand binding on the ion permeation in KCNQ1 potassium channel*. PLoS One, 2018. **13**(2): p. e0191905.
121. Hughes, T.E.T., et al., *Structural insights on TRPV5 gating by endogenous modulators*. Nat Commun, 2018. **9**(1): p. 4198.
122. Hansen, S.B., X. Tao, and R. MacKinnon, *Structural basis of PIP<sub>2</sub> activation of the classical inward rectifier K<sup>+</sup> channel Kir2.2*. Nature, 2011. **477**(7365): p. 495-8.
123. Whorton, M.R. and R. MacKinnon, *Crystal structure of the mammalian GIRK2 K<sup>+</sup> channel and gating regulation by G proteins, PIP<sub>2</sub>, and sodium*. Cell, 2011. **147**(1): p. 199-208.
124. Sala-Rabanal, M., et al., *Secreted CLCA1 modulates TMEM16A to activate Ca(2+)-dependent chloride currents in human cells*. Elife, 2015. **4**.

125. Session, A.M., et al., *Genome evolution in the allotetraploid frog Xenopus laevis*. Nature, 2016. **538**(7625): p. 336-343.
126. Wozniak, K.L., et al., *The TMEM16A channel mediates the fast polyspermy block in Xenopus laevis*. J Gen Physiol, 2018.
127. Wuhr, M., et al., *Deep proteomics of the Xenopus laevis egg using an mRNA-derived reference database*. Curr Biol, 2014. **24**(13): p. 1467-75.
128. Tembo, M. and A.E. Carlson, *Under pressure: Ano1 mediates pressure sensing in the lymphatic system*. J Gen Physiol, 2019. **151**(4): p. 404-406.
129. Zawieja, S.D., et al., *Ano1 mediates pressure-sensitive contraction frequency changes in mouse lymphatic collecting vessels*. J Gen Physiol, 2019. **151**(4): p. 532-554.
130. Wozniak, K.L., et al., *PLC and IP3-evoked Ca(2+) release initiate the fast block to polyspermy in Xenopus laevis eggs*. J Gen Physiol, 2018.
131. Heinze, C., et al., *Disruption of vascular Ca2+-activated chloride currents lowers blood pressure*. J Clin Invest, 2014. **124**(2): p. 675-86.
132. Mall, M.A. and L.J. Galiotta, *Targeting ion channels in cystic fibrosis*. J Cyst Fibros, 2015. **14**(5): p. 561-70.
133. He, M., et al., *Cytoplasmic Cl(-) couples membrane remodeling to epithelial morphogenesis*. Proc Natl Acad Sci U S A, 2017. **114**(52): p. E11161-e11169.
134. Deba, F. and B.F. Bessac, *Anoctamin-1 Cl(-) channels in nociception: activation by an N-aroylaminothiazole and capsaicin and inhibition by T16A[inh]-A01*. Mol Pain, 2015. **11**: p. 55.
135. Ji, Q., et al., *Recent advances in TMEM16A: Structure, function, and disease*. J Cell Physiol, 2019. **234**(6): p. 7856-7873.
136. Le, S.C., et al., *Molecular basis of PIP2-dependent regulation of the Ca(2+)-activated chloride channel TMEM16A*. Nat Commun, 2019. **10**(1): p. 3769.
137. Yu, K., et al., *A network of phosphatidylinositol 4,5-bisphosphate binding sites regulates gating of the Ca(2+)-activated Cl(-) channel ANO1 (TMEM16A)*. Proc Natl Acad Sci U S A, 2019. **116**(40): p. 19952-19962.
138. Hill-Eubanks, D.C., et al., *Calcium signaling in smooth muscle*. Cold Spring Harb Perspect Biol, 2011. **3**(9): p. a004549.
139. Marin, K., *Calcium Signaling*. 14 February 2012 ed. 2012. 1073-1094.

140. Hilgemann, D.W., *Local PIP(2) signals: when, where, and how?* Pflugers Arch, 2007. **455**(1): p. 55-67.
141. McLaughlin, S., et al., *PIP(2) and proteins: interactions, organization, and information flow.* Annu Rev Biophys Biomol Struct, 2002. **31**: p. 151-75.
142. Wang, J. and D.A. Richards, *Segregation of PIP2 and PIP3 into distinct nanoscale regions within the plasma membrane.* Biol Open, 2012. **1**(9): p. 857-62.
143. van den Bogaart, G., et al., *Membrane protein sequestering by ionic protein-lipid interactions.* Nature, 2011. **479**(7374): p. 552-5.
144. Ni, Y.L., A.S. Kuan, and T.Y. Chen, *Activation and inhibition of TMEM16A calcium-activated chloride channels.* PLoS One, 2014. **9**(1): p. e86734.
145. Yuan, H., et al., *Divalent cations modulate TMEM16A calcium-activated chloride channels by a common mechanism.* The Journal of membrane biology, 2013. **246**(12): p. 893-902.
146. Clapham, D.E., *Calcium signaling.* Cell, 2007. **131**(6): p. 1047-58.
147. Berg, J., H. Yang, and L.Y. Jan, *Ca<sup>2+</sup>-activated Cl<sup>-</sup> channels at a glance.* J Cell Sci, 2012. **125**(Pt 6): p. 1367-71.
148. Kang, M. and H.G. Othmer, *The variety of cytosolic calcium responses and possible roles of PLC and PKC.* Physical biology, 2007. **4**(4): p. 325-343.
149. Seo, J.B., et al., *Charge Shielding of PIP2 by Cations Regulates Enzyme Activity of Phospholipase C.* PLoS One, 2015. **10**(12): p. e0144432.
150. Bleasdale, J.E., et al., *Inhibition of phospholipase C dependent processes by U-73, 122.* Adv Prostaglandin Thromboxane Leukot Res, 1989. **19**: p. 590-3.
151. Jin, W., et al., *U73122 inhibits phospholipase C-dependent calcium mobilization in neuronal cells.* Brain Res, 1994. **642**(1-2): p. 237-43.
152. Lam, A.K. and R. Dutzler, *Calcium-dependent electrostatic control of anion access to the pore of the calcium-activated chloride channel TMEM16A.* Elife, 2018. **7**.
153. Han, Y., et al., *Two Ca(2+)-Binding Sites Cooperatively Couple Together in TMEM16A Channel.* J Membr Biol, 2016. **249**(1-2): p. 57-63.
154. Ta, C.M., et al., *Mechanism of allosteric activation of TMEM16A/ANO1 channels by a commonly used chloride channel blocker.* Br J Pharmacol, 2016. **173**(3): p. 511-28.
155. Mowry, K.L., *Using the Xenopus Oocyte Toolbox.* Cold Spring Harb Protoc, 2020.

156. Wozniak, K.L., et al., *The TMEM16A channel mediates the fast polyspermy block in Xenopus laevis*. J Gen Physiol, 2018. **150**(9): p. 1249-1259.
157. Suh, B.C. and B. Hille, *Electrostatic interaction of internal Mg<sup>2+</sup> with membrane PIP<sub>2</sub> Seen with KCNQ K<sup>+</sup> channels*. J Gen Physiol, 2007. **130**(3): p. 241-56.
158. Kozak, J.A., et al., *Charge screening by internal pH and polyvalent cations as a mechanism for activation, inhibition, and rundown of TRPM7/MIC channels*. J Gen Physiol, 2005. **126**(5): p. 499-514.
159. Zhelay, T., et al., *Depletion of plasma membrane-associated phosphoinositides mimics inhibition of TRPM7 channels by cytosolic Mg(2+), spermine, and pH*. J Biol Chem, 2018. **293**(47): p. 18151-18167.
160. Xie, J., et al., *Phosphatidylinositol 4,5-bisphosphate (PIP(2)) controls magnesium gatekeeper TRPM6 activity*. Sci Rep, 2011. **1**: p. 146.
161. McDonald, L.J. and M.D. Mammack, *Phosphoinositide hydrolysis by phospholipase C modulated by multivalent cations La(3+), Al(3+), neomycin, polyamines, and melittin*. J Lipid Mediat Cell Signal, 1995. **11**(1): p. 81-91.
162. Wuhr, M., et al., *Deep proteomics of the Xenopus laevis egg using an mRNA-derived reference database*. Curr Biol, 2014. **24**(13): p. 1467-1475.
163. Wozniak, K.L., et al., *PLC and IP3-evoked Ca(2+) release initiate the fast block to polyspermy in Xenopus laevis eggs*. J Gen Physiol, 2018. **150**(9): p. 1239-1248.
164. Yang, H., et al., *TMEM16F forms a Ca<sup>2+</sup>-activated cation channel required for lipid scrambling in platelets during blood coagulation*. Cell, 2012. **151**(1): p. 111-22.
165. Xiao, Q., et al., *Voltage- and calcium-dependent gating of TMEM16A/Ano1 chloride channels are physically coupled by the first intracellular loop*. Proc Natl Acad Sci U S A, 2011. **108**(21): p. 8891-6.
166. Sala-Rabanal, M., et al., *Modulation of TMEM16A channel activity by the von Willebrand factor type A (VWA) domain of the calcium-activated chloride channel regulator 1 (CLCA1)*. J Biol Chem, 2017. **292**(22): p. 9164-9174.
167. Wang, H., et al., *Cell-specific mechanisms of TMEM16A Ca(2+)-activated chloride channel in cancer*. Molecular cancer, 2017. **16**(1): p. 152-152.
168. Patel, P., et al., *Standardized Hypertension Management to Reduce Cardiovascular Disease Morbidity and Mortality Worldwide*. Southern medical journal, 2018. **111**(3): p. 133-136.

169. Snow, P., et al., *Fertilization stimulates an increase in inositol trisphosphate and inositol lipid levels in Xenopus eggs*. *Developmental biology*, 1996. **180**(1): p. 108-118.